7.04 Analytical Approaches to Mantle Dynamics

N. M. Ribe, Institut de Physique du Globe, Paris, France

7.04.1 Introduction

Geodynamics is the study of how Earth materials deform and flow over long ($\geq 10^2$–10^3 years) timescales. It is thus a science with dual citizenship: at once a central discipline within the Earth sciences and a branch of fluid dynamics more generally.

The basis of fluid dynamics is a set of general conservation laws for mass, momentum, and energy, which are usually formulated as partial differential equations (PDEs) (Batchelor, 1967, chapter 3). However, because these equations apply to all fluid flows, they describe none in particular, and must therefore be supplemented by material constitutive relations and initial and/or boundary conditions that are appropriate for a particular phenomenon of interest. The result, often called a model problem, is the ultimate object of study in fluid mechanics.

Once posed, a model problem can be solved in one of three ways. The first is to construct a physical analog in the laboratory and let nature do the solving. The experimental approach has long played a central role in geodynamics, and is discussed in Chapter 1.03. Another approach is to solve the model problem numerically on a computer, using one of the methods discussed in Chapter 1.05. The third possibility, the subject of the present chapter, is to solve the problem analytically.

Admittedly, analytical approaches are most effective when the model problem at hand is relatively simple, and lack some of the flexibility of the best experimental and numerical methods. However, they compensate for this by providing a degree of understanding and insight that no other method can match. What is more, they also play a critical role in the interpretation of experimental and numerical results. For example, dimensional analysis is required to ensure proper scaling of experimental and numerical results to the Earth; and local scaling analysis of numerical output can reveal underlying laws that are obscured by numerical tables and graphical images. For all these reasons, the central role that analytical methods have always played in geodynamics is unlikely to diminish.

The purpose of this chapter is to survey the principal analytical methods of geodynamics and the major results that have been obtained using them. These methods are remarkably diverse, and require a correspondingly broad and comprehensive treatment. However, it is equally important to highlight

the common structures and styles of argumentation that give analytical geodynamics an impressive unity. In this spirit, we begin with a discussion of the art of formulating geophysical model problems, focusing on three paradigmatic phenomena (heat transfer from magma diapirs, gravitational instability of buoyant layers, and plume–lithosphere interaction (PLI)) that will subsequently reappear in the course of the chapter treated by different methods. Thus, heat transfer from diapirs is treated using dimensional analysis (Sections 7.04.3.1 and 7.04.3.2), scaling analysis (Section 7.04.3.3), and boundary-layer (BL) theory (Section 7.04.7.1.2); gravitational instability using scaling analysis (Section 7.04.4.3), long-wave analysis (Section 7.04.8.3), and linear stability analysis (Section 7.04.9.1); and PLI using lubrication theory and scaling analysis (Sections 7.04.8.1 and 7.04.8.2). Moreover, the discussions of these and other phenomena are organized as much as possible around three recurrent themes. The first is the importance of scaling arguments (and the scaling laws to which they lead) as tools for understanding physical mechanisms and applying model results to the Earth. Examples of scaling arguments can be found in Sections 7.04.3.3, 7.04.4.3, 7.04.7.2, 7.04.8.2, 7.04.9.2.5, 7.04.9.2.6, 7.04.9.3.1, and 7.04.9.3.4. The second is the ubiquity of self-similar behavior in geophysical flows, which typically occurs in parts of the spatiotemporal flow domain that are sufficiently far from the inhomogeneous initial or boundary conditions that drive the flow to be uninfluenced by their structural details (Sections 7.04.4.1, 7.04.4.2, 7.04.5.3.3, 7.04.5.3.4, 7.04.7.1.1, 7.04.7.3, 7.04.8.1, 7.04.8.2, and 7.04.9.3.4). The third theme is asymptotic analysis, in which the smallness of some crucial parameter in the model problem is exploited to simplify the governing equations, often via a reduction of their dimensionality (Sections 7.04.4.1, 7.04.5.7, 7.04.7, 7.04.7.2, 7.04.8.1, 7.04.8.3, 7.04.8.4, 7.04.8.5, 7.04.8.6, 7.04.9.2.5, 7.04.9.2.6, 7.04.9.3.2, 7.04.9.3.3, and 7.04.9.3.4). While these themes by no means encompass everything the chapter contains, they can serve as threads to guide the reader through what might otherwise appear a trackless labyrinth of miscellaneous methods.

A final aim of the chapter is to introduce some less familiar methods, drawn from other areas of fluid mechanics, that deserve to be better known among geodynamicists. Examples include the use of Papkovich–Fadle eigenfunction expansions (Section 7.04.5.4.1) and complex variables (Section 7.04.5.5) for two-dimensional (2-D) Stokes flows, solutions in bispherical coordinates for 3-D Stokes flows (Section 7.04.5.4.3), and multiple-scale analysis of modulated convection rolls (Sections 7.04.9.2.5 and 7.04.9.2.6).

Table 1 Frequently used abbreviations

Abbreviation	Meaning
1-D	One-dimensional
2-D	Two-dimensional
3-D	Three-dimensional
BL	Boundary layer
BVP	Boundary-value problem
CMB	Core–mantle boundary
LHS	Left-hand side
MEE	Method of eigenfunction expansions
MMAE	Method of matched asymptotic expansions
ODE	Ordinary differential equation
PDE	Partial differential equation
PLI	Plume-lithosphere interaction
RHS	Right-hand side
R-T	Rayleigh–Taylor
SBT	Slender-body theory
TBL	Thermal boundary layer

Throughout this chapter, unless otherwise stated, Greek indices range over the values 1 and 2; Latin indices range over 1, 2, and 3; and the standard summation convention over repeated subscripts is assumed. Subscript notation (e.g., u_i, e_{ij}) and vector notation (e.g., $\mathbf{u}$, $\mathbf{e}$) are used interchangeably as convenience dictates, and the notations $(x, y, z) = (x_1, x_2, x_3)$ for Cartesian coordinates and $(u, v, w) = (u_1, u_2, u_3)$ for the corresponding velocity components are equivalent. Unit vectors are denoted by symbols $\mathbf{e}_x$, $\mathbf{e}_r$, etc. Partial derivatives are denoted either by subscripts or by the symbol ∂, and $\partial_i = \partial/\partial x_i$. Thus, for example,

$$T_x = \partial_x T = \partial_1 T = \frac{\partial T}{\partial x} = \frac{\partial T}{\partial x_1} \qquad [1]$$

The symbols $\Re[\ldots]$ and $\Im[\ldots]$ denote the real and imaginary parts, respectively, of the bracketed quantities. Frequently used abbreviations are listed in **Table 1**.

7.04.2 Formulating Geodynamical Model Problems: Three Case Studies

Ideally, a geodynamical model should respect two distinct criteria: it should be sufficiently simple that the essential physics it embodies can be easily understood, yet sufficiently complex and realistic that it can be used to draw inferences about the Earth. It is seldom easy to satisfy both these desiderata in a single model; and so most geophysicists tend to emphasize one or the other, according to temperament and education.

However, there is a way around this dilemma: to investigate not just a single model, but rather a hierarchical series of models of gradually increasing complexity and realism. Such an investigation – whether carried out by one individual or by many – is a cumulative one in which the initial study of a highly simplified model provides the physical understanding required to guide the formulation and investigation of more complex models. To show how this process works in practice, I have chosen three exemplary geophysical phenomena as case studies: heat transfer from mantle diapirs; buoyant instability of thermal boundary layers (TBLs); and the interaction of mantle plumes with the lithosphere. Mathematical detail and bibliographical references are kept to a minimum in order to focus on the conceptual structure of the hierarchical approach.

7.04.2.1 Heat Transfer from Mantle Diapirs

Our first example is the ascent of a hot blob or diapir of magma through the lithosphere, a possible mechanism for the formation of island-arc volcanoes (Marsh and Carmichael, 1974; Marsh, 1978). To evaluate this model, one needs to know how far the diapir can move through the colder surrounding material before losing so much of its excess heat that it solidifies. **Figure 1** illustrates a series of model problems that can be used to investigate this question.

Probably the simplest model that still retains much of the essential physics (Marsh, 1978) can be formulated by assuming that (1) the diapir is spherical and has a constant radius; (2) the diapir's interior temperature is uniform and (3) does not vary with time; (4) the ascent speed and (5) the temperature of the lithosphere far from the diapir are constants; (6) the lithosphere is a uniform viscous fluid with constant physical properties; and (7) the viscosity of the diapir is much less than that of the lithosphere. The result is the model shown in **Figure 1(a)**, in which an effectively inviscid fluid sphere with radius a and temperature ΔT moves at constant speed U through a fluid with constant density ρ, thermal diffusivity κ, and viscosity ν, and constant temperature $T = 0$ far from the sphere. An analytical solution for the rate of heat transfer q from the diapir (Section 7.04.7.1.2) can now be obtained if one makes the additional (and realistic) assumption (8) that the Peclet number $Pe \equiv Ua/\kappa \gg 1$, in which case the temperature variations around the leading hemisphere of the diapir are confined to a thin BL of

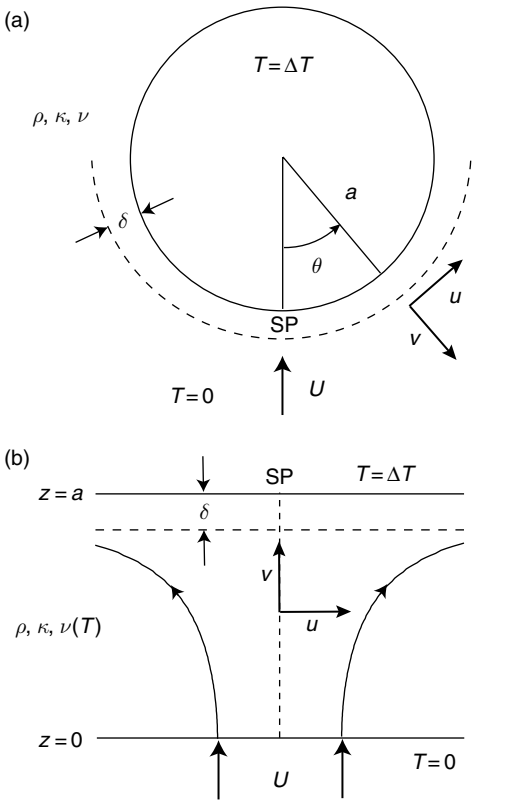

Figure 1 Models for the heat transfer from an ascending magma diapir. (a) Original model in spherical geometry. A sphere of radius a and constant temperature ΔT is immersed in an infinite fluid with density ρ, kinematic viscosity ν, and thermal diffusivity κ. The fluid far from the sphere moves with a constant streaming speed U, and its temperature is zero. The colatitude measured from the upstream stagnation point (SP) is θ, and the components of the velocity in the colatitudinal and radial directions are u and v, respectively. In the limit $Ua/\kappa \gg 1$, temperature variations in the hemisphere $\theta \leq \pi/2$ are confined to a boundary layer of thickness $\delta \ll a$. The viscosity ν may be constant (Marsh, 1978) or temperature-dependent (Morris, 1982). (b) Modified stagnation-point flow model of Morris (1982). The surface of the hot sphere is replaced by the plane $z = a$, and the steady streaming velocity U is imposed as a boundary condition at $z = 0$.

thickness $\delta \ll a$ (**Figure 1(a)**). One thereby finds (see Section 7.04.3.3 for the derivation)

$$q \sim k_c a \Delta T Pe^{1/2} \qquad [2]$$

where k_c is the thermal conductivity.

While the model just described provides a first estimate of how the heat transfer scales with the ascent speed and the radius and excess temperature of the diapir, it is far too simple for direct application to the Earth. A more realistic model can be obtained by relaxing assumptions (3) and (5), allowing the temperatures of the diapir and the ambient lithosphere to vary with

time. If these variations are slow enough, the heat transfer at each instant will be described by a law of the form [2], but with a time-dependent excess temperature $\Delta T(t)$. A model of this type was proposed by Marsh (1978), who obtained a solution in the form of a convolution integral for the evolving temperature of a diapir ascending through a lithosphere with a prescribed far-field temperature $T_{\text{lith}}(t)$.

A different extension of the simple model of **Figure 1(a)**, also suggested by Marsh (1978), begins from the observation that the viscosity of mantle materials decreases strongly with increasing temperature. A hot diapir will therefore be surrounded by a thin halo of softened lithosphere, which will act as a lubricant and increase the diapir's ascent speed. The effectiveness of this mechanism depends on whether the halo is thick enough, and/or has a viscosity low enough, to carry a substantial fraction of the volume flux $\sim\pi a^2 U$ that the sphere must displace in order to move. Formally, this model is obtained by replacing the constant viscosity ν in **figure 1(a)** by one that depends exponentially on temperature as $\nu = \nu_0 \exp(-T/\Delta T_r)$.

While this new variable-viscosity model is more realistic and dynamically richer than the original model, its spherical geometry makes analytical solution impossible except in certain limiting cases (Morris, 1982; Ansari and Morris, 1985). However, closer examination reveals that the spherical geometry is not in fact essential: all that matters is that the flow outside the softened halo varies over a characteristic length scale a that greatly exceeds the halo thickness. This recognition led Morris (1982) to study a simpler model in which the flow around the sphere is replaced by a stagnation-point flow between two planar boundaries $z = 0$ and $z = a$ (**Figure 1(b)**). The model equations now admit 1-D solutions $T = T(z)$ and $\nu = \nu(z)$ for the temperature and the vertical velocity, respectively, which can be determined using the method of matched asymptotic expansions (MMAE) (Section 7.04.7.2) in the limit of large viscosity contrast $\Delta T/\Delta T_r \gg 1$ (Morris, 1982).

7.04.2.2 Plume Formation in TBLs

Our second example (**Figure 2**) is the formation of plumes via the gravitational instability of a horizontal TBL. The first step in formulating a model for this process is to choose a simple representation for the relevant physical properties (density, viscosity, and thermal diffusivity) of the fluid. Because these depend on pressure, temperature, and (possibly) chemical composition, they will vary continuously with depth in the

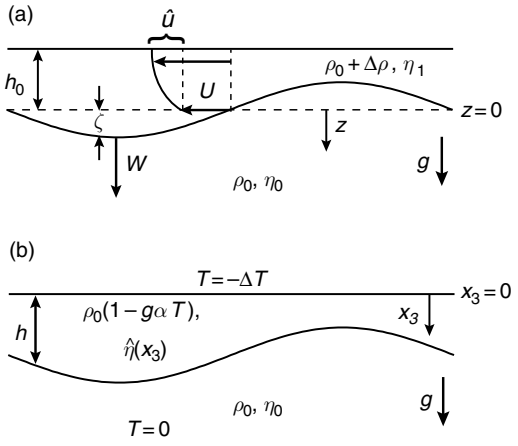

Figure 2 Models for plume formation in a dense/cold thermal boundary layer. (a) Rayleigh–Taylor instability of a layer of fluid with density $\rho_0 + \Delta\rho$ and viscosity η_1 above a half-space of fluid with density ρ_0 and viscosity η_0. The initial thickness of the dense layer is h_0, and the deformation of the interface is ζ. The maximum values of the horizontal and vertical velocities at the interface $z = \zeta$ are U and W, respectively, and $\hat{u}$ is the magnitude of the change in horizontal velocity across the layer. (b) Buoyant instability of a cold thermal boundary layer. The upper surface $x_3 = 0$ of a fluid half-space is held at a fixed temperature $-\Delta T$ relative to the interior. The density of the fluid varies with temperature as $\rho = \rho_0(1 - g\alpha T)$, where α is the thermal expansion coefficient. The thickness of the boundary layer is $h(x_1, x_2, t)$ and the viscosity within it is $\hat{\eta}(x_3)$.

TBL and with time (due to thermal diffusion). As a first approximation, however, one can model the depth distribution of the fluid properties as a nondiffusing and spatially discontinuous two-fluid configuration in which a dense layer with constant thickness h_0, density $\rho_0 + \Delta\rho$, and viscosity η_1 overlies a half-space with density ρ_0 and viscosity η_0 (**Figure 2(a)**). The case of a less-dense BL beneath a denser fluid is obtained by turning the system upside down and switching the sign of $\Delta\rho$. Because both configurations are gravitationally unstable, any small perturbation of the interface between the two fluids will grow with time via the Rayleigh–Taylor (R–T) instability. The growth rate of an infinitesimal sinusoidal perturbation with arbitrary wave number k can be determined analytically (Selig, 1965; Whitehead and Luther, 1975) via a standard linear stability analysis (Section 7.04.9.1).

While the simple RT model embodies some of the essential physics of plume formation, it is unable to describe such crucial features as the characteristic periodicity of TBL instabilities (Howard, 1964). For this purpose, a more realistic model that incorporates a diffusing temperature field is required. **Figure 2(b)** shows such a model (Canright, 1987; Lemery *et al.*,

2000), in which a diffusive TBL grows away from a cold surface and subsequently becomes unstable. The density of the fluid varies linearly with temperature, and the viscosity $\hat{\eta}$ can vary as a function of the depth x_3 within the TBL. The additional assumptions that the wavelength of the instability greatly exceeds the thickness of the TBL and that the horizontal components of the fluid velocity are constant across it then permit an analytical reduction of the full 3-D equations to an equivalent set of 2-D equations for the horizontal velocities and the first moment of the temperature in the TBL (Section 7.04.8.3).

7.04.2.3 Plume–Lithosphere Interaction

PLI refers to the processes that occur after a rising mantle plume strikes the base of the lithosphere. Because the plume fluid is buoyant relative to its surroundings, it will spread beneath the lithosphere, eventually forming a thin layer or pancake whose lateral dimensions greatly exceed its thickness.

Figure 3 shows a series of fluid dynamical models that have been used to study PLI, beginning with the kinematic model of Sleep (1987) (**Figure 3(a)**). Sleep's insight was that the flow associated with a plume rising beneath a moving plate can be regarded as the sum of two parts: a (horizontal) radial flow representing buoyant plume fluid emanating from a steady localized source at the top of the plume conduit; and an ambient mantle wind in the direction of the plate motion. Fluid from the source can travel only a finite distance upstream against the wind before being blown back downstream again, leading to the formation of a stagnation point (labeled SP in **Figure 3(a)**) at which the wind speed just equals the speed of radial outflow from the source. The stagnation streamline that passes through this point (heavy line in **Figure 3(a)**) divides the (x, y) plane into an inner region containing fluid from the source, and an outer region containing fluid brought in from upstream by the wind. The stagnation streamline resembles the shape of the topographic swell around the Hawaiian island chain (Richards *et al.*, 1988).

While the kinematic model of Sleep (1987) nicely illustrates the geometry of PRI, it neglects the (driving) buoyancy force and (resisting) viscous force that control the spreading of the plume pancake. We now seek the simplest possible model that embodies these dynamics. Following the logic of Section 7.04.2.2, we replace the continuous variation of fluid properties by a two-fluid structure, comprising a pancake with constant viscosity η spreading in an ambient fluid with viscosity η_m. We further assume that η_m/η is not too large, so that the influence of the ambient mantle on the spreading of the plume pancake can be neglected. Another simplifying assumption (to be relaxed later) is that the plate does not move with respect to the source of plume fluid. Finally, we suppose that the strength of the source is constant. The result is the viscous gravity current model (Huppert, 1982), wherein

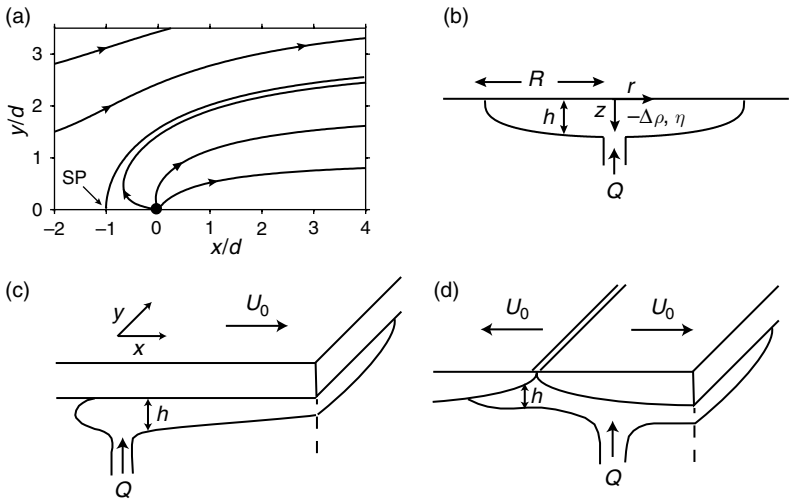

Figure 3 Hierarchy of models for plume–lithosphere interaction. (a) Steady streamlines for the 2-D kinematic model of Sleep (1987). The source is indicated by the black circle, the heavy solid line is the stagnation streamline, and d is the distance between the source and the stagnation point SP. (b) Spreading beneath a rigid surface of an axisymmetric current of viscous fluid with viscosity η and anomalous density $-\Delta\rho$, supplied at a volumetric rate Q. (c) Same as (b), but beneath a rigid plate moving at speed U_0. (d) Same as (c), but beneath two plates separated by a spreading ridge with half-spreading rate U_0.

fluid with viscosity η and anomalous density $-\Delta\rho$ relative to its surroundings is supplied at a constant volumetric rate Q and spreads beneath a stationary rigid surface (**Figure 3(b)**). The analytical solution for the closely related problem of a current with constant volume V is discussed in Section 7.04.8.1.

The next step is to generalize the gravity current model by allowing the plate to move with a constant velocity U_0 relative to the source (Olson, 1990). The resulting refracted plume model (**Figure 3(c)**) is in essence a dynamically self-consistent extension of the 2-D kinematic model of Sleep (1987), and is discussed further in Section 7.04.8.2.

As a final illustration, **Figure 3(d)** shows a further extension of the refracted plume model in which the uniform plate is replaced by two plates separated by a spreading ridge. Despite the increased complexity of this plume–ridge interaction model, analytical methods can still profitably be applied to it (Ribe *et al.*, 1995).

7.04.3 Dimensional and Scaling Analysis

The goal of studying model problems in fluid mechanics is typically to determine functional relations, or scaling laws, that obtain between certain parameters of interest and the various other parameters on which they depend. Two simple yet powerful methods that can be used for this purpose are dimensional analysis and scaling analysis.

7.04.3.1 Buckingham's Π-Theorem and Dynamical Similarity

Dimensional analysis begins from the principle that the validity of physical laws cannot depend on the units in which they are expressed. An important consequence of this principle is the Π-theorem of Buckingham (1914).

Suppose that there exists a (generally unknown) functional relationship among N-dimensional parameters $P_1\ P_2, \ldots, P_N$, such that

$$f_1(P_1,\ P_2, \ldots,\ P_N) = 0 \qquad [3]$$

Let $M < N$ be the number of the parameters P_n which have independent physical dimensions (note that a dimensionally consistent functional relationship among the parameters P_n is impossible if $M = N$). In most (but not all!) cases, M is just the number of independent units that enter into the problem, for example, $M = 3$ for mechanical problems involving units of m, kg, and s and $M = 4$ for thermomechanical problems involving temperature (units K) in addition. The Π-theorem states that the functional relationship [3] is equivalent to a relation of the form

$$f_2(\Pi_1,\ \Pi_2, \ldots,\ \Pi_{N-M}) = 0 \qquad [4]$$

where $\Pi_1,\ \Pi_2, \ldots,\ \Pi_{N-M}$ are $N-M$ independent dimensionless combinations (or groups) of the dimensional parameters P_n. The fact that all systems of units (SI, cgs, etc.) are equivalent requires that each dimensionless group Π_i be a product of powers of the dimensional parameters P_n; no other functional form preserves the value of the dimensionless group when the system of units is changed. The function f_2, by contrast, can have any form. While the total number of independent groups Π_i is fixed ($\equiv N-M$), the definitions of the individual groups are arbitrary and can be chosen as convenient. A more detailed discussion and proof of the Π-theorem can be found in Barenblatt (1996, chapter 1).

The Π-theorem is the basis for the concept of dynamical similarity, according to which two physical systems behave similarly (i.e., proportionally) if they have the same values of the dimensionless groups Π_i that define them. The crucial point is that two systems may have identical values of Π_i even though they are of very different size, that is, even if the values of the dimensional parameters P_n are very different. Dynamical similarity is thus a natural generalization of the concept of geometrical similarity, whereby, for example, two triangles of different sizes are similar if they have the same values of the dimensionless parameters (angles and ratios of sides) that define them. Geometrical similarity is a necessary, but not a sufficient, condition for dynamical similarity.

The importance of dynamical similarity for physical modeling is that it allows results obtained in the laboratory or on a computer to be applied to another system with very different scales of length, time, etc. Its power derives from the fact that the function f_2 in [4] has M fewer arguments than the original function f_1. Thus, an experimentalist or numerical analyst who seeks to determine how a target dimensional parameter P_1 depends on the other $N-1$ parameters need not vary all of the latter individually; it suffices to vary only $N-M-1$ dimensionless parameters. Consequently, if the variation of a given dimensional parameter requires $\approx$10 samplings, then use of the Π-theorem reduces the effort involved in searching

the parameter space by a factor $\approx 10^M$ (Barenblatt, 1996; see also Chapter 7.02) By the same token, the Π-theorem makes possible a far more economical representation of experimental or numerical data. As an example, suppose that we have $N = 5$ dimensional parameters P_1–P_5 from which $N - M = 2$ independent dimensionless groups Π_1 and Π_2 can be formed. To represent our data without the help of the Π-theorem, we would need many shelves (one for each value of P_5), each containing many books (one for each value of P_4), each containing many pages (one for each value of P_3), each containing a plot of P_2 versus P_1. By using the Π-theorem, however, we can collapse the whole library onto a single plot of Π_2 versus Π_1.

As a simple illustration of the Π-theorem, consider again the model for heat transfer from a hot sphere (**Figure 1(a)**). Suppose that we wish to determine the radial temperature gradient β (proportional to the local conductive heat flux) as a function of position on the sphere's surface. A list of all the relevant parameters includes the following eight (units in parentheses): $\beta(\mathrm{K\,m^{-1}})$, $a(\mathrm{m})$, $U(\mathrm{m\,s^{-1}})$, $\rho(\mathrm{kg\,m^{-3}})$, $\nu(\mathrm{m^2\,s^{-1}})$, $\kappa(\mathrm{m^2\,s^{-1}})$, $\Delta T(\mathrm{K})$, and θ (dimensionless). However, ρ can be eliminated immediately because it is the only parameter that involves units of mass: no dimensionless group containing it can be defined. The remaining parameters are $N = 7$ in number, $M = 3$ of which (e.g., a, ΔT, and U) have independent units, so $N - M = 4$ independent dimensionless groups can be formed. It is usually good practice to start by defining a single group containing the target parameter (β here.) While inspection usually suffices, one can also proceed more formally by writing the group (Π_1 say) as a product of the desired parameter (β) and unknown powers of any set of M parameters with independent dimensions, for example, $\Pi_1 = \beta a^{n_1} \Delta T^{n_2} U^{n_3}$. The requirement that Π_1 be dimensionless then implies $n_1 = 1$, $n_2 = -1$, and $n_3 = 0$. Additional groups are then obtained by applying the same procedure to the remaining dimensional parameters in the list (κ and ν in this case.) Finally, any remaining parameters in the list that are already dimensionless (θ in this case) can be used as groups by themselves. For the hot sphere, the result is

$$\frac{\beta a}{\Delta T} = \mathrm{fct}\left(\frac{Ua}{\kappa},\ \frac{Ua}{\nu},\ \theta\right) \qquad [5]$$

where fct is an unknown function. The groups $Ua/\kappa \equiv Pe$, $Ua/\kappa \equiv Re$, and $\beta a/\Delta T \equiv \mathcal{N}$ are traditionally called the Peclet number, the Reynolds number, and the (local) Nusselt number, respectively (the last to be distinguished from the global Nusselt number $Nu \equiv \int_s \mathcal{N}\ \mathrm{d}S$ that measures the total heat flux across the sphere's surface S.) As we remarked earlier, the definitions of the dimensionless groups in a relation like [5] are not unique. Thus one can replace any group by the product of itself and arbitrary powers of the other groups, for example, Pe in [5] by the Prandtl number $\nu/\kappa \equiv Pe/Re$. Furthermore, it often (but not always!) happens that the target parameter ceases to depend on a dimensionless group whose value is very large or very small. For example, in a very viscous fluid such as the mantle, $Re << 1$ because inertia is negligible, and so Re no longer appears as an argument in [5].

7.04.3.2 Nondimensionalization

When the equations governing the dynamics of the problem at hand are known, another method of dimensional analysis becomes available: nondimensionalization. We illustrate this using the same example of a hot sphere.

The first step is to write down the governing equations, together with all the relevant initial and boundary conditions. Because the problem is both steady and axisymmetric, the dependent variables are the temperature $T(r, \theta)$ and the velocity $\mathbf{u}(r, \theta)$, where r and θ are the usual spherical coordinates. If viscous dissipation is negligible, the governing equations and boundary conditions are (*see* Chapter 7.06)

$$\begin{gathered}\nabla \cdot \mathbf{u} = 0, \quad \mathbf{u} \cdot \nabla T = \kappa \nabla^2 T, \\ \mathbf{u} \cdot \nabla \mathbf{u} = -\rho^{-1} \nabla p + \nu \nabla^2 \mathbf{u}\end{gathered} \qquad [6a]$$

$$\begin{aligned}T(a,\ \theta) - \Delta T = T(\infty,\ \theta) &= \mathbf{u}(a,\ \theta) \\ &= \mathbf{u}(\infty,\ \theta) - U\mathbf{e}_z = 0\end{aligned} \qquad [6b]$$

where $\mathbf{e}_z$ is a unit vector in the direction of the steady stream far from the sphere. The next step is to define dimensionless variables (denoted, e.g., by primes) using scales that appear in the equations and/or initial and boundary conditions. An obvious (but not unique) choice is $r' = r/a$, $T' = T/\Delta T$, $\mathbf{u}' = \mathbf{u}/U$, and $p' = a(p - p_0)/\rho\nu U$, where p_0 is the (dynamically insignificant) pressure far from the sphere. Substituting these definitions into [6] and immediately dropping the primes to avoid notational overload, we obtain the dimensionless BVP:

$$\begin{gathered}\nabla \cdot \mathbf{u} = 0, \quad Pe\,\mathbf{u} \cdot \nabla T = \nabla^2 T, \\ Re\,\mathbf{u} \cdot \nabla \mathbf{u} = -\nabla p + \nabla^2 \mathbf{u}\end{gathered} \qquad [7a]$$

$$T(1, \theta) - 1 = T(\infty, \theta) = \mathbf{u}(1, \theta) = \mathbf{u}(\infty, \theta) - \mathbf{e}_z = 0 \qquad [7b]$$

where Pe and Re are the Peclet and Reynolds numbers defined in Section 7.04.3.1. Now because these are the only dimensionless parameters appearing in [7a] and [7b], the dimensionless temperature must have the form $T = T(r, \theta, Pe, Re)$. Differentiating this with respect to r and evaluating the result on the surface $r = 1$ to obtain the quantity $\beta a/\Delta T$, we find the same result [5] as we did using the Π-theorem.

Whether one chooses to do dimensional analysis using the Π-theorem or nondimensionalization depends on the problem at hand. The Π-theorem is of course the only choice if the governing equations are not known, but its effective use then requires a good intuition of what the relevant physical parameters are. When the governing equations are known, nondimensionalization is usually the best choice, as the relevant physical parameters appear explicitly in the equations and initial/boundary conditions.

7.04.3.3 Scaling Analysis

Except when $N - M = 1$, dimensional analysis yields a relation involving an unknown function of one or more dimensionless arguments. To determine the functional dependence itself, methods that go beyond dimensional analysis are required. The most detailed information is provided by a full analytical or numerical solution of the problem, but finding such solutions is rarely easy. Scaling analysis is a powerful intermediate method that provides more information than dimensional analysis while avoiding the labor of a complete solution. It proceeds by estimating the orders of magnitude of the different terms in a set of governing equations, using both known and unknown quantities, and then exploiting the fact that the terms must balance (the definition of an equation!) to determine how the unknown quantities depend on the known.

To illustrate this, we consider once again the problem of determining the local Nusselt number $\mathcal{N}$ for the hot sphere, but now in the specific limit $Re \ll 1$ and $Pe \gg 1$. Recall that Re measures the ratio of advection to diffusion of gradients in velocity (≡vorticity), while Pe does the same for gradients in temperature. In the limit $Re \ll 1$, advection of velocity gradients is negligible relative to diffusion everywhere in the flow field, and $\mathbf{u}$ is given by the classic Stokes–Hadamard solution for slow viscous flow around a sphere of another fluid (Section 7.04.5.3.2). When $Pe \gg 1$, temperature gradients are transported by advection with negligible diffusion everywhere except in a thin TBL of thickness $\delta(\theta) \ll a$ around the leading hemisphere where advection and diffusion are of the same order. Because radial temperature gradients greatly exceed surface-tangential gradients within this layer, the temperature distribution there is described by the simplified BL forms of the continuity and energy equations (cf. Section 7.04.7)

$$a \sin\theta v_r + (u \sin\theta)_\theta = 0 \qquad [8a]$$

$$a^{-1} u T_\theta + v T_r = \kappa T_{rr} \qquad [8b]$$

where $u(r, \theta)$ and $v(r, \theta)$ are the tangential (θ) and radial (r) components of the velocity, respectively, and subscripts indicate partial derivatives. Equations [8] are obtained from [145] by setting $x = a\theta$ and $r = a \sin\theta$.

We begin by determining the relative magnitudes of the velocity components u and v in the BL. While these can be found directly from the Stokes–Hadamard solution, it is more instructive to do a scaling analysis of the continuity equation [8a]. Now $v_r \sim \Delta v/\delta$, where Δv is the change in v across the BL; but because $v(a, \theta) = 0$, $\Delta v = v$. Similarly, $u_\theta \sim \Delta u/\Delta\theta$, where Δu is the change in u over an angle $\Delta\theta$ of order unity from the forward stagnation point $\theta = 0$ toward the equator $\theta = \pi/2$. But because $u(r, 0) = 0$, $\Delta u = u$. The continuity equation therefore implies

$$v \sim (\delta/a) u \qquad [9]$$

We turn now to the left-hand side (LHS) of the energy equation [8b], whose two terms represent advection of temperature gradients in the tangential and radial directions, respectively. Now the radial temperature gradient $T_r \sim \Delta T/\delta$ greatly exceeds the tangential gradient $a^{-1} T_\theta \sim \Delta T/a$, but this difference is compensated by the smallness of the radial velocity $v \sim (\delta/a)u$, and so the terms representing tangential and radial advection are of the same order. The balance of advection and diffusion in the BL is therefore $a^{-1} u T_\theta \sim \kappa T_{rr}$, which together with $T_{rr} \sim \Delta T/\delta^2$ implies

$$\delta^2 \sim \kappa a/u \qquad [10]$$

It remains only to determine an expression for u, which depends on the ratio γ of the viscosity of the sphere to that of the surrounding fluid. We consider the limiting cases $\gamma \ll 1$ (a traction-free sphere) and $\gamma \gg 1$ (an effectively rigid sphere). Because the fluid outside the sphere has constant viscosity, $\mathbf{u}$ varies smoothly over a length scale $\sim a$. Within the TBL,

therefore, **u** can be approximated by the first term of its Taylor series expansion in the radial distance $r - a \equiv \zeta$ away from the sphere's surface. If the sphere is traction free, $u_\zeta|_{\zeta=0} = 0$, implying that $u \sim U$ is constant across the TBL to lowest order. If however the sphere is rigid, $u|_{\zeta=0} = 0$ and $u \sim (\zeta/a)U$. The tangential velocity u at the outer edge $\zeta \sim \delta$ of the TBL is therefore

$$u \sim (\delta/a)^n U \qquad [11]$$

where $n = 0$ for a traction-free sphere and $n = 1$ for a rigid sphere. Substituting [11] into [10] and noting that $\mathcal{N} \sim a/\delta$, we obtain

$$\mathcal{N} \sim Pe^{1/(n+2)} f_n(\theta) \qquad [12]$$

where $f_n(\theta)$ ($n = 1$ or 2) are unknown functions. Thus when $Pe \gg 1$, $\mathcal{N} \sim Pe^{1/2}$ if the sphere is traction-free and $\mathcal{N} \sim Pe^{1/3}$ if it is rigid. $\mathcal{N}$ is greater in the former case because the tangential velocity u, which carries the heat away from the sphere, is $\sim U$ across the whole TBL.

7.04.4 Self-Similarity and Intermediate Asymptotics

In geophysics and in fluid dynamics more generally, one often encounters functions that exhibit the property of scale-invariance or self-similarity. As an illustration, consider a function $f(y, t)$ of two arbitrary variables y and t. The function f is self-similar if it has the form

$$f(y, t) = G(t) F\left(\frac{y}{\delta(t)}\right) \qquad [13]$$

where F, G, and δ are arbitrary functions and $\eta \equiv y/\delta(t)$ is the similarity variable. Self-similarity simply means that curves of f versus y for different values of t can be obtained from a single universal curve $F(\eta)$ by stretching its abscissa and ordinate by factors $\delta(t)$ and $G(t)$, respectively.

Self-similarity is closely connected with the concept of intermediate asympotics (Barenblatt, 1996). In many physical situations, one is interested in the behavior of a system at intermediate times, long after it has become insensitive to the details of the initial conditions but long before it reaches a final equilibrium state. The behavior of the system at these intermediate times is often self-similar, as we now illustrate using a simple example of conductive heat transfer (Barenblatt, 1996, Section 7.04.2.1).

7.04.4.1 Conductive Heat Transfer

Consider the 1-D conductive heat transfer in a rod $y \in [0, L]$ in which the initial temperature is zero everywhere except in a heated segment of length h centered at $y = y_0$ (**Figure 4**). The width of the heated segment is much smaller than the distance to either end of the rod, and the segment is much closer to the left end than to the right end, that is, $h \ll y_0$ and $y_0 \ll L - y_0$. The ends of the rod are held at zero temperature, and its sides are insulated.

The equation and initial/boundary conditions governing the temperature $T(y, t)$ in the rod are

$$T_t = \kappa T_{yy} \qquad [14a]$$

$$T(y, 0) = T_0(y), \quad T(0, t) = T(L, t) = 0 \qquad [14b]$$

where $T_0(y)$ is the concentrated initial temperature distribution. While it is relatively easy to solve [14a] and [14b] numerically for an arbitrary initial temperature $T_0(y)$, such an approach would not reveal the essential fact that the solution has two distinct intermediate asymptotic, self-similar stages. The first obtains long after the temperature distribution has forgotten the details of the initial distribution $T_0(y)$, but long before it feels the influence of the left boundary condition $T(0, t) = 0$, that is, for (roughly) $0.1h^2/\kappa \ll t \ll 0.1y_0^2/\kappa$. In this time range, the rod appears effectively infinite, and the integrated temperature anomaly

$$Q = \int_{-\infty}^{\infty} T(y, t)\mathrm{d}y \qquad [15]$$

is constant. The temperature T can depend only on Q, κ, t, and $y - y_0$, and only three of these five parameters have independent dimensions. Applying the Π-theorem with $N = 5$ and $M = 3$, we find

$$T = \frac{Q}{(\kappa t)^{1/2}} F_1(\eta), \quad \eta = \frac{y - y_0}{(\kappa t)^{1/2}} \qquad [16]$$

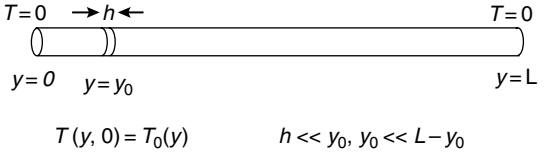

Figure 4 Model for 1-D conductive heat transfer in a rod $y \in [0, L]$ in which the initial temperature is zero everywhere except in a heated segment of length h centered at $y = y_0$. The width of the heated segment is much smaller than the distance to either end of the rod, and the segment is much closer to the left end than to the right end. Both ends of the rod are held at zero temperature, and its sides are insulated.

which is of the general self-similar form [13]. Substituting [16] into [14a] and [15], we find that F_1 satisfies

$$2F_1'' + \eta F_1' + F_1 = 0, \qquad \int_{-\infty}^{\infty} F_1 \, \mathrm{d}\eta = 1 \qquad [17]$$

Upon solving [17] subject to $F_1(\pm\infty) = 0$, [16] becomes

$$T = \frac{Q}{2\sqrt{\pi\kappa t}} \exp\left[-\frac{(y-y_0)^2}{4\kappa t}\right] \qquad [18]$$

The second intermediate asymptotic stage occurs long after the temperature distribution has begun to be influenced by the left boundary condition $T(0, t) = 0$, but long before the influence of the right boundary condition $T(L, t) = 0$ is felt, or $y_0^2/\kappa \ll t \ll 0.1(L - y_0)^2/\kappa$. During this time interval, the rod is effectively semi-infinite, and the temperature satisfies the boundary conditions

$$T(0,\ t) = T(\infty,\ t) = 0 \qquad [19]$$

The essential step in determining the similarity solution is to identify a conserved quantity. Multiplying [14a] by y, integrating from $y = 0$ to $y = \infty$, and then taking the time derivative outside the integral sign, we obtain

$$\frac{\mathrm{d}}{\mathrm{d}t} \int_0^{\infty} yT \, \mathrm{d}y = \kappa \int_0^{\infty} yT_{yy} \mathrm{d}y \qquad [20]$$

However, the RHS of [20] is zero, as can be shown by integrating by parts, applying the conditions [19], and noting that $yT_y|_{y=\infty} = 0$ because $T_y \to 0$ more rapidly (typically exponentially) than $y \to \infty$. The temperature moment

$$M = \int_0^{\infty} yT \, \mathrm{d}y \qquad [21]$$

is therefore constant; and because the initial temperature distribution is effectively a delta-function concentrated at $y = y_0$, $M = Qy_0$. Now in the time interval in question, the influence of the temperature distribution that existed at the time $\approx 0.1y_0^2/\kappa$ when the heated region first reached the near end $y = 0$ of the rod will no longer be felt. The temperature will therefore no longer depend on y_0, but only on M, κ, y, and $t - t_0$, where t_0 is the effective starting time for the second stage, to be determined later. Applying the Π-theorem as before, we find

$$T = \frac{M}{\kappa(t-t_0)} F_2(\eta), \qquad \eta = \frac{y}{\sqrt{\kappa(t-t_0)}} \qquad [22]$$

Now substitute [22] into [14a] and [21], and solve the resulting equations subject to $F_2(0) = F_2(\infty) = 0$, whereupon [22] becomes

$$T = \frac{My}{2\sqrt{\pi}[\kappa(t-t_0)]^{3/2}} \exp\left[-\frac{y^2}{4\kappa(t-t_0)}\right] \qquad [23]$$

The final step is to determine the starting time $t_0 = -y_0^2/6\kappa$ (Barenblatt, 1996, p. 74). Because $t_0 < 0$, that is, before the rod was originally heated, it represents a virtual starting time with respect to which the behavior of the second stage is self-similar.

7.04.4.2 Classification of Self-Similar Solutions

The solutions [18] and [23] are examples of what Barenblatt (1996) calls self-similar solutions of the first kind, for which dimensional analysis (in some cases supplemented by scaling analysis of the governing equations) suffices to find the similarity variable. They are distinguished from self-similar solutions of the second kind, for which the similarity variable can only be found by solving an eigenvalue problem. We will meet some examples of these below, in the sections on viscous eddies in a corner (Section 7.04.5.3.4) and the spreading of viscous gravity currents (Section 7.04.8.1).

An example of a self-similar solution that does not fit naturally into either class is the impulsive cooling of a half-space deforming in pure shear. Suppose that the half-space $y \geq 0$ has temperature $T = 0$ initially, and that at time $t = 0$ the temperature at its surface $y = 0$ is suddenly decreased by an amount ΔT. The 2-D velocity field in the half-space is $\mathbf{u} = \dot{\epsilon}(x\mathbf{e}_x - y\mathbf{e}_y)$, where $\dot{\epsilon}$ is the constant rate of extension of the surface $y = 0$ and $\mathbf{e}_x$ and $\mathbf{e}_y$ are unit vectors parallel to and normal to the surface, respectively. Given this velocity field, a temperature field $T = T(y, t)$ that is independent of the lateral coordinate x is an allowable solution of the governing advection–diffusion equation $T_t + \mathbf{u} \cdot \nabla T = \kappa \nabla^2 T$, which takes the form

$$T_t - \dot{\epsilon} y T_y = \kappa T_{yy} \qquad [24]$$

subject to the conditions $T(y, 0) = T(\infty, t) = T(0, t) + \Delta T = 0$. The limit $\dot{\epsilon} = 0$ corresponds to the classic problem of the impulsive cooling of a static half-space.

Neither dimensional analysis nor scaling analysis is sufficient to determine the similarity variable, which does not have the standard power-law monomial form. However, the solution can be found via a generalized

form of the familiar separation-of-variables procedure often used to solve PDEs such as Laplace's equation. Note first that the amplitude ΔT of the temperature in the half-space is a constant. This implies that the function $G(t)$ in the similarity transformation [13] must be independent of time, whence $T(y, t) = \Delta T F(y/\delta(t))$. Substituting this expression into [24] and bringing all terms involving $\delta(t)$ to the LHS, we obtain

$$\frac{\delta\left(\dot{\delta} + \dot{\epsilon}\delta\right)}{\kappa} = -\frac{F''}{\eta F'} \qquad [25]$$

where dots and primes denote differentiation with respect to t and $\eta \equiv y/\delta(t)$, respectively. Now the LHS of [25] is a function of t only, whereas the RHS depends on y through the similarity variable η. Equation [25] is therefore consistent only if both sides are equal to a constant λ^2, which is positive because $\dot{\delta} > 0$. The solutions for δ and F subject to the conditions $\delta(0) = F(\infty) = F(0) - 1 = 0$ are

$$F = \operatorname{erfc}\frac{\lambda y}{\sqrt{2}\delta}, \quad \delta = \lambda\left\{\frac{\kappa}{\dot{\epsilon}}[1 - \exp(-2\dot{\epsilon}t)]\right\}^{1/2} \qquad [26]$$

Evidently λ cancels out when the solution for δ is substituted into the solution for F, because different values of λ merely correspond to different (arbitrary) definitions of the thermal layer thickness δ. With $\dot{\epsilon} = 0$ and the conventional choice $\lambda = \sqrt{2}$, we recover the well-known solution $\delta = 2\sqrt{\kappa t}$ for a static half-space. However, when $\dot{\epsilon} > 0$, the BL thickness approaches a steady-state value $\delta = (2\kappa/\dot{\epsilon})^{1/2}$ for which the downward diffusion of temperature gradients is balanced by upward advection, and the similarity variable involves an exponential function of time. The only reliable way to find such nonstandard self-similar solutions is the separation-of-variables procedure outlined above. But the same procedure works just as well for problems with similarity variables of standard form, and therefore will be used throughout this chapter.

In conclusion, we note that similarity transformations can also be powerful tools for reducing and interpreting the output of numerical models. As a simple example, suppose that some such model yields values of a dimensionless parameter W as a function of two dimensionless groups Π_1 and Π_2. Depending on the physics of the problem, it may be possible to express the results in the self-similar form

$$W(\Pi_1,\ \Pi_2) = F_1(\Pi_1)F_2\left(\frac{\Pi_1}{F_3(\Pi_2)}\right) \qquad [27]$$

where F_1–F_3 are functions to be determined numerically. A representation of the form [27] is not guaranteed to exist, but when it does it provides a compact way of representing multidimensional numerical data by functions of a single variable that can be fit by simple analytical expressions. An example of the use of this technique for a problem involving five dimensionless groups is the lubrication theory model for plume–ridge interaction of Ribe and Delattre (1998).

7.04.4.3 Intermediate Asymptotics with Respect to Parameters: The R–T Instability

The concept of intermediate asymptotics is not limited to self-similar behavior of systems that evolve in time, but also applies in a more general way to functions of one or more parameters that exhibit simple (typically power-law) behavior in some asymptotically defined region of the parameter space. Because power-law scaling usually results from a simple dynamical balance between two competing effects, the identification of intermediate asymptotic limits that have this form is crucial for a physical understanding of the system in question.

The dynamical significance of intermediate asymptotic limits and the role that scaling arguments play in identifying them are nicely illustrated by the RT instability of a fluid layer with density $\rho_0 + \Delta\rho$, viscosity η_1, and thickness h_0 above a fluid half-space with density ρ_0 and viscosity η_0 (**Figure 2(a)**). The following discussion is adapted from Canright and Morris (1993).

Linear stability analysis of this problem (cf. Section 7.04.9.1) shows that an infinitesimal sinusoidal perturbation $\zeta = \zeta_0 \sin kx$ of the initially flat interface $z = 0$ in **Figure 2(a)** grows exponentially at a rate (Whitehead and Luther, 1975)

$$s = s_1\frac{\gamma}{2\epsilon}\left[\frac{\gamma(C-1) + S - 2\epsilon}{\gamma^2(S+2\epsilon) + 2\gamma C + S - 2\epsilon}\right] \qquad [28]$$

where $s_1 = g\Delta\rho h_0/\eta_1$, $\gamma = \eta_1/\eta_0$, $\epsilon = h_0 k$, $C = \cos\mathrm{h}(2\epsilon)$, and $S = \sin\mathrm{h}(2\epsilon)$. Here we shall consider only the long-wavelength limit $\epsilon \ll 1$, for which [28] reduces to

$$\frac{s}{s_1} \sim \frac{\epsilon\gamma(2\epsilon + 3\gamma)}{2(2\epsilon^3 + 3\gamma + 6\epsilon\gamma^2)} \qquad [29]$$

where the viscosity contrast γ is arbitrary.

By noting the ranges of $\gamma(\epsilon)$ for which different pairs of terms in [29] (one each in the numerator and the denominator) are dominant, one finds that [29] has four intermediate asymptotic limits: $\gamma \ll \epsilon^3$, $\epsilon^3 \ll \gamma \ll \epsilon$, $\epsilon \ll \gamma \ll \epsilon^{-1}$, and $\gamma \gg \epsilon^{-1}$. The essential

Table 2 Rayleigh–Taylor instability: intermediate asymptotic limits

Limit	γ	W/U	$\hat{u}/U$	Balancing pressure	s
1	$\ll\epsilon^3$	ϵ^2/γ	ϵ/γ	$p_0 \sim \eta_0 kW$	$\Delta\rho g/2k\eta_0$
2	$\epsilon^3 \ll \gamma \ll \epsilon$	ϵ^2/γ	ϵ/γ	$p_1 \sim \eta_1 \hat{u}/h_0^2 k \sim \eta_1 W/h_0^3 k^2$	$\Delta\rho g h_0^3 k^2/3\eta_1$
3	$\epsilon \ll \gamma \ll \epsilon^{-1}$	ϵ	ϵ/γ	$p_1 \sim \eta_1 \hat{u}/h_0^2 k \sim \eta_0 W/h_0^2 k$	$\Delta\rho g h_0^2 k/2\eta_0$
4	$\gg\epsilon^{-1}$	ϵ	ϵ^2	$p_1 \sim \eta_1 kU \sim \eta_1 W/h_0$	$\Delta\rho g h_0/4\eta_1$

dynamics associated with each are summarized in columns 3–5 of **Table 2**. Column 3 shows the ratio of the amplitudes of the vertical (W) and horizontal (U) components of the velocity at the interface (**Figure 2(a)**). As γ increases, the motion of the interface changes from dominantly vertical in limit 1 to dominantly horizontal in limits 3 and 4. The ratio of shear deformation to plug flow in the layer is measured by the ratio $\hat{u}/U$ (column 4), where $\hat{u}$ is the change in horizontal velocity across the layer (**Figure 2(a)**). The layer deforms mainly by shear in limits 1 and 2, and by plug flow in limits 3 and 4.

The growth rate is determined by whether the interfacial buoyancy $\sim g\Delta\rho\zeta_0$ is supported by the pressure p_1 in the layer or the pressure p_0 in the half-space. Column 5 of **Table 2** gives the expression for the pressure that balances the buoyancy in each limit, and column 6 shows the corresponding growth rate $s = W/\zeta_0$. While the pressures can be calculated directly from the analytical solution of the problem (Section 7.04.9.1), it is more revealing to obtain them via a scaling analysis of the horizontal component $\partial_x p = \eta\nabla^2 u$ of the momentum equation. In the half-space, the only length scale is k^{-1}, so that $\partial_x \sim \partial_z \sim k$. The continuity equation then implies $u \sim w$. The magnitude of $u \sim w$ is set by the larger of the two components of the velocity at the interface, namely, $u \sim [U, W]$, where $[\ldots]$ denotes the maximum of the enclosed quantities. Turning now to the layer, we note that the horizontal and vertical length scales are different, so that $\partial_x \sim k$ and $\partial_z \sim h_0^{-1}$. Moreover, $\nabla^2 u \sim [\hat{u}/h_0^2, k^2 U]$ is the sum of terms arising from the shear and plug flow components of u. We thereby find

$$p_1 \sim \frac{\eta_1}{h_0^2 k}\left[\hat{u},\ \epsilon^2 U\right], \quad p_0 \sim \eta_0 k[U,\ W] \qquad [30]$$

In view of the pressure scales [30] and those for W/U and $\hat{u}/U$ from **Table 2**, the essential dynamics of each of the four intermediate limits can be summarized as follows. In limit 1, the half-space feels the layer as an effectively traction-free boundary, the buoyancy is balanced by the pressure $p_0 \sim \eta_0 kW$ in the half-space, and s is controlled by the half-space viscosity η_0. In limit 2, the half-space still sees the layer as traction-free, but the pressure $p_1 \sim \eta_1 \hat{u}/h_0^2 k$ induced by shear flow in the layer is nevertheless sufficient to balance the buoyancy. Because the layer deforms mostly in shear, $\hat{u}$ is related directly to W via the continuity equation ($W \sim \epsilon\hat{u}$), so s is controlled by the layer viscosity η_1. In limit 3, each layer feels the shear stress applied by the other. While the buoyancy is still balanced by the shear-induced pressure in the layer, the dominance of plug flow means that $\hat{u}$ and W are no longer related via the continuity equation, but rather by the matching condition on the shear stress. The growth rate is therefore controlled by the half-space viscosity η_0. Finally, in limit 4 the layer feels the half-space as a traction-free boundary, the buoyancy is balanced by the pressure $p_1 \sim \eta_1 kU$ induced by plug flow in the layer, and s is controlled by the layer viscosity η_1.

7.04.5 Slow Viscous Flow

Flows with negligible inertia are fundamental in the Earth's mantle, where the Reynolds number $Re \approx 10^{-20}$. A particularly important subclass of inertialess flow – variously called slow, creeping, or low Reynolds number flow – comprises flows in which the fluid is incompressible, isothermal, and has a rheology with no memory (elasticity). These conditions, while obviously restrictive, are nevertheless sufficiently realistic to have served as a basis for many important geophysical models.

7.04.5.1 Basic Equations and Theorems

The most general equations required to describe the slow viscous flows discussed in this section are (*see* Chapter 7.06)

$$\partial_j u_j = 0 \qquad [31a]$$

$$\partial_j \sigma_{ij} + b_i = 0 \qquad [31b]$$

$$b_i = -\rho\partial_i\chi \qquad [31c]$$

$$\nabla^2\chi = 4\pi G\rho \qquad [31d]$$

$$\sigma_{ij} = -p + 2\eta e_{ij}, \quad e_{ij} = \frac{1}{2}\left(\partial_i u_j + \partial_j u_i\right) \qquad [31e]$$

$$\eta = \eta_0 (I/I_0)^{-1+1/n}, \quad I = \left(e_{ij}e_{ij}\right)^{1/2} \qquad [31f]$$

where u_i is the velocity vector, σ_{ij} is the stress tensor, b_i is the gravitational body force per unit volume, χ is the gravitational potential, ρ is the density, p is the pressure, η is the viscosity, and e_{ij} is the strain-rate tensor with second invariant I. Equation [31a] is the incompressibility condition. Equation [31b] expresses conservation of momentum in the absence of inertia, and states that the net force (viscous plus gravitational) acting on each fluid element is zero. Equation [31d] is Poisson's equation for the gravitational potential. Equation [31e] is the standard constitutive relation for a viscous fluid. Finally, [31f] is the strain-rate-dependent viscosity for a power-law fluid (sometimes called a generalized Newtonian fluid), where η_0 is the viscosity at a reference strain rate $I = I_0$ and n is the power-law exponent. A Newtonian fluid has $n = 1$, while the rheology of dry olivine deforming by dislocation creep is well described by [31f] with $n \approx 3.5$ (Bai *et al.*, 1991). A discussion of more complicated non-Newtonian fluids is beyond the scope of this chapter; the interested reader is referred to Bird *et al.* (1987).

Viscous flow described by [31] can be driven either externally, by velocities and/or stresses imposed at the boundaries of the flow domain, or internally, by buoyancy forces (internal loads) arising from lateral variations of the density ρ. On the scale of the whole mantle, the influence of long-wavelength lateral variations of ρ on the gravitational potential χ (self-gravitation) is significant and cannot be neglected. In modeling flow on smaller scales, however, one generally ignores Poisson's equation [31d] and replaces $\nabla\chi$ in [31c] by a constant gravitational acceleration $-\mathbf{g}$.

Slow viscous flow exhibits the property of instantaneity: u_i and σ_{ij} at each instant are determined throughout the fluid solely by the distribution of forcing (internal loads and/or boundary motions) acting at that instant. Instantaneity requires that the fluid have no memory (elasticity) and that acceleration and inertia be negligible; there is then no time lag between the forcing and the fluid's response to it. A corollary is that slow viscous flow is quasi-static, any time-dependence being due entirely to the time-dependence of the forcing.

The theory of slow viscous flow is most highly developed for the special case of Newtonian fluids (Stokes flow), and several excellent monographs on the subject exist (Ladyzhenskaya, 1963; Langlois, 1964; Happel and Brenner, 1991; Kim and Karrila, 1991; Pozrikidis, 1992). Relative to general slow viscous flow, Stokes flow exhibits the important additional properties of linearity and reversibility. Linearity implies that for a given geometry, a sum of different solutions (e.g., for different forcing distributions) is also a solution. It also implies that u_i and σ_{ij} are directly proportional to the forcing that generates them, and hence for example, that the force acting on a body in Stokes flow is proportional to its speed. Reversibility refers to the fact that changing the sign of the forcing terms reverses the signs of u_i and σ_{ij} for all material particles. The reversibility principle is especially powerful when used in conjunction with symmetry arguments. It implies, for example, that a body with fore-aft symmetry falling freely in any orientation in Stokes flow experiences no torque, and that the lateral separation of two spherical diapirs with different radii is the same before and after their interaction (Manga, 1997).

An important theorem concerning Stokes flow is the 'Lorentz reciprocal theorem,' which relates two different Stokes flows (u_i, σ_{ij}, b_i) and $(u_i^*, \sigma_{ij}^*, b_i^*)$. This theorem is the starting point for the boundary-integral representation of Stokes flow derived in Section 7.04.5.6.4. Consider the scalar quantity $u_i^*\partial_j\sigma_{ij}$, which we manipulate as follows:

$$\begin{aligned} u_i^*\partial_j\sigma_{ij} &= \partial_j\left(u_i^*\sigma_{ij}\right) - \sigma_{ij}\partial_j u_i^* \\ &= \partial_j\left(u_i^*\sigma_{ij}\right) - \left(-p\delta_{ij} + 2\eta e_{ij}\right)\partial_j u_i^* \\ &= \partial_j\left(u_i^*\sigma_{ij}\right) - 2\eta e_{ij}e_{ij}^* \end{aligned} \qquad [32]$$

By subtracting from [32] the analogous expression with the starred and unstarred fields interchanged and setting $\partial_j\sigma_{ij} = -b_i$ and $\partial_j\sigma_{ij}^* = -b_i^*$, we obtain the differential form of the Lorentz reciprocal theorem:

$$\partial_j\left(u_i^*\sigma_{ij} - u_i\sigma_{ij}^*\right) = u_j b_j^* - u_j^* b_j \qquad [33]$$

An integral form of the reciprocal theorem is obtained by integrating [33] over a volume V bounded by a surface S and applying the divergence theorem, yielding

$$\int_S u_i^*\sigma_{ij}n_j\,\mathrm{d}S + \int_V b_j u_j^*\,\mathrm{d}V = \int_S u_i\sigma_{ij}^*n_j\,\mathrm{d}S + \int_V b_j^* u_j\,\mathrm{d}V \qquad [34]$$

where n_j is the outward unit normal to S.

Two additional theorems for Stokes flow concern the total rate of energy dissipation

$$E = 2\eta \int_V e_{ij} e_{ij} \mathrm{d}V \qquad [35]$$

in a volume V. The first states that the solution of the Stokes equations subject to given boundary conditions is unique, and is most easily proved by showing that the energy dissipated by the difference of two supposedly different solutions is zero (Kim and Karrila, 1991, p. 14.) The second is the minimum dissipation theorem, which states that a solution of the Stokes equations for given boundary conditions dissipates less energy than any other solenoidal vector field satisfying the same boundary conditions (Kim and Karrila, 1991, p. 15.) Note that this theorem merely compares a Stokes flow with other flows that do not satisfy the Stokes equations. It says nothing about the relative rates of dissipation of Stokes flows with different geometries and/or boundary conditions, and therefore its use as a principle of selection among such flows is not justified.

7.04.5.2 Potential Representations for Incompressible Flow

In an incompressible flow satisfying $\nabla \cdot \mathbf{u} = 0$, only $N-1$ of the velocity components u_i are independent, where $N=3$ in general and $N=2$ for 2-D and axisymmetric flows. This fact allows one to express all the velocity components in terms of derivatives of $N-1$ independent scalar potentials, thereby reducing the number of independent variables in the governing equations. The most commonly used potentials are the streamfunction ψ (for $N=2$) and the poloidal potential $\mathcal{P}$ and the toroidal potential $\mathcal{T}$ (for $N=3$). Below we give expressions for the components of $\mathbf{u}$ in terms of these potentials in Cartesian (x, y, z), cylindrical (ρ, ϕ, z), and spherical (r, θ, ϕ) coordinates, together with the PDEs they satisfy for the important special case of constant viscosity.

7.04.5.2.1 2-D and axisymmetric flows

A 2-D flow is one in which the velocity vector $\mathbf{u}$ is everywhere perpendicular to a fixed direction ($\mathbf{e}_z$ say) in space. The velocity can then be represented in terms of a streamfunction by

$$\mathbf{u} = \mathbf{e}_z \times \nabla\psi = -\mathbf{e}_x\psi_y + \mathbf{e}_y\psi_x = -\mathbf{e}_\phi\psi_\rho + \frac{\mathbf{e}_\rho}{\rho}\psi_\phi \qquad [36]$$

The PDE satisfied by ψ is obtained by applying the operator $\mathbf{e}_z \times \nabla$ to the momentum equation [31b] with the constitutive law [31e]. If the viscosity is constant and $b_i = 0$, ψ satisfies the biharmonic equation

$$\nabla_1^4\psi = 0, \quad \nabla_1^2 = \partial_{xx}^2 + \partial_{yy}^2 = \rho^{-1}\partial_\rho\left(\rho\partial_\rho\right) + \rho^{-2}\partial_{\phi\phi}^2 \qquad [37]$$

An axisymmetric flow (without swirl) is one in which $\mathbf{u}$ at any point lies in the plane containing the point and some fixed axis ($\mathbf{e}_z$, say). For this case,

$$\mathbf{u} = \frac{\mathbf{e}_\phi}{\rho} \times \nabla\psi = -\frac{\mathbf{e}_z}{\rho}\psi_\rho + \frac{\mathbf{e}_\rho}{\rho}\psi_z \qquad [38a]$$

$$\mathbf{u} = \frac{\mathbf{e}_\phi}{r\sin\theta} \times \nabla\psi = \frac{\mathbf{e}_\theta}{r\sin\theta}\psi_r - \frac{\mathbf{e}_r}{r^2\sin\theta}\psi_\theta \qquad [38b]$$

where ψ is referred to as the Stokes streamfunction. The PDE satisfied by the Stokes streamfunction is obtained by applying the operator $\mathbf{e}_\phi \times \nabla$ to the momentum equation. For a fluid with constant viscosity and no body force, the result is

$$E^4\psi = 0,$$
$$E^2 = \frac{h_3}{h_1h_2}\left[\frac{\partial}{\partial q_1}\left(\frac{h_2}{h_1h_3}\frac{\partial}{\partial q_1}\right) + \frac{\partial}{\partial q_2}\left(\frac{h_1}{h_2h_3}\frac{\partial}{\partial q_2}\right)\right] \qquad [39]$$

where (q_1, q_2) are orthogonal coordinates in any half-plane normal to $\mathbf{e}_\phi$, (h_1, h_2) are the corresponding scale factors, and h_3 is the scale factor for the azimuthal coordinate ϕ. Thus $(q_1, q_2, h_1, h_2, h_3) = (z, \rho, 1, 1, \rho)$ in cylindrical coordinates and $(q_1, q_2, h_1, h_2, h_3) = (r, \theta, 1, r, r\sin\theta)$ in spherical coordinates. The operator E^2 is in general different from the Laplacian operator

$$\nabla_1^2 = \frac{1}{h_1h_2h_3}\left[\frac{\partial}{\partial q_1}\left(\frac{h_2h_3}{h_1}\frac{\partial}{\partial q_1}\right) + \frac{\partial}{\partial q_2}\left(\frac{h_1h_3}{h_2}\frac{\partial}{\partial q_2}\right)\right] \qquad [40]$$

the two being identical only for 2-D flows ($h_3 = 1$).

7.04.5.2.2 3-D flows

The most commonly used (but not the only) potential representation of 3-D flows in geophysics is a decomposition of the velocity $\mathbf{u}$ into poloidal and toroidal components (Backus, 1958; Chandrasekhar, 1981). This representation requires the choice of a preferred direction, which is usually chosen to be an upward vertical ($\mathbf{e}_z$) or radial ($\mathbf{e}_r$) unit vector. Relative to Cartesian coordinates, the poloidal/toroidal decomposition has the form

$$\mathbf{u} = \nabla \times (\mathbf{e}_z \times \nabla\mathcal{P}) + \mathbf{e}_z \times \nabla\mathcal{T}$$
$$= \mathbf{e}_x\left(-\mathcal{P}_{xz} - \mathcal{T}_y\right) + \mathbf{e}_y\left(-\mathcal{P}_{yz} + \mathcal{T}_x\right) + \mathbf{e}_z\nabla_1^2\mathcal{P} \qquad [41]$$

where $\mathcal{P}$ is the poloidal potential and $\mathcal{T}$ is the toroidal potential. The associated vorticity $\boldsymbol{\omega} \equiv \boldsymbol{\nabla} \times \mathbf{u}$ is

$$\boldsymbol{\omega} = \mathbf{e}_x\left(\nabla^2\mathcal{P}_y - \mathcal{T}_{xz}\right) + \mathbf{e}_y\left(-\nabla^2\mathcal{P}_x - \mathcal{T}_{yz}\right) + \mathbf{e}_z\nabla_1^2\mathcal{T} \quad [42]$$

Inspection of [41] and [42] immediately reveals the fundamental distinction between the poloidal and toroidal fields: the former has no vertical vorticity, while the latter has no vertical velocity.

The PDEs satisfied by $\mathcal{P}$ and $\mathcal{T}$ are obtained by applying the operators $\boldsymbol{\nabla} \times (\mathbf{e}_z \times \boldsymbol{\nabla})$ and $\mathbf{e}_z \times \boldsymbol{\nabla}$, respectively, to the momentum equation [31b] and [31e]. Supposing that the viscosity is constant but retaining a body force $\mathbf{b} \equiv -g\delta\rho\mathbf{e}_z$ where $\delta\rho(\mathbf{x})$ is a density anomaly, we find

$$\nabla_1^2\nabla^4\mathcal{P} = \frac{g}{\eta}\nabla_1^2\delta\rho, \quad \nabla_1^2\nabla^2\mathcal{T} = 0 \quad [43]$$

Note that the equation for $\mathcal{T}$ is homogeneous, implying that flow driven by internal density anomalies in a fluid with constant viscosity is purely poloidal. The same is true in a fluid whose viscosity varies only as a function of depth, although the equations satisfied by $\mathcal{P}$ and $\mathcal{T}$ are more complicated than [43]. When the viscosity varies laterally, however, the equations for $\mathcal{P}$ and $\mathcal{T}$ are coupled, and internal density anomalies drive a toroidal flow that is slaved to the poloidal flow. Toroidal flow will also be driven by any surface boundary conditions having a nonzero vertical vorticity, even if the viscosity does not vary laterally.

Because of the Earth's spherical geometry, the spherical-coordinate form of the poloidal–toroidal representation is particularly important in geophysics. However, the definitions of $\mathcal{P}$ and $\mathcal{T}$ used by different authors sometimes differ by a sign and/or a factor of r. Following Forte and Peltier (1987)

$$\begin{aligned}\mathbf{u} &= \boldsymbol{\nabla} \times (r\mathbf{e}_r \times \boldsymbol{\nabla}\mathcal{P}) + r\mathbf{e}_r \times \boldsymbol{\nabla}\mathcal{T} \\ &= \mathbf{e}_\theta\left[-\frac{1}{r}(r\mathcal{P})_{r\theta} - \frac{\mathcal{T}_\phi}{\sin\theta}\right] + \mathbf{e}_\phi\left[-\frac{1}{r\sin\theta}(r\mathcal{P})_{r\phi} + \mathcal{T}_\theta\right] \\ &\quad + \frac{\mathbf{e}_r}{r}\mathcal{B}^2\mathcal{P}\end{aligned} \quad [44]$$

where

$$\mathcal{B}^2 = \frac{1}{\sin\theta}\frac{\partial}{\partial\theta}\sin\theta\frac{\partial}{\partial\theta} + \frac{1}{\sin^2\theta}\frac{\partial^2}{\partial\phi^2} \quad [45]$$

Another common convention is that of Chandresekhar (1981, appendix III), who uses a poloidal potential $\Phi \equiv -r\mathcal{P}$ and a toroidal potential $\Psi \equiv -r\mathcal{T}$.

Two additional quantities of interest are the lateral divergence $\boldsymbol{\nabla}_1 \cdot \mathbf{u}$ and the radial component $\mathbf{e}_r \cdot (\boldsymbol{\nabla} \times \mathbf{u})$ of the vorticity, which are

$$\boldsymbol{\nabla}_1 \cdot \mathbf{u} = -\mathcal{B}^2\left[\frac{1}{r^2}(r\mathcal{P})_r\right], \quad \mathbf{e}_r \cdot (\boldsymbol{\nabla} \times \mathbf{u}) = \frac{\mathcal{B}^2\mathcal{T}}{r} \quad [46]$$

The lateral divergence depends only on the poloidal component of the flow, whereas the radial vorticity depends only on the toroidal component. At the Earth's surface $r = a$, therefore, divergent and convergent plate boundaries (where $\boldsymbol{\nabla}_1 \cdot \mathbf{u} \neq 0$) are associated with poloidal flow, while transform faults (where $\mathbf{e}_r \cdot (\boldsymbol{\nabla} \times \mathbf{u}) \neq 0$) reflect toroidal flow.

The PDEs satisfied by $\mathcal{P}$ and $\mathcal{T}$ in a fluid of constant viscosity in spherical coordinates are obtained by applying the operators $\boldsymbol{\nabla} \times (r\mathbf{e}_r \times \boldsymbol{\nabla})$ and $r\mathbf{e}_r \times \boldsymbol{\nabla}$, respectively, to the momentum equation [31b] and [31e], yielding

$$\mathcal{B}^2\nabla^4\mathcal{P} = \frac{g}{\eta r}\mathcal{B}^2\delta\rho, \quad \mathcal{B}^2\nabla^2\mathcal{T} = 0 \quad [47]$$

Because the above equation for $\mathcal{T}$ is homogeneous, the remarks following [43] apply also to spherical geometry.

7.04.5.3 Classical Exact Solutions

The equations of slow viscous flow admit exact analytical solutions in a variety of geophysically relevant geometries. Some of the most useful of these solutions are the following:

7.04.5.3.1 Steady unidirectional flow

The simplest conceivable fluid flow is a steady unidirectional flow with a velocity $w(x, y, t)\mathbf{e}_z$, where (x, y) are Cartesian coordinates in the plane normal to $\mathbf{e}_z$. If the viscosity is constant and inertia is negligible, w satisfies (Batchelor, 1967)

$$\eta\nabla_1^2 w = -G \quad [48]$$

where $-G \equiv p_z$ is a constant pressure gradient and η is the viscosity. Two special cases are of interest in geophysics. The first is the steady Poiseuille flow through a cylindrical pipe of radius a driven by a pressure gradient $-G$, for which the velocity w and the volume flux Q are

$$w = \frac{G}{4\eta}\left(a^2 - r^2\right), \quad Q \equiv 2\pi\int_0^a rw\,\mathrm{d}r = \frac{\pi G a^4}{8\eta} \quad [49]$$

Poiseuille flow in a vertical pipe driven by an effective pressure gradient $g\Delta\rho$ has been widely used as a

model for the ascent of buoyant fluid in the conduit or tail of a mantle plume (e.g., Whitehead and Luther, 1975). The second case is that of a 2-D channel $0 \leq y \leq d$ bounded by rigid walls in which flow is driven by a combination of an applied pressure gradient $-G$ and motion of the boundary $y = d$ with speed U_0 in its own plane. For this case,

$$w = \frac{G}{2\eta} y(d-y) + \frac{U_0 y}{d} \qquad [50]$$

An example of a geodynamical application of [50] is the asthenosphere flow model of Yale and Phipps Morgan (1998).

7.04.5.3.2 Stokes–Hadamard solution for a sphere

Another classical result that is useful in geophysics is the Stokes–Hadamard solution for the flow in and around a fluid sphere with radius a and viscosity η_1 in an unbounded fluid with viscosity $\eta_0 = \eta_1/\gamma$ and velocity $U\mathbf{e}_z$ far from the sphere (Batchelor, 1967, pp. 230–238). The outer ($n = 0$) and inner ($n = 1$) streamfunctions are $\psi_n = Ua^2 \sin^2\theta f_n(r)$, where

$$f_0 = \frac{(2+3\gamma)\hat{r} - \gamma\hat{r}^{-1} - 2(1+\gamma)\hat{r}^2}{4(1+\gamma)}, \quad f_1 = \frac{\hat{r}^2 - \hat{r}^4}{4(1+\gamma)} \qquad [51]$$

and $\hat{r} = r/a$. The drag on the sphere is

$$\mathbf{F} = 4\pi\alpha\eta_0 U \frac{1+3\gamma/2}{1+\gamma}\mathbf{e}_z \qquad [52]$$

If the densities of the two fluids differ such that $\rho_1 = \rho_0 + \Delta\rho$, the steady velocity $\mathbf{V}$ of the sphere as it moves freely under gravity is obtained by equating $\mathbf{F}$ to the Archimedean buoyancy force, yielding

$$\mathbf{V} = \frac{a^2 \mathbf{g}\Delta\rho}{3\eta_0} \frac{1+\gamma}{1+3\gamma/2} \qquad [53]$$

where $\mathbf{g}$ is the gravitational acceleration. The speed of an effectively inviscid sphere ($\gamma = 0$) is only 50% greater than that of a rigid sphere ($\gamma \to \infty$). Equation [53] has been widely used to estimate the ascent speed of plume heads (e.g., Whitehead and Luther, 1975) and isolated thermals (e.g., Griffiths, 1986) in the mantle.

7.04.5.3.3 Models for subduction zones and ridges

Two-dimensional viscous flow in a fluid wedge driven by motion of the boundaries (corner flow) has been widely used to model mantle flow in subduction zones and beneath mid-ocean ridges. **Figures 5(a)** and **5(b)** show the geometry of the simplest corner-flow models of these features, due respectively to McKenzie (1969) and Lachenbruch and Nathenson (1974).

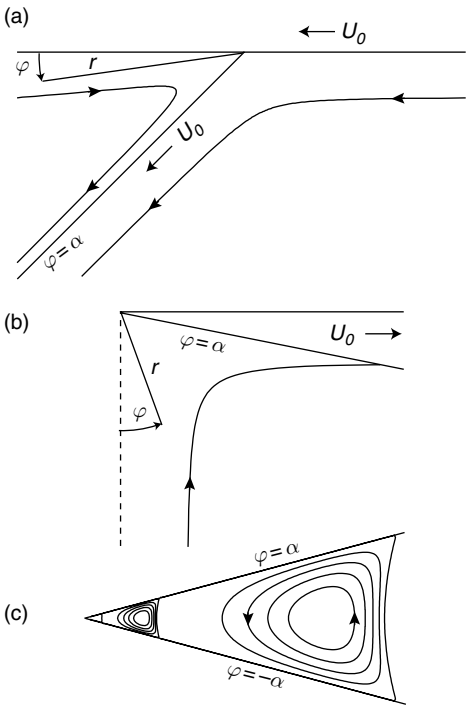

Figure 5 Models for slow viscous flow in wedge-shaped regions. (a) subduction zone; (b) mid-ocean ridge; (c) self-similar viscous corner eddies generated by an agency far from the corner. In all models, streamlines (for Newtonian rheology) are shown by solid lines with arrows.

The models of **Figures 5(a)** and **5(b)** admit analytical solutions for both Newtonian and power-law rheology. The boundary conditions for both models can be satisfied by a self-similar (of the first kind; cf. Section 7.04.4.2) streamfunction $\psi = -U_0 rF(\varphi)$, where (r, φ) are polar coordinates. The only nonzero component of the strain-rate tensor $\mathbf{e}$ is $e_{r\theta} = U_0(F + F'')/2r$, whence the second invariant of $\mathbf{e}$ is $I \equiv \left(e_{ij}e_{ij}\right)^{1/2} = \sqrt{2}e_{r\theta}$. The equation satisfied by F is obtained by applying the operator $\mathbf{e}_z \times \nabla$ to the momentum equation [31b] with the power-law constitutive relation [31e] and [31f], where $\mathbf{e}_z$ is a unit vector normal to the flow plane. The result is

$$\left(\frac{\mathrm{d}^2}{\mathrm{d}\varphi^2} + \frac{2n-1}{n^2}\right)(F'' + F)^{1/n} = 0 \qquad [54]$$

where n is the power-law index. The associated pressure, obtained by integrating the $\mathbf{e}_r$-component of the momentum equation with respect to r subject to the condition of vanishing pressure at $r = \infty$ is

$p = -\eta U_0 r^{-1}\,(F' + F''')$. Equation [54] can be solved analytically if n is any positive integer (Tovish *et al.*, 1978). The values most relevant to geophysics (*see* Chapter 1.02) are $n = 1$ and $n = 3$, for which the general solutions are

$$F_1 = A_1 \sin\varphi + B_1 \cos\varphi + C_1 \varphi \sin\varphi + D_1 \varphi \cos\varphi \qquad [55]$$

$$F_3 = A_3 \sin\varphi + B_3 \cos\varphi + C_3 H(\varphi,\ D_3) \qquad [56]$$

respectively, where

$$H(\varphi,\ D_3) = 27 \cos\frac{\sqrt{5}}{3}(\varphi + D_3) - \cos\sqrt{5}(\varphi + D_3) \qquad [57]$$

and $A_n - D_n$ are arbitrary constants for $n = 1$ and $n = 3$ that are determined by the boundary conditions. For the ridge model,

$$\{A_1,\ B_1,\ C_1,\ D_1\} = \frac{\{c^2,\ 0,\ 0,\ -1\}}{\alpha - sc} \qquad [58]$$

$$\{A_3,\ B_3,\ C_3,\ D_3\} = \left\{-C_3(b_1 s + b_1' c),\ 0,\ \frac{1}{b_1' s - b_1 c},\ \frac{3\pi}{2\sqrt{5}}\right\} \qquad [59]$$

where $s = \sin\alpha$, $c = \cos\alpha$, $b_1 = H(\alpha,\ D_3)$, and $b_1' = H_\varphi(\alpha,\ D_3)$. For the Newtonian ($n = 1$) subduction model in the wedge $0 \le \varphi \le \alpha$,

$$\{A_1,\ B_1,\ C_1,\ D_1\} = \frac{\{\alpha s,\ \ 0,\ \ \alpha c - s,\ \ -\alpha s\}}{\alpha^2 - s^2} \qquad [60]$$

For the power-law ($n = 3$) subduction model in $0 \le \varphi \le \alpha$, D_3 satisfies $b_1 - b_0 c - b_0' s = 0$ and the other constants are

$$C_3 = (b_1' + b_0 s - b_0' c)^{-1}, \quad B_3 = -b_0 C_3, \quad A_3 = -b_0' C_3 \qquad [61]$$

where $b_0 = H(0,\ D_3)$, and $b_0' = H_\varphi(0,\ D_3)$. If needed, the solutions in the wedge $\alpha \le \varphi \le \pi$ can be obtained from [55] and [56] by applying the boundary conditions shown in **Figure 5(a)**. The solution [60] together with the corresponding one for the wedge $\alpha \le \varphi \le \pi$ was the basis for Stevenson and Turner's (1977) hypothesis that the angle of subduction is controlled by the balance between the hydrodynamic lifting torque and the opposing gravitational torque acting on the slab. Their results were extended to power-law fluids by Tovish *et al.* (1978).

7.04.5.3.4 Viscous eddies

Another important exact solution for slow viscous flow describes viscous eddies near a sharp corner (Moffatt, 1964). This solution is an example of a self-similar solution of the second kind (Section 7.04.4.2), the determination of which requires the solution of an eigenvalue problem. Here we consider only Newtonian fluids; for power-law fluids, see Fenner (1975).

The flow domain is a 2-D wedge $|\varphi| \le \alpha$ bounded by rigid walls (**Figure 5(c)**). Flow in the wedge is driven by an agency (e.g., stirring) acting at a distance $\sim r_0$ from the corner. We seek to determine the asymptotic character of the flow near the corner, that is, in the limit $r/r_0 \to 0$. Because the domain of interest is far from the driving agency, we anticipate that the flow will be self-similar.

The streamfunction satisfies the biharmonic equation [37], which admits separable solutions of the form

$$\psi = r^\lambda F(\varphi) \qquad [62]$$

Substituting [62] into [37], we find that F satisfies

$$F'''' + \left[\lambda^2 + (\lambda - 2)^2\right] F'' + \lambda^2 (\lambda - 2)^2 = 0 \qquad [63]$$

where primes denote $\mathrm{d}/\mathrm{d}\varphi$. For all λ except 0, 1, and 2, the solution of [63] is

$$F = A\cos\lambda\varphi + B\sin\lambda\varphi + C\cos(\lambda - 2)\varphi + D\sin(\lambda - 2)\varphi \qquad [64]$$

where A–D are arbitrary constants. The solutions for $\lambda = 0$, 1, and 2 do not exhibit eddies (the solution with $\lambda = 1$ is the one used in the models of subduction zones and ridges in Section 7.04.5.3.3).

The most interesting solutions are those for which $\psi(r,\ \varphi)$ is an even function of φ. Application of the rigid-surface boundary conditions $F(\pm\alpha) = F'(\pm\alpha) = 0$ to [64] with $B = D = 0$ yields two equations for A and C that have a nontrivial solution only if

$$\sin 2(\lambda - 1)\alpha + (\lambda - 1)\sin 2\alpha = 0 \qquad [65]$$

The only physically relevant roots of [65] are those with $\Re(\lambda) > 0$, corresponding to solutions that are finite at $r = 0$. When $2\alpha < 146°$, these roots are all complex; let $\lambda_1 \equiv p_1 + iq_1$ be the root with the smallest real part, corresponding to the solution that decays least rapidly towards the corner. **Figure 5(c)** shows the streamlines $\Re(r^\lambda F) = \mathrm{cst}$ for $2\alpha = 30°$, for which $p_1 = 4.22$ and $q_1 = 2.20$. The flow comprises an infinite sequence of self-similar eddies with alternating senses of rotation, whose successive intensities decrease by a factor $\exp(\pi p_1/q_1) \approx 414$ towards the corner. In the limit $\alpha = 0$ corresponding to flow between parallel planes, $p_1 = 4.21$ and $q_1 = 2.26$, all the eddies have the same size ($\approx$2.78 times the channel width), and the intensity ratio ≈ 348.

In a geophysical context, corner eddies are significant primarily as a simple model for the tendency of forced viscous flows in domains with large aspect ratio to break up into separate cells. An example (Section 7.04.9.3), is steady 2-D cellular convection at high Rayleigh number, in which Stokes flow in the isothermal core of a cell is driven by the shear stresses applied to it by the thermal plumes at its ends. When the aspect ratio (width/depth) $\beta = 1$, the core flow comprises a single cell ; but when $\beta = 2.5$, the flow separates into two distinct eddies (Jimenez and Zufiria, 1987, Figure 2).

7.04.5.4 Superposition and Eigenfunction Expansion Methods

The linearity of the equations governing Stokes flow is the basis of two powerful methods for solving Stokes flow problems in regular domains: the methods of superposition and eigenfunction expansion. In both methods, a complicated flow is represented by infinite sums of elementary separable solutions of the Stokes equations for the coordinate system in question, and the unknown coefficients in the expansion are determined to satisfy the boundary conditions. In the superposition method, the individual separable solutions do not themselves satisfy all the boundary conditions in any of the coordinate directions. In the method of eigenfunction expansions (henceforth MEE), by contrast, the separable solutions are true eigenfunctions that satisfy all the (homogeneous) boundary conditions at both ends of an interval in one of the coordinate directions, so that the unknown constants are determined entirely by the boundary conditions in the other direction(s). Let us turn now to some concrete illustrations of these methods in three coordinate systems of geophysical interest: 2-D Cartesian, spherical, and bispherical.

7.04.5.4.1 2-D flow in Cartesian coordinates

The streamfunction ψ for 2-D Stokes flow satisfies the biharmonic equation [37], which has the general solution

$$\psi = f_1(x+iy) + f_2(x-iy) + (y+ix)f_3(x+iy) + (y-ix)f_4(x-iy) \quad [66]$$

where f_1–f_4 are arbitrary functions of their (complex) arguments. However, the most useful solutions for applications are the separable solutions that vary periodically in one direction. Setting $\psi \propto \exp ikx$ and solving [37] by separation of variables, we find

$$\psi = [(A_1 + A_2 y)\exp(-ky) + (A_3 + A_4 y)\exp ky]\exp ikx \quad [67]$$

where A_1–A_4 are arbitrary functions of k. An analogous solution is obtained by interchanging x and y in [67], and both solutions remain valid if k is complex.

The solution [67] has been widely used in geodynamics to describe flows generated by loads that vary sinusoidally in the horizontal direction (e.g., Fleitout and Froidevaux, 1983.) The representation of more general flows, however, typically requires the use of a superposition or an eigenfunction expansion. To illustrate the use of these two methods, we consider the problem of driven cavity flow in a rectangular domain $x \in [-\beta/2, \beta/2]$, $y \in [-1/2, 1/2]$ with impermeable ($\psi = 0$) boundaries (**Figure 6**). The sidewalls $x = \pm\beta/2$ and the bottom $y = -1/2$ are rigid and motionless, while the upper boundary $y = 1/2$ moves in its own plane with velocity $U(x)$ (**Figure 6**, boundary conditions a).

In the superposition method, the solution is represented as a sum of two ordinary Fourier series in the two coordinate directions. The flow is the sum of two parts that are even and odd functions of y,

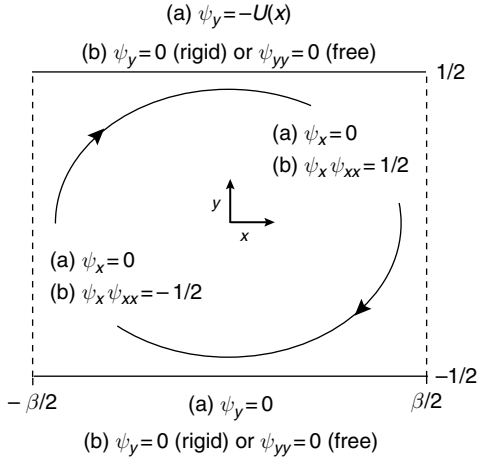

Figure 6 Geometry and boundary conditions for (a) driven cavity flow and (b) steady cellular convection in a rectangle $x \in [-\beta/2, \beta/2]$, $y \in [-1/2, 1/2]$ with impermeable boundaries. All lengths are nondimensionalized by the height of the rectangle.

respectively, and the representation for the even part is (Meleshko, 1996)

$$\psi = \sum_{m=1}^{\infty} A_m F(y,\ p_m,\ 1)\cos p_m x + \sum_{n=1}^{\infty} B_n F(x,\ q_n,\ \beta)\cos q_n y \qquad [68a]$$

$$p_m = \frac{2m-1}{\beta}\pi, \qquad q_n = (2n-1)\pi \qquad [68b]$$

$$F(z,\ k,\ r) = \frac{r\tanh(rk/2)\cosh kz - 2z\sinh kz}{2\cosh(rk/2)} \qquad [68c]$$

where A_m and B_n are undetermined coefficients. Due to the choice of the wave numbers p_m and q_n and the function $F(z,k,r)$ (which vanishes at $z=\pm r/2$), each of the series in [68a] satisfies the impermeability condition $\psi=0$ on all boundaries. Moreover, because the trigonometric systems $\cos p_m x$ and $\cos q_n y$ are complete, the superposition [68] (with suitable choices of A_m and B_n) can represent arbitrary distributions of tangential velocity on $y=\pm 1/2$ and $x=\pm\beta/2$.

Unlike the superposition method, the MEE makes use of so-called Papkovich–Fadle eigenfunctions $\phi(x)$ that satisfy all the homogeneous boundary conditions in the direction (x in this case) perpendicular to two motionless walls. For simplicity, suppose that $U(x)=U(-x)$, so that ψ is an even function of x. The even eigenfunctions on the canonical unit interval $x \in [-1/2,\ 1/2]$ are obtained by substituting $\psi=\phi(x)\exp(\lambda y)$ into the biharmonic equation [37] and solving the resulting equation for ϕ subject to the conditions $\phi(\pm 1/2)=\phi_x(\pm 1/2)=0$, yielding

$$\phi_n(x) = x\sin\lambda_n x - \frac{1}{2}\tan\frac{\lambda_n}{2}\cos\lambda_n x \qquad [69]$$

where λ_n are the first-quadrant complex roots of $\sin\lambda_n + \lambda_n = 0$. The streamfunction for the flow in the cavity with $x \in [-\beta/2, \beta/2]$ (**Figure 6**) can then be written as (Shankar, 1993)

$$\psi = \sum_{n=1}^{\infty}\left\{ A_n\Phi_n \exp\left[-\lambda_n\left(y+\frac{1}{2}\right)\right] + \bar{A}_n\bar{\Phi}_n \exp\left[-\bar{\lambda}_n\left(y+\frac{1}{2}\right)\right] + B_n\Phi_n \exp\left[-\lambda_n\left(\frac{1}{2}-y\right)\right] + \bar{B}_n\bar{\Phi}_n \exp\left[-\bar{\lambda}_n\left(\frac{1}{2}-y\right)\right]\right\} \qquad [70]$$

where $\Phi_n=\phi_n(x/\beta)$, overbars denote complex conjugation, and the constants A_n and B_n are chosen to satisfy the boundary conditions at $y=\pm 1/2$. The difficulty, however, is that the reduced biharmonic equation $(d^2/dx^2+\lambda^2)^2\phi=0$ satisfied by the eigenfunctions ϕ_n is not self-adjoint, as can be seen by rewriting it in the form

$$\frac{d^2}{dx^2}\begin{pmatrix}\phi\\ -\lambda^{-2}\phi''\end{pmatrix} = \lambda^2\begin{pmatrix}0 & -1\\ 1 & -2\end{pmatrix}\begin{pmatrix}\phi\\ -\lambda^{-2}\phi''\end{pmatrix} \qquad [71]$$

and noting that the square matrix on the RHS is not Hermitian. Consequently, the eigenfunctions ϕ_n are not mutually orthogonal, which makes the determination of A_n and B_n a nontrivial matter. One solution is to use a complementary set of adjoint eigenfunctions χ_m which are biorthogonal to the set ϕ_n, although considerable care must then be taken to ensure convergence of the expansion (see Katopodes *et al.* (2000) for a discussion and references to the relevant literature). A cruder but very effective approach is to determine A_n and B_n via a numerical least-squares procedure that minimizes the misfit of the solution [70] to the boundary conditions (Shankar, 1993; Bloor and Wilson, 2006). Shankar (2005) showed how this approach can be extended to an irregular domain by embedding the latter in a larger, regular domain on which a complete set of eigenfunctions exists.

Another geophysically relevant 2-D Stokes problem that can be solved using superposition and eigenfunction expansion methods is that of the flow within the isothermal core of a vigorous (high Rayleigh number) convection cell. The boundary conditions for this case (**Figure 6**, conditions b) comprise either rigid ($\psi_y=0$) or traction-free ($\psi_{yy}=0$) conditions at $y=\pm 1/2$ and nonlinear sidewall conditions $\psi_x\psi_{xx}=\pm 1/2$ (derived in Section 7.04.9.3.2) that represent the shear stresses applied to the core by the buoyant thermal plumes. If the boundaries $y=\pm 1/2$ are traction free, the conditions $\psi=\psi_{yy}=0$ involve only even derivatives of ψ, and are satisfied identically if $\psi\propto\cos q_n y$ where q_n is defined by [68b]. The streamfunction that also satisfies the sidewall impermeability conditions $\psi(\pm\beta/2, y)=0$ is (Roberts, 1979)

$$\psi = \sum_{n=0}^{\infty} A_n F(x,\ q_n,\ \beta)\cos q_n y \qquad [72]$$

where $F(x, q_n, \beta)$ is defined by [68c]. The constants A_n are then determined iteratively to satisfy the boundary conditions $\psi_x\psi_{xx}(\pm\beta/2, y)=\pm 1/2$. Strictly speaking, [72] is an eigenfunction expansion, because the functions $\cos q_n y$ satisfy all the homogeneous

boundary conditions at $y = \pm 1/2$. In practice, however, the term eigenfunction expansion is usually reserved for expressions like [70] that involve a sequence of complex wave numbers λ_n. No such terminological ambiguity applies for a convection cell bounded by rigid surfaces, for which the flow can be represented by the eigenfunction expansion (Roberts, 1979)

$$\psi = \sum_{n=1}^{\infty} \left[A_n \phi_n(y) \cosh \lambda_n x + \bar{A}_n \bar{\phi}_n(y) \cosh \bar{\lambda}_n x \right] \qquad [73]$$

Other examples of the use of superposition and eigenfunction expansion methods for cellular convection problems can be found in Turcotte (1967), Turcotte and Oxburgh (1967), Olson and Corcos (1980), Morris and Canright (1984), and Busse *et al.* (2006).

7.04.5.4.2 Spherical coordinates

Lamb (1932) derived a general solution of the equations of Stokes flow in spherical coordinates (r, θ, ϕ). Because the pressure p satisfies Laplace's equation, it may be expressed as a sum of solid spherical harmonics p_l:

$$p = \sum_{l=-\infty}^{\infty} p_l, \quad p_l = r^l \sum_{m=-l}^{l} c_{lm} Y_l^m(\theta, \phi) \qquad [74]$$

where Y_l^m are surface spherical harmonics and c_{lm} are complex coefficients. The velocity $\mathbf{u}$ can then be written

$$\mathbf{u} = \sum_{l=-\infty}^{\infty} [\nabla \Phi_l + \nabla \times (\mathbf{x} \chi_l)] + \sum_{\substack{l=-\infty \\ l \neq 1}}^{\infty} \left[\frac{(1/2)(l+3) r^2 \nabla p_l - l \mathbf{x} p_l}{\eta (l+1)(2l+3)} \right] \qquad [75]$$

where η is the viscosity, $\mathbf{x}$ is the position vector and Φ_l and χ_l are solid spherical harmonics of the form [74] but with different coefficients. The first sum in [75] is the solution of the homogeneous Stokes equations $\nabla^2 \mathbf{u} = 0$, $\nabla \cdot \mathbf{u} = 0$, whereas the second sum is the particular solution of $\nabla^2 \mathbf{u} = \nabla p / \eta$. A recent application of [75] is the solution of Gomilko *et al.* (2003) for steady Stokes flow driven by the motion of one of three mutually perpendicular walls that meet in a corner, a 3-D generalization of the 2-D corner-flow model (**Figure 5(a)**). The main difficulty in using Lamb's solution is in applying boundary conditions, because the elements of [75], while complete, do not form an orthogonal basis for vector functions on the surface of a sphere in the way that standard spherical harmonics form an orthonormal basis for scalar functions. Methods for dealing with this problem are discussed in chapter 4 of Kim and Karrila (1991).

7.04.5.4.3 Bispherical coordinates

Flow in a domain bounded by nonconcentric spheres is a useful model for the interaction of one buoyant diapir or plume head with another or with a flat interface (i.e., a sphere of infinite radius). Such flow problems can often be solved analytically using bispherical coordinates (ξ, θ, ϕ), which are related to the Cartesian coordinates (x, y, z) by

$$(x, y, z) = \frac{(a \sin\theta \cos\phi, \ a \sin\theta \sin\phi, \ a \sinh\xi)}{\cosh\xi - \cos\theta} \qquad [76]$$

where a is a fixed length scale. Surfaces of constant ξ are nonconcentric spheres with their centers on the axis $x = y = 0$, and $\xi = 0$ corresponds to the plane $z = 0$ (**Figure 7**). For axisymmetric (i.e., independent of ϕ) Stokes flow, the general solution for the streamfunction ψ and the pressure p is (Stimson and Jeffreys, 1926)

$$\psi = (\cosh\xi - \eta)^{-3/2} \sum_{n=0}^{\infty} C_{n+1}^{-1/2}(\eta) \left[a_n \cosh \beta_{-1} \xi + b_n \sinh \beta_{-1} \xi + c_n \cosh \beta_3 \xi + d_n \sinh \beta_3 \xi \right] \qquad [77a]$$

$$p = (\cosh\xi - \eta)^{-1/2} \sum_{n=0}^{\infty} \left[A_n \exp \beta_1 \xi + B_n \exp(-\beta_1 \xi) \right] P_n(\eta), \qquad [77b]$$

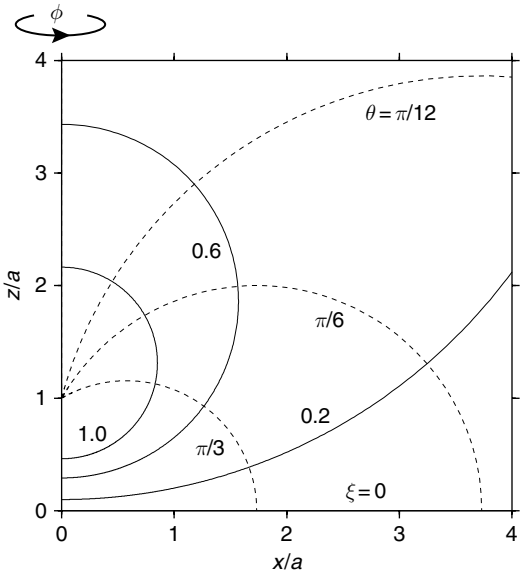

Figure 7 Bispherical coordinates (ξ, θ, ϕ) defined by [76]. Selected lines of constant ξ (solid) and constant θ (dashed) are shown.

where $\eta = \cos\theta$, $\beta_m = n + m/2$, $C_{n+1}^{-1/2}$ is a Gegenbauer polynomial of order $n+1$ and degree $-1/2$, P_n is a Legendre polynomial, and $a_n - d_n$, A_n, and B_n are arbitrary constants. Koch and Ribe (1989) used a solution of the form [77] to model the effect of a viscosity contrast on the topography and gravity anomalies produced by the motion of a buoyant and deformable fluid sphere beneath a free surface of a fluid with a different viscosity. A representation of general nonaxisymmetric flows in bispherical coordinates was derived by Lee and Leal (1980), and used to determine the flow due to the arbitrary motion of a sphere near a plane wall.

7.04.5.5 The Complex-Variable Method for 2-D Flows

A powerful method for 2-D Stokes flows and analogous problems in elasticity (Muskhelishvili, 1953) is based on the Goursat representation of a biharmonic function ψ in terms of two analytic functions ϕ and χ of the complex variable $z \equiv x + \mathrm{i}y$:

$$\psi = \Re[\bar{z}\phi(z) + \chi(z)] \qquad [78]$$

where an overbar denotes complex conjugation. If ψ is the streamfunction of a 2-D flow, then the velocity components $u = -\psi_y$ and $v = \psi_x$ are

$$v - iu = \phi(z) + z\overline{\phi'(z)} + \overline{\chi'(z)} \qquad [79]$$

the vorticity $\omega \equiv \nabla^2\psi$ and the pressure p are

$$\omega + ip/\eta = 4\phi'(z) \qquad [80]$$

where η is the viscosity and the components of the stress tensor are

$$\sigma_{xx} = -2\eta\Im[2\phi'(z) - \bar{z}\phi''(z) - \chi''(z)] \qquad [81a]$$

$$\sigma_{yy} = -2\eta\Im[2\phi'(z) + \bar{z}\phi''(z) + \chi''(z)] \qquad [81b]$$

$$\sigma_{xy} = 2\eta\Re[\bar{z}\phi''(z) + \chi''(z)] \qquad [81c]$$

The Goursat representation reduces the task of solving the biharmonic equation to one of finding two analytic functions that satisfy the relevant boundary conditions. The method is most powerful when used in conjunction with conformal mapping, which allows a flow domain with a complex shape to be mapped onto a simpler one (such as the interior of the unit circle). A remarkable example is Jeong and Moffatt's (1992) analytical solution for the formation of a cusp above a vortex dipole located at depth d beneath the free surface of a viscous fluid. In the geodynamically relevant limit of zero surface tension, the surface displacement $y(x)$ satisfies $x^2 y = -(y + 2d/3)^3$, which has an infinitely sharp cusp at $(x,y) = (0, -2d/3)$. Although the model is too idealized for direct application to the mantle, its dynamics are relevant to the formation of cusp-like features by entrainment in thermochemical convection (Davaille, 1999).

7.04.5.6 Singular Solutions and the Boundary-Integral Representation

The Stokes equations admit a variety of singular solutions in which the velocity and/or the pressure becomes infinite at one or more points in space. Such solutions are the basis of the boundary-integral representation, whereby a Stokes flow in a given domain is expressed in terms of surface integrals of velocities and stresses over the domain boundaries. The dimensionality of the problem is thereby reduced by one (from 3-D to 2-D or from 2-D to 1-D), making possible a powerful numerical technique – the boundary element method – that does not require discretization of the whole flow domain (Pozrikidis, 1992.)

The most useful singular solutions fall into two classes: those involving point forces, and those associated with volume sources and sinks.

7.04.5.6.1 Flow due to point forces

The most important singular solution of the Stokes equations is that due to a point force F_i, or Stokeslet, applied at a position $\mathbf{x}'$ in the fluid. The velocity u_i and stress tensor σ_{ij} induced at any point $\mathbf{x}$ satisfy

$$\partial_j \sigma_{ij} = -F_i \delta(\mathbf{x} - \mathbf{x}'), \quad \partial_j u_j = 0 \qquad [82]$$

where $\delta(\mathbf{x} - \mathbf{x}') = \delta(x_1 - x_1')\delta(x_2 - x_2')\delta(x_3 - x_3')$ and δ is the Dirac delta-function. Here and throughout Section 7.04.5.6, vector arguments of functions are denoted using boldfaced vector notation, while other quantities are written using Cartesian tensor (subscript) notation. In an infinite fluid, the required boundary conditions are that $u_i \to 0$ and $\sigma_{ij} \to -p_0\delta_{ij}$ as $|\mathbf{x} - \mathbf{x}'| \to \infty$, where p_0 is the (dynamically irrelevant) far-field pressure. Because the response of the fluid is proportional to the applied force, $u_i = \mathcal{J}_{ij}F_j/\eta$ and $\sigma_{ik} = K_{ijk}F_j$, where η is the viscosity and $\mathcal{J}_{ij}$ and K_{ijk} are tensorial Green's functions representing the response to a unit force. Substituting these expressions into [82] and eliminating the arbitrary vector F_j, we obtain

$$\partial_i K_{ijk} = -\delta_{jk}\delta(\mathbf{x} - \mathbf{x}'), \quad \partial_i \mathcal{J}_{ij} = 0 \qquad [83]$$

The solutions of [83] can be found using a Fourier transform (Kim and Karrila, 1991, p. 33) or by reducing [83] to Poisson's equation (Pozrikidis, 1992, p. 22), and are

$$\mathcal{J}_{ij}(\mathbf{r}) = \frac{1}{8\pi}\left(\frac{\delta_{ij}}{r} + \frac{r_i r_j}{r^3}\right), \quad K_{ijk}(\mathbf{r}) = -\frac{3}{4\pi}\frac{r_i r_j r_k}{r^5} \qquad [84]$$

where $\mathbf{r} = \mathbf{x} - \mathbf{x}'$ and $r = |\mathbf{r}|$. The tensor $\mathcal{J}_{ij}$ is often called the Oseen tensor. The analogs of [84] for a 2-D flow are

$$\mathcal{J}_{ij}(\mathbf{r}) = \frac{1}{4\pi}\left(-\delta_{ij}\ln r + \frac{r_i r_j}{r^2}\right), \quad K_{ijk}(\mathbf{r}) = -\frac{1}{\pi}\frac{r_i r_j r_k}{r^4} \qquad [85]$$

The expression [85] for $\mathcal{J}_{ij}$ does not vanish as $r \to \infty$, which is related to the fact that a 2-D Stokes flow around an infinitely long cylinder does not exist (Stokes's paradox). Below we will see how this paradox is resolved by the presence of a boundary.

Starting from the Stokeslet solution, one can use the principle of superposition to construct an infinite variety of additional singular solutions. An example is the flow due to a force dipole, comprising a point force F_i at $\mathbf{x}'$ and an equal and opposite force $-F_i$ at $\mathbf{x}' - d\mathbf{n}$, where $\mathbf{n}$ is a unit vector directed from the negative to the positive force. The associated velocity field is $u_i(\mathbf{x}) = [\mathcal{J}_{ij}(\mathbf{r}) - \mathcal{J}_{ij}(\mathbf{r} + d\mathbf{n})]F_j$. In the limit $d \to 0$ with $dF_j n_k$ fixed,

$$u_i = dF_j n_k G^{\mathrm{FD}}_{ijk} \qquad [86a]$$

$$G^{\mathrm{FD}}_{ijk}(\mathbf{r}) = -\partial_k \mathcal{J}_{ij}(\mathbf{r}) \equiv \frac{1}{8\pi}\left[\frac{\delta_{ij}r_k - \delta_{ik}r_j - \delta_{jk}r_i}{r^3} + \frac{3r_i r_j r_k}{r^5}\right] \qquad [86b]$$

where G^{FD}_{ijk} is the force-dipole Green's function. The force-dipole moment $dn_j F_k$ is sometimes decomposed into symmetric (stresslet) and antisymmetric (rotlet) parts (Kim and Karrila, 1991, Section 7.04.2.5.)

7.04.5.6.2 Flows due to point sources

The basic singular solution of the second class is that associated with a volume source of strength Q at $\mathbf{x}'$, which generates a spherically symmetric flow

$$u_i = \frac{Qr_i}{4\pi r^3} \qquad [87]$$

The flow due to a source doublet comprising a source and sink with equal strengths Q separated by a vector $d\mathbf{n}$ pointing from the sink to the source is

$$u_i = Qdn_j G^{\mathrm{SD}}_{ij},$$
$$G^{\mathrm{SD}}_{ij}(\mathbf{r}) = -\frac{1}{4\pi}\partial_j\left(\frac{r_i}{r^3}\right) \equiv \frac{1}{4\pi}\left(\frac{3r_i r_j}{r^5} - \frac{\delta_{ij}}{r^3}\right) \qquad [88]$$

7.04.5.6.3 Singular solutions in the presence of a boundary

The flow produced by a point force is modified by the presence of an impermeable wall. Consider a force F_i at a point $\mathbf{x}'$ located a distance d from the wall, and let $\mathbf{n}$ be a unit vector normal to the wall directed towards the side containing $\mathbf{x}'$ (**Figure 8(a)**). The modified velocity can be written as $u_i = G^{\mathrm{B}}_{ij}F_j$, where $G^{\mathrm{B}}_{ij}(\mathbf{x}, \mathbf{x}')$ is a Green function that satisfies all the required boundary conditions at the wall. Its general form is

$$G^{\mathrm{B}}_{ij}(\mathbf{x},\ \mathbf{x}') = \mathcal{J}_{ij}(\mathbf{x} - \mathbf{x}') + G^{\mathrm{IM}}_{ij}(\mathbf{x} - \mathbf{x}^{\mathrm{IM}}) \qquad [89]$$

where G^{IM}_{ij} is a Green function that is singular at the image point $\mathbf{x}^{\mathrm{IM}} = \mathbf{x}' - 2d\mathbf{n}$ (**Figure 8a**).

The two limiting cases of greatest interest are traction-free and rigid walls. Because a traction-free wall is equivalent to a plane of mirror symmetry, the modified flow for this case can be constructed simply by adding a reflected Stokeslet with strength $\mathbf{R} \cdot \mathbf{F} \equiv \mathbf{F}^*$ at the image point $\mathbf{x}^{\mathrm{IM}}$, where $R_{ij} \equiv \delta_{ij} - 2n_i n_j$ is a reflection tensor that reverses the sign of the wall-normal component of a vector while leaving its wall-parallel components unchanged (**Figure 8(a)**). Therefore

$$G^{\mathrm{IM}}_{ij}(\mathbf{r}^{\mathrm{IM}}) = R_{jk}\mathcal{J}_{ik}(\mathbf{r}^{\mathrm{IM}}) \qquad [90]$$

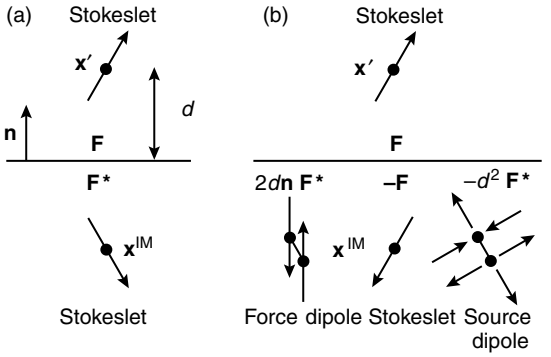

Figure 8 Singular solutions required to describe the flow due to a point force **F** located at a point $\mathbf{x}'$ a distance d above a plane wall. The boundary conditions on the wall (horizontal lines) are satisfied by adding one or more singular solutions at the image point $\mathbf{x}^{\mathrm{IM}} \equiv \mathbf{x}' - 2d\mathbf{n}$, where $\mathbf{n}$ is the unit vector normal to the wall. The strength or moment of each required singular solution is indicated, and $\mathbf{F}^*$ is the reflection of the vector **F** across the wall. (a) traction-free wall; (b) rigid wall.

where $\mathbf{r}^{\mathrm{IM}} = \mathbf{x} - \mathbf{x}^{\mathrm{IM}}$. If the surface is rigid, the boundary conditions can be satisfied by adding three different singular solutions at $\mathbf{x}^{\mathrm{IM}}$: a Stokeslet with strength $-\mathbf{F}$, a force dipole with moment $2d\mathbf{n}\mathbf{F}^*$, and a source dipole with strength $-d^2\mathbf{F}^*$ (**Figure 8(b)**) The result is (Blake, 1971)

$$G_{ij}^{\mathrm{IM}}(\mathbf{r}^{\mathrm{IM}}) = -\mathcal{J}_{ij}(\mathbf{r}^{\mathrm{IM}}) + 2dR_{jl}n_k G_{ikl}^{\mathrm{FD}}(\mathbf{r}^{\mathrm{IM}}) - d^2 R_{jk} G_{ik}^{\mathrm{SD}}(\mathbf{r}^{\mathrm{IM}}) \quad [91]$$

where G_{ij}^{FD} and G_{ij}^{SD} are defined by [86b] and [88], respectively.

Expressions analogous to those above also apply to 2-D flow in the presence of a boundary. The basic idea is illustrated by the free-surface case, for which both [89] and [90] remain valid if $\mathcal{J}_{ij}$ has its 2-D form [85]. Now, however, the presence of the image singularity G_{ij}^{IM} cancels the logarithmic divergence of $\mathcal{J}_{ij}$ at large distances from the point force, thereby resolving Stokes's paradox and rendering the problem well-posed. A rigid surface has the same effect, although the corresponding expressions for the Green's function are more complicated.

7.04.5.6.4 Boundary-integral representation

The boundary-integral representation for Stokes flow expresses the velocity u_i at any point in a fluid volume V bounded by a surface S in terms of the velocity and traction on S. The starting point is the integral form [34] of the Lorentz reciprocal theorem. Let (u_i, σ_{ij}) be the flow of interest in a fluid with no distributed body forces ($b_i = 0$), and let $u_i^* \equiv \mathcal{J}_{ij}(\mathbf{x}-\mathbf{x}')F_j/\eta$ and $\sigma_{ik}^* \equiv K_{ijk}(\mathbf{x}-\mathbf{x}')F_j$ be the flow produced by a point force $b_i^* \equiv F_i\delta(\mathbf{x}-\mathbf{x}')$ at the point $\mathbf{x}'$. Substituting these expressions into [34] and dropping the arbitrary vector F_i, we obtain

$$\frac{1}{\eta}\int_S \mathcal{J}_{ij}(\mathbf{x}-\mathbf{x}')\sigma_{ik}(\mathbf{x})n_k(\mathbf{x})\mathrm{d}S(\mathbf{x}) - \int_V u_j(\mathbf{x})\delta(\mathbf{x}-\mathbf{x}')\mathrm{d}V(\mathbf{x}) = \int_S K_{ijk}(\mathbf{x}-\mathbf{x}')u_i(\mathbf{x})n_k(\mathbf{x})\mathrm{d}S(\mathbf{x}) \quad [92]$$

where the normal $\mathbf{n}$ points out of V. Now

$$\int_V u_j(\mathbf{x})\delta(\mathbf{x}-\mathbf{x}')\mathrm{d}V = \chi(\mathbf{x}')u_j(\mathbf{x}') \quad [93]$$

where $\chi(\mathbf{x}') = 0$, $1/2$, or 1 depending on whether $\mathbf{x}'$ lies outside V, right on S, or inside V, respectively. Substituting [93] into [92] and interchanging the roles of $\mathbf{x}$ and $\mathbf{x}'$, we obtain the boundary-integral representation

$$\frac{1}{\eta}\int_{S'} \mathcal{J}_{ij}\sigma_{ik}n_k\mathrm{d}S' - \int_{S'} K_{ijk}u_i n_k \mathrm{d}S' = \chi(\mathbf{x})u_j(\mathbf{x}) \quad [94]$$

where the arguments of the quantities in the integrands ($\mathbf{x}'$ for n_k, σ_{ik}, and u_i; $\mathbf{x}'-\mathbf{x}$ for $\mathcal{J}_{ij}$ and K_{ijk}) have been suppressed for brevity and $\mathrm{d}S' = \mathrm{d}S(\mathbf{x}')$. The first integral in [94] represents the velocity due to a surface distribution of point forces with density $\sigma_{ik}n_k\,\mathrm{d}S'$. It is called the single-layer potential by analogy to the electrostatic potential generated by a surface distribution of electric charges. The second integral, called the double-layer potential, represents the velocity field generated by the sum of a distribution of sources and sinks and a symmetric distribution of force dipoles (Kim and Karrila, 1991, Section 7.04.2.4.2).

An important extension of the integral representation [94] is to the buoyancy-driven motion of a fluid drop with viscosity $\eta_2 \equiv \gamma\eta_1$ and density $\rho_2 \equiv \rho_1 + \Delta\rho$ in another fluid with viscosity η_1 and density ρ_1 (Pozrikidis, 1990; Manga and Stone, 1993.) Let S, V_1, and V_2 be the surface of the drop and the volumes outside and inside it, respectively. We begin by writing separate integral equations of the form [94] for each fluid:

$$-\frac{1}{\eta_1}\int_{S'} \mathcal{J}_{ij}\sigma_{ik}^{(1)}n_k\mathrm{d}S' + \int_{S'} K_{ijk}u_i^{(1)}n_k\mathrm{d}S' = \chi_1(\mathbf{x})u_j^{(1)}(\mathbf{x}) \quad [95a]$$

$$\frac{1}{\eta_2}\int_{S'} \mathcal{J}_{ij}\sigma_{ik}^{(2)}n_k\mathrm{d}S' - \int_{S'} K_{ijk}u_i^{(2)}n_k\mathrm{d}S' = \chi_2(\mathbf{x})u_j^{(2)}(\mathbf{x}) \quad [95b]$$

where $\mathbf{n}$ points out of the drop and the volume (V_1 or V_2) in which a given quantity is defined as indicated by a superscript in parentheses. Here $\chi_1(\mathbf{x}) = 0$, $1/2$, or 1 if $\mathbf{x}$ is in V_2, right on S, or in V_1, respectively, and $\chi_2(\mathbf{x})$ is defined similarly but with the subscripts 1 and 2 interchanged. Now multiply [95b] by γ, add the result to [95a], and apply the matching conditions $u_j^{(1)} = u_j^{(2)} = u_j$ and $(\sigma_{ik}^{(1)} - \sigma_{ik}^{(2)})n_k = n_i\Delta\rho g_k x_k'$ on S, where g_k is the gravitational acceleration. The result is

$$\chi_1(\mathbf{x})u_j^{(1)}(\mathbf{x}) + \gamma\chi_2(\mathbf{x})u_j^{(2)}(\mathbf{x}) - (1-\gamma)\int_{S'} K_{ijk}u_i n_k \mathrm{d}S' = -\frac{g_k\Delta\rho}{\eta_1}\int_{S'} \mathcal{J}_{ij}n_i x_k'\mathrm{d}S' \quad [96]$$

For points $\mathbf{x}$ on S, [96] reduces to

$$\frac{1}{2}u_j(\mathbf{x}) - \frac{1-\gamma}{1+\gamma}\int_{S'} K_{ijk}u_i n_k \mathrm{d}S' = -\frac{g_k\Delta\rho}{\eta_1(1+\gamma)}\int_{S'} \mathcal{J}_{ij}n_i x_k'\mathrm{d}S' \quad (\mathbf{x}\in S) \quad [97]$$

a Fredholm integral equation of the second kind for the velocity $\mathbf{u}$ of the interface. Once $\mathbf{u}$ on S has been determined by solving [97], $\mathbf{u}$ at points in V_1 and V_2 can be determined if desired from [96]. A generalization of [97] to $N > 1$ interacting drops was derived by Manga and Stone (1993).

The integral equation [97], which must in general be solved numerically, has been used in geodynamics to model systems comprising distinct fluids with different viscosities. Manga and Stone (1993) solved the N-drop generalization of [97] using the boundary element method (Pozrikidis, 1992) to investigate the buoyancy-driven interaction between two drops in an infinite fluid with a different viscosity. Manga *et al.* (1993) used a similar method to study the interaction of plume heads with compositional discontinuities in the Earth's mantle. The deformation of viscous blobs in a 2-D cellular flow was investigated by Manga (1996), who concluded that geochemical reservoirs can persist undisturbed for relatively long times if they are 10–100 times more viscous than the surrounding mantle. Finally, Manga (1997) showed that the deformation-induced mutual interactions of deformable diapirs in a rising cloud causes the diapirs progressively to cluster, but that the rate of this clustering is probably too slow to affect significantly the lateral spacing of rising diapirs in the mantle.

7.04.5.7 Slender-Body Theory

Slender-body theory (SBT) is concerned with Stokes flow around thin rod-like bodies whose length greatly exceeds their other two dimensions. The approach takes its departure from Stokes's paradox: the fact that a solution of the equations for Stokes flow around an infinitely long circular cylinder moving steadily in an unbounded viscous fluid does not exist, due to a logarithmic singularity that makes it impossible to satisfy all the boundary conditions (Batchelor, 1967). However, the problem can be regularized in one of three ways: by including inertia, by making the length of the cylinder finite, or by making the domain bounded. SBT is concerned with the second (and by extension the third) of these possibilities.

The canonical problem of SBT is to determine the force $\mathbf{F}$ on a rod of length 2ℓ and radius $a \ll \ell$ moving with uniform velocity $\mathbf{U}$ in a viscous fluid. The solution can be found using the MMAE, which exploits the fact that the flow field comprises two distinct regions characterized by very different length scales. The first or inner region includes points whose radial distance ρ from the rod is small compared to their distance from the rod's nearer end. In this region, the fluid is not affected by the ends of the rod, and sees it as an infinite cylinder with radius a. The second, outer region $\rho \gg a$ is at distances from the rod that are large compared to its radius. Here, the fluid is unaffected by the rod's finite radius, and sees it as a line distribution of point forces with effectively zero thickness. The basic idea of the MMAE is to obtain two different asymptotic expansions for the velocity field that are valid in the inner and outer regions, respectively, and then to match them together in an intermediate or overlap region where both expansions must coincide.

As the details of the matching are rather complicated, we defer our discussion of the method to Section 7.04.2, where it will be applied in the context of BL theory. Here we simply quote the lowest-order result that the force on a cylinder whose axis is parallel to a unit vector $\mathbf{e}_z$ is

$$\mathbf{F} = -4\pi\eta\ell\epsilon[2\mathbf{U} - (\mathbf{U}\cdot\mathbf{e}_z)\mathbf{e}_z] \qquad [98]$$

where $\epsilon = (\ln 2\ell/a)^{-1}$. The force on a cylinder moving normal to its axis ($\mathbf{U}\cdot\mathbf{e}_z = 0$) is thus twice that on one moving parallel to its axis. For further details and extensions of SBT, see Batchelor (1970), Cox (1970), Keller and Rubinow (1976), and Johnson (1980). Geophysically relevant applications of SBT include Olson and Singer (1985), who used [98] to predict the rise velocity of buoyant quasi-cylindrical (diapiric) plumes. Koch and Koch (1995) used an expression analogous to [98] for an expanding ring to model the buoyant spreading of a viscous drop beneath the free surface of a much more viscous fluid. Whittaker and Lister (2006a) presented a model for a creeping plume above a planar boundary from a point source of buoyancy, in which they modeled the flow outside the plume as that due to a line distribution of Stokeslets.

7.04.5.8 Flow Driven by Internal Loads

Because inertia is negligible in the mantle, the flow at each instant is determined entirely by the distribution of internal density anomalies (loads) at that instant. This principle is the basis of a class of internal loading models in which an instantaneous mantle flow field is determined by convolving a load distribution with a Green function that represents the mantle's response to a unit load. However, it proves convenient here to define the unit load not as a point force, but rather as a surface force concentrated at a single radius and whose amplitude is proportional to a spherical harmonic $Y_l^m(\theta, \phi)$ of degree l and order m.

Because the Stokes equations are separable in spherical coordinates, the Green function representing the response to an harmonic surface load of a given degree and order satisfies an ordinary differential equation (ODE) in the radial coordinate r that can be solved analytically. This approach was pioneered by Parsons and Daly (1983) for a plane layer with constant viscosity, and was extended by Richards and Hager (1984), Ricard *et al.* (1984), and Forte and Peltier (1987) to spherical geometry with self-gravitation and radially variable viscosity. To illustrate the method, we sketch below Forte and Peltier's (1987) analytical derivation of the Green function for a self-gravitating mantle with uniform viscosity.

7.04.5.8.1 Wave-domain Green functions

Our starting point is the equations [31] with $n=1$ that govern slow flow in an incompressible, self-gravitating, Newtonian mantle. Let

$$\rho = \rho_0 + \hat{\rho}(r,\ \theta,\ \phi), \quad \boldsymbol{\sigma} = \boldsymbol{\sigma}_0(r) + \hat{\boldsymbol{\sigma}}(r,\ \theta,\ \phi), \quad \chi = \chi_0(r) + \hat{\chi}(r,\ \theta,\ \phi) \qquad [99]$$

where hatted quantities are perturbations of the field variables about a reference hydrostatic state denoted by a subscript 0. Substituting [99] into [31b] and [31d] and neglecting products of perturbation quantities, we obtain

$$0 = \boldsymbol{\nabla}\cdot\hat{\boldsymbol{\sigma}} + \mathbf{g}_0\hat{\rho} - \rho_0\boldsymbol{\nabla}\hat{\chi} \qquad [100a]$$

$$\nabla^2\hat{\chi} = 4\pi G\hat{\rho} \qquad [100b]$$

where $\mathbf{g}_0 = -\boldsymbol{\nabla}\chi_0$. The third term on the RHS of [100b] represents the buoyancy force acting on the internal density anomalies, and the fourth represents the additional force associated with the perturbations in the gravitational potential that they induce (self-gravitation). For consistency with other sections of this chapter, the signs of all gravitational potentials (χ_0, $\hat{\chi}$, etc.) referred to below are opposite to those of Forte and Peltier (1987).

As noted in Section 7.04.5.2, the flow driven by internal density anomalies in a fluid with constant or depth-dependent viscosity is purely poloidal. The poloidal potential $\mathcal{P}(r, \theta, \phi)$ satisfies the first of equations [47], which remain valid in a self-gravitating mantle. We now substitute into this equation the expansions

$$\mathcal{P} = \sum_{l=0}^{\infty}\sum_{m=-l}^{l}\mathcal{P}_l^m(r)\,Y_l^m(\theta,\ \phi), \qquad \hat{\rho} = \sum_{l=0}^{\infty}\sum_{m=-l}^{l}\hat{\rho}_l^m(r)\,Y_l^m(\theta,\ \phi) \qquad [101]$$

where $Y_l^m(\theta, \phi)$ are surface spherical harmonics satisfying $\mathcal{B}^2 Y_l^m = -l(l+1)Y_l^m$ and $\mathcal{B}^2$ is defined by [45]. We thereby find that $\mathcal{P}_l^m(r)$ satisfies

$$\mathcal{D}_l^2\mathcal{P}_l^m(r) = \frac{g_0\hat{\rho}_l^m}{\eta r}, \quad \mathcal{D}_l = \frac{\mathrm{d}^2}{\mathrm{d}r^2} + \frac{2}{r}\frac{\mathrm{d}}{\mathrm{d}r} - \frac{l(l+1)}{r^2} \qquad [102]$$

where the gravitational acceleration g_0 has been assumed constant (Forte and Peltier, 1987). Now define a poloidal Green's function $P_l(r, r')$ that satisfies

$$\mathcal{D}_l^2 P_l(r,\ r') = \delta(r - r') \qquad [103]$$

$P_l(r, r')$ represents the poloidal flow generated at the radius r by an infinitely thin density contrast of spherical harmonic degree l and unit amplitude located a radius r'. The poloidal flow due to a distributed density anomaly $\hat{\rho}_l^m(r)$ is then obtained by convolving $\hat{\rho}_l^m(r)$ with the Green's function, yielding

$$\mathcal{P}_l^m(r) = \frac{g_0}{\eta}\int_{a_2}^{a_1}\frac{\hat{\rho}_l^m(r')}{r'}P_l(r,\ r')\mathrm{d}r' \qquad [104]$$

where a_2 and a_1 are the inner and outer radii of the mantle, respectively.

At all radii $r \neq r'$, the Green's function $P_l(r, r')$ satisfies the homogeneous form of [103], which has the general solution

$$P_l(r,\ r') = A_n r^l + B_n r^{-l-1} + C_n r^{l+2} + D_n r^{-l+1} \qquad [105]$$

where $A_n - D_n$ are undetermined constants with $n=1$ for $r' < r \leq a_1$ and $n=2$ for $a_2 \leq r < r'$. These eight constants are determined by the boundary conditions at $r = a_1$ and $r = a_2$ and by matching conditions at $r = r'$. The vanishing of the radial velocity at $r = a_1$ and $r = a_2$ requires

$$P_l(a_1,\ r') = P_l(a_2,\ r') = 0 \qquad [106]$$

and the vanishing of the shear stress requires

$$\frac{\mathrm{d}^2 P_l}{\mathrm{d}r^2}(a_1,\ r') = \frac{\mathrm{d}^2 P_l}{\mathrm{d}r^2}(a_2,\ r') = 0 \qquad [107]$$

Turning now to the matching conditions, we define $[A] \equiv A(r'+) - A(r'-)$ to be the jump in the quantity A across the radius $r = r'$. Continuity of the normal and tangential velocities and the shear stress requires

$$[P_l] = \left[\frac{\mathrm{d}P_l}{\mathrm{d}r}\right] = \left[\frac{\mathrm{d}^2 P_l}{\mathrm{d}r^2}\right] = 0 \qquad [108]$$

The normal stress, however, is discontinous at $r = r'$. By integrating [103] from $r'-$ to $r'+$ and applying [108], we find

$$\left[\frac{\mathrm{d}^3 P_l}{\mathrm{d}r^3}\right] = 1 \qquad [109]$$

Substitution of [105] into [106]–[109] yields eight equations for A_n–D_n, the solutions of which are

$$\begin{aligned} C_n &= -\frac{B_n}{a_n^{2l+3}} \\ &= \frac{1}{2(2l+3)(2l+1)(r')^{l-1}} \\ &\quad \times \frac{(a_1/a_n)^{2l+3} - (r'/a_2)^{2l+3}}{1-(a_1/a_2)^{2l+3}} \end{aligned} \qquad [110a]$$

$$\begin{aligned} D_n &= -a_n^{2l-1} A_n \\ &= \frac{a_n^{2l-1}}{2(4l^2-1)(r')^{l-3}} \frac{(a_1/a_n)^{2l-1} - (r'/a_2)^{2l-1}}{1-(a_1/a_2)^{2l-1}} \end{aligned} \qquad [110b]$$

The next step is to determine the gravitational potential anomaly. Because the flow induces deformations (dynamic topography) of the Earth's surface and of the core–mantle boundary (CMB), the total potential anomaly is

$$\hat{\chi}_l^m(r) = (\hat{\chi}_0)_l^m(r) + (\hat{\chi}_1)_l^m(r) + (\hat{\chi}_2)_l^m(r) \qquad [111]$$

where $\hat{\chi}_0$, $\hat{\chi}_1$, and $\hat{\chi}_2$ are the potentials associated with the internal load, the deformation $\hat{a}_1$ of the Earth's surface, and the deformation $\hat{a}_2$ of the CMB, respectively. To determine $\hat{\chi}_0$, we note that the general solution of [100b] is

$$\hat{\chi}(\mathbf{x}) = -G \int_V \frac{\hat{\rho}(\mathbf{x}')}{|\mathbf{x}-\mathbf{x}'|} \mathrm{d}V' \qquad [112]$$

where $\mathbf{x}$ is the 3-D position vector and the integral is over the whole mantle. We now invoke the expansion (Jackson, 1975, p. 102)

$$\begin{aligned} |\mathbf{x}-\mathbf{x}'|^{-1} &= 4\pi \sum_{l=0}^{\infty} \sum_{m=-l}^{l} \frac{1}{2l+1} \\ &\quad \times \frac{r_<^l}{r_>^{l+1}} Y_l^m(\theta,\ \phi)\, \bar{Y}_l^m(\theta',\ \phi') \end{aligned} \qquad [113]$$

where $r_< = \min(r, r')$ and $r_> = \max(r, r')$ and an overbar denotes complex conjugation. Substituting [113] into [112] and integrating over θ' and ϕ', we obtain

$$(\hat{\chi}_0)_l^m(r) = -\frac{4\pi G}{2l+1} \int_{a_2}^{a_1} (r')^2 \frac{r_<^l}{r_>^{l+1}} \hat{\rho}_l^m(r') \mathrm{d}r' \qquad [114]$$

Expressions for $\hat{\chi}_1$ and $\hat{\chi}_2$ can be obtained from [114] by replacing $\hat{\rho}_l^m(r')$ by $(\rho_0 - \rho_w)\ (\hat{a}_1)_l^m \delta(r'-a_1)$ and $(\rho_c - \rho_0)\ (\hat{a}_2)_l^m \delta(r'-a_2)$, respectively, where ρ_w is the density of seawater and ρ_c is the core density. The results are

$$(\hat{\chi}_1)_l^m(r) = -\frac{4\pi G a_1}{2l+1} (\rho_0 - \rho_\mathrm{w}) \left(\frac{r}{a_1}\right)^l (\hat{a}_1)_l^m \qquad [115a]$$

$$(\hat{\chi}_2)_l^m(r) = -\frac{4\pi G a_2}{2l+1} (\rho_\mathrm{c} - \rho_0) \left(\frac{a_2}{r}\right)^{l+1} (\hat{a}_2)_l^m \qquad [115b]$$

The boundary deformations $\hat{a}_n$ are determined from the principle that the normal stress must be continuous across the deformed surfaces $r = a_n + \hat{a}_n \equiv r_n$. This is equivalent to the requirement that the nonhydrostatic normal stress $\hat{\sigma}_{rr}$ acting on the reference surfaces $r = a_n$ be equal to the weight of the topography there. Expanded in spherical harmonics, this condition reads

$$-\hat{p}_l^m(a_n) + 2\eta \frac{\mathrm{d}\hat{w}_l^m}{\mathrm{d}r}(a_n) = -g_0 \Delta\rho_n (\hat{a}_n)_l^m \qquad [116]$$

where p is the nonhydrostatic pressure, w is the radial velocity, $\Delta\rho_1 = \rho_0 - \rho_\mathrm{w}$, and $\Delta\rho_2 = \rho_0 - \rho_\mathrm{c}$. An expression for $\hat{p}$ in terms of the poloidal scalar is obtained by integrating the $\mathbf{e}_\theta$-component of the momentum equation [100a] and expanding the result in spherical harmonics:

$$\hat{p}_l^m = -\eta \frac{\mathrm{d}}{\mathrm{d}r}\left(r D_l \mathcal{P}_l^m\right) - \rho_0 \hat{\chi}_l^m \qquad [117]$$

Substituting [117] and $\hat{w}_l^m = -l(l+1)\mathcal{P}_l^m/r$ into [116] and applying the boundary conditions [106], we obtain

$$(\hat{a}_n)_l^m = \Delta\rho_n^{-1} \left[X_l^m(a_n) - \frac{\rho_0}{g_0} \hat{\chi}_l^m(a_n) \right] \qquad [118a]$$

$$X_l^m(r) = \frac{\eta}{g_0} \left[-r\frac{\mathrm{d}^3}{\mathrm{d}r^3} + \frac{3l(l+1)}{r} \frac{\mathrm{d}}{\mathrm{d}r} \right] \mathcal{P}_l^m(r) \qquad [118b]$$

Now by substituting [115] into [111] and using [118a], we obtain the following expression for the total gravitational potential:

$$\begin{aligned} \hat{\chi}_l^m(r) &= (\hat{\chi}_0)_l^m(r) - \frac{4\pi a_1 G}{2l+1} \left(\frac{r}{a_1}\right)^l \left[X_l^m(a_1) - \frac{\rho_0}{g_0} \hat{\chi}_l^m(a_1) \right] \\ &\quad + \frac{4\pi a_2 G}{2l+1} \left(\frac{a_2}{r}\right)^{l+1} \left[X_l^m(a_2) - \frac{\rho_0}{g_0} \hat{\chi}_l^m(a_2) \right] \end{aligned} \qquad [119]$$

The boundary potentials $\hat{\chi}_l^m(a_1)$ and $\hat{\chi}_l^m(a_2)$ are determined by solving the coupled equations obtained by evaluating [119] at $r = a_1$ and $r = a_2$, and are then eliminated from [119]. Next, the resulting equation for $\hat{\chi}_l^m$ is rewritten as a convolution integral using [114], [118b], [104], [105], and [110]. Finally, the result is evaluated at $r = a_1$ to obtain the surface potential

$$\hat{\chi}_l^m(a_1) = -\frac{4\pi a_1 G}{2l+1} \int_{a_2}^{a_1} G_l(r') \hat{\rho}_l^m(r') \mathrm{d}r' \qquad [120]$$

where the Green function or kernel G_l is

$$G_l(r) = \left(1 - K_1 + K_2 K_r \beta^{2l+1}\right)^{-1} \left(\frac{r}{a_1}\right)^{l+2} \times \left\{ 1 - K_r \beta \left(\frac{a_2}{r}\right)^{2l+1} - E_1 \left(1 - K_r \beta^{2l+2}\right) \left(\frac{a_1}{r}\right)^{l+2} - E_2 (1 - K_r \beta) \left(\frac{a_2}{r}\right)^{l+2} \right\} \quad [121a]$$

$$E_n = \frac{l(l+2)}{2l+1} \left(\frac{a_n}{r}\right)^{l-2} \frac{(r/a_1)^{2l-1} - (a_2/a_n)^{2l-1}}{1 - \beta^{2l-1}} + \frac{l(l-1)}{2l+1} \left(\frac{a_n}{r}\right)^{l} \frac{(r/a_1)^{2l+3} - (a_2/a_n)^{2l+3}}{1 - \beta^{2l+3}} \quad [121b]$$

$$K_n = \frac{4\pi a_n \rho_0 G}{(2l+1) g_0}, \quad K_r = \frac{K_1}{1 + K_2}, \quad \beta = \frac{a_2}{a_1} \quad [121c]$$

Figure 9 shows $G_l(r)$ for $l = 2$ and $l = 10$, both with (solid lines) and without ($K_1 = K_2 = 0$; dashed lines) self-gravitation. The kernels are negative at all radii because the negative gravitational potential of the deformed upper surface exceeds the positive contribution of the internal mass anomaly itself. The maximum potential anomaly is produced by loads in the mid-mantle when $l = 2$, and in the upper mantle when $l = 10$. The effect of self-gravitation is nearly a factor of 2 for $l = 2$, but only about 10% for $l = 10$.

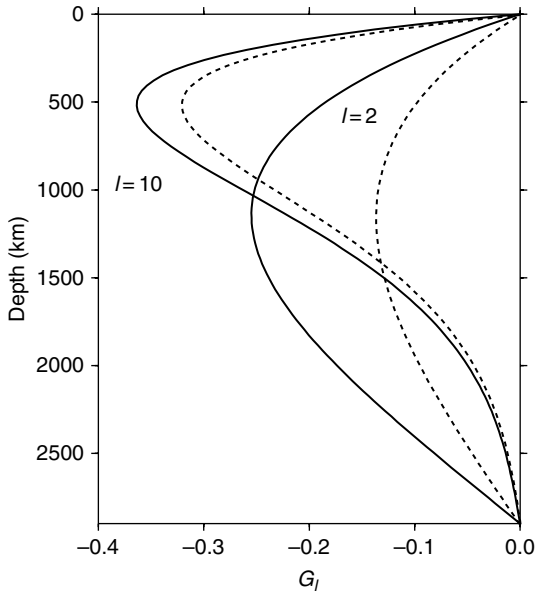

Figure 9 Gravitational potential kernels $G_l(r)$ defined by [121] as functions of depth for spherical harmonic degrees $l = 2$ and $l = 10$, with (solid lines) and without (dashed lines) self-gravitation.

An expression analogous to [121] for a mantle comprising an upper layer $r > a_1 - z$ with viscosity η_U and a lower layer $r < a_1 - z$ with viscosity η_L is given by Forte and Peltier (1987). The general effect of a viscosity contrast $\eta_L/\eta_U > 1$ is to enhance the dynamic deformation of the CMB and reduce that of the upper surface. The reduced (negative) gravitational potential anomaly of the upper surface then counteracts less effectively the positive anomaly due the (sinking) load, with the result that $G_l(r)$ increases at all depths relative to the kernels for $\eta_L/\eta_U = 1$. For $\eta_L/\eta_U = 30$ and $z = 670$ km, for example, $G_{10}(r) > 0$ for all r, while $G_2(r)$ is positive in the upper mantle and negative in the lower mantle (Forte and Peltier, 1987, figure 17).

The simplest application of the kernel approach (e.g., Hager *et al.*, 1985; Forte and Peltier, 1987) is to start with a load function $\hat{\rho}(r,\theta,\phi)$ estimated from seismic tomography or the global distribution of subducted lithosphere, and then to determine by repeated forward modeling the values of η_L/η_U and z for which geoid and other anomalies (surface divergence, surface topography, etc.) predicted by formulae like [120] best match their observed counterparts on the real Earth. A robust result of the early studies that has been confirmed by later work (e.g., Mitrovica and Forte, 2004) is that the lower mantle must be more viscous than the upper mantle by a factor $\eta_L/\eta_U \sim 10 - 100$. In many of these studies, the kernels were obtained using an alternative analytical technique, the propagator matrix method, discussed next.

7.04.5.8.2 The propagator-matrix method

The analytical Green function approach outlined in Section 7.04.5.8.1 for a constant-viscosity mantle can in principle be extended to models comprising any number N of discrete layers with different viscosities. In practice, however, the rapidly increasing complexity of the analytical expressions limits the method to $N = 2$ (Forte and Peltier, 1987). A more efficient approach for models with multiple layers is the propagator-matrix method, whereby a flow solution is propagated from one layer interface to the next by simple matrix multiplication. The method is in fact applicable to any system of linear ODEs with constant coefficients of the form

$$\frac{d\mathbf{y}}{dz} = \mathbf{A}\mathbf{y} + \mathbf{b}(z) \quad [122]$$

where $\mathbf{y}(z)$ is a vector of dependent variables, $\mathbf{A}$ is a constant square matrix, and $\mathbf{b}(z)$ is an inhomogeneous

vector. The general solution of [122] is (Gantmacher, 1960, I, p. 120, eqn [53])

$$\mathbf{y}(z) = \mathbf{P}(z,\ z_0)\mathbf{y}(z_0) + \int_{z_0}^{z} \mathbf{P}(z,\ \zeta)\mathbf{b}(\zeta)\mathrm{d}\zeta \qquad [123a]$$

$$\mathbf{P}(z,\ z_0) = \exp[\mathbf{A}(z-z_0)] \qquad [123b]$$

where $\mathbf{y}(z_0)$ is the solution vector at the reference point $z = z_0$ and $\mathbf{P}(z,\ z_0)$ is the propagator matrix. The form of the solution [123] is identical to that for a scalar variable $y(z)$, except that the argument of the exponential in [123b] is now a matrix rather than a scalar quantity. Analytical expressions for functions of matrices such as [123b] are given by Gantmacher (1960, vol. I, pp. 95–110).

As an illustration, we determine the propagator matrix for a poloidal flow driven by internal density anomalies in a self-gravitating spherical shell with radially variable viscosity $\eta(r)$ and laterally averaged density $\rho(r)$ (Hager and O'Connell, 1981; Richards and Hager, 1984). As in Section 7.04.5.8.1, we suppose that the driving density anomaly is $\hat{\rho}_l^m(r)Y_l^m(\theta,\phi)$, where Y_l^m is a surface spherical harmonic.

The first step is to transform the equations governing the flow in the mantle to the canonical form [122], where $\mathbf{A}$ – to repeat – is a constant matrix. The standard Stokes equations [31] for our model mantle do not have this form for three reasons: (1) the fluid properties $\eta(r)$ and $\rho(r)$ vary with radius; (2) the expression for the differential operator $\boldsymbol{\nabla}$ in spherical coordinates involves the scale factor r^{-1}; and (3) a system of first-order equations cannot be written in terms of the primitive variables u_i and p. Difficulty (1) is circumvented by dividing the mantle into N discrete layers $n = 1, 2, \ldots, N$, in each of which the viscosity η_n and the density ρ_n is constant. Difficulty (2) is overcome by using a transformed radial variable $z = \ln(r/a_1)$, where a_1 is the outer radius of the mantle. Finally, one circumvents (3) by using the independent variables

$$\mathbf{y} = \left[\hat{u},\ \hat{v},\ \frac{r\hat{\sigma}_{rr}}{\eta_0},\ \frac{r\hat{\sigma}_{r\theta}}{\eta_0},\ \frac{\rho_0 r\hat{\chi}}{\eta_0},\ \frac{\rho_0 r^2\partial_r\hat{\chi}}{\eta_0}\right]^{\mathrm{T}} \qquad [124]$$

where $\hat{u}$ and $\hat{v}$ are the $\mathbf{e}_r$- and $\mathbf{e}_0$-components of the velocity, respectively, η_0 and ρ_0 are reference values of the viscosity and density, respectively, and the spherical harmonic dependence of each variable ($\hat{u}$, $\hat{\chi}_{rr}$, $\hat{\chi}$, and $\partial_r\hat{\chi} \propto Y_l^m$, $\hat{v}$ and $\hat{\sigma}_{r\theta} \propto \partial_\theta Y_l^m$) has been suppressed for clarity. The Stokes equations within each layer n then takes the form [122] with

$$\mathbf{A} = \begin{bmatrix} -2 & L & 0 & 0 & 0 & 0 \\ -1 & 1 & 0 & 1/\eta^* & 0 & 0 \\ 12\eta^* & -6L\eta^* & 1 & L & 0 & \rho^* \\ -6\eta^* & 2(2L-1)\eta^* & -1 & -2 & \rho^* & 0 \\ 0 & 0 & 0 & 0 & 1 & 1 \\ 0 & 0 & 0 & 0 & L & 0 \end{bmatrix} \qquad [125a]$$

$$\mathbf{b} = \left[0,\ 0,\ r^2 g_0(r)\hat{\rho}(r)/\eta_0,\ 0,\ 0,\ -4\pi r^3 G\rho_0\hat{\rho}(r)/\eta_0\right]^{\mathrm{T}} \qquad [125b]$$

where $L = l(l+1)$, $\eta^* = \eta_n/\eta_0$, and $\rho^* = \rho_n/\rho_0$. Further simplification is achieved by recasting the density anomaly $\hat{\rho}(r)$ as a sum of equivalent surface density contrasts $\hat{\sigma}_n$ (units kg m^{-2}) localized at the midpoints r_n of the layers, according to

$$\hat{\rho}(r) = \sum_n \delta(r-r_n)\hat{\sigma}_n \qquad [126]$$

In practice, $\hat{\sigma}_n$ is different in each layer, while η_n and ρ_n may be constant over several adjacent layers. For a group of M such adjacent layers bounded by the depths z and z_0, the solution [123a] now takes the approximate form

$$\mathbf{y}(z) = \mathbf{P}(z,\ z_0)\mathbf{y}(z_0) + \sum_{m=1}^{M} \mathbf{P}(z,\ z_m)\mathbf{b}_m \qquad [127a]$$

$$\mathbf{b}_m = \left[0,\ 0,\ r_m g_0(r_m)\hat{\sigma}_m/\eta_0,\ 0,\ 0,\ -4\pi r_m^2 G\rho_0\hat{\sigma}_m/\eta_0\right]^{\mathrm{T}} \qquad [127b]$$

where $z_m = \ln(r_m/a_1)$. To use [127], one must apply boundary conditions at the CMB and at the Earth's surface, taking into account the dynamic topography of these boundaries (Richards and Hager, 1984, Appendix 1).

An analytical expression for $\mathbf{P}(z,\ z_0)$ can be written in terms of the minimal polynomial $\psi(\lambda)$ of $\mathbf{A}$. For the matrix [125a], $\psi(\lambda)$ is identical to the characteristic polynomial, and is

$$\psi(\lambda) = \prod_{i=1}^{4}(\lambda-\lambda_i)^{m_i} \qquad [128a]$$

$$\lambda_1 = l+1, \quad \lambda_2 = -l, \quad \lambda_3 = l-1, \quad \lambda_4 = -l-2 \qquad [128b]$$

$$m_1 = m_2 = 2, \quad m_3 = m_4 = 1 \qquad [128c]$$

where λ_1–λ_4 are the four distinct eigenvalues of $\mathbf{A}$. Following Gantmacher (1960, I, pp. 95–102)

$$\mathbf{P}(z,\ z_0) = \sum_{k=1}^{4}\sum_{j=1}^{m_k} \alpha_{kj}(\mathbf{A}-\lambda_k\mathbf{I})^{j-1}\Psi_k \qquad [129]$$

where

$$\alpha_{kj} = \frac{1}{(j-1)!}\frac{\mathrm{d}^{j-1}}{\mathrm{d}\lambda^{j-1}}\left[\frac{\exp\lambda(z-z_0)}{\psi_k(\lambda)}\right]_{\lambda=\lambda_k} \qquad [130]$$

$$\psi_k(\lambda) = \frac{\psi(\lambda)}{(\lambda-\lambda_k)^{m_k}}, \quad \Psi_k = \prod_{\substack{i=1\\ i\neq k}}^{4}(\mathbf{A}-\lambda_i\mathbf{I})^{m_i} \qquad [131]$$

and $\mathbf{I}$ is the identity matrix.

7.04.6 Elasticity and Viscoelasticity

Fluid convection with a period $\tau \sim 10^{15}$ s is the extreme limit of a spectrum of deformational processes in the mantle spanning an enormous range of timescales, including postglacial rebound ($\tau \sim 10^{11}$ s), the Chandler wobble ($\tau \sim 4\times 10^{7}$ s), and elastic free oscillations ($\tau \sim 10$–10^{3} s). All these processes can be understood by regarding the mantle as a viscoelastic body that deforms as a fluid when $\tau \gg \tau_{\mathrm{M}}$ and as an elastic solid when $\tau \ll \tau_{\mathrm{M}}$, where τ_{M} is the Maxwell time of the material. τ_{M} is just the ratio of the viscosity of the material to its elastic shear modulus, and is of the order of a few hundred years ($\sim 10^{10}$ s) in the mantle.

Because the theory of viscous flow is valid only at very long-periods ($\tau \gg \tau_{\mathrm{M}}$), other rheological models are required to understand phenomena with shorter periods. The two most commonly used models are the linear elastic solid (for short periods $\tau \ll \tau_{\mathrm{M}}$) and the linear Maxwell solid (for intermediate periods $\tau \sim \tau_{\mathrm{M}}$.) The reader is referred to Chapter 7.06 for a more extensive discussion of these models. Here we focus on the mathematical analogies (correspondence principles) among the viscous, elastic, and viscoelastic models and the powerful analytical techniques these analogies make possible.

7.04.6.1 Correspondence Principles

Stokes (1845) and Rayleigh (1922) demonstrated the existence of a mathematical correspondence (the Stokes–Rayleigh analogy) between small incompressible deformations of an elastic solid and slow flows of a viscous fluid. As discussed in Chapter 7.06, the constitutive law for a linear (Hookean) elastic solid is

$$\sigma_{ij} = Kv_{kk}\delta_{ij} + 2\mu\left(v_{ij} - \frac{1}{3}v_{kk}\delta_{ij}\right) \qquad [132]$$

where σ_{ij} is the stress tensor, $v_{ij} \equiv (\partial_i v_j + \partial_j v_i)/2$ is the linearized strain tensor, v_i is the displacement vector, K is the bulk modulus, and μ is the shear modulus. Alternatively, [132] can be written in terms of the Young's modulus E and Poisson's ratio σ, which are related to K and μ by

$$E = \frac{9K\mu}{3K+\mu}, \quad \sigma = \frac{3K-2\mu}{2(3K+\mu)} \qquad [133]$$

An incompressible elastic solid corresponds to the limits $K/E \to \infty$, $\sigma \to 1/2$, and an incompressible deformation to the limit $\Delta \to 0$. As these limits are approached, however, the product $-K\Delta$ tends to a finite value, the pressure p. Equation [132] then becomes

$$\sigma_{ij} = -p\delta_{ij} + 2\mu v_{ij} \qquad [134]$$

which is identical to the constitutive relation [31e] for a viscous fluid if the shear modulus μ and the displacement v_i are replaced by the viscosity η and the velocity u_i, respectively. Consequently, solutions of problems in linear elasticity and Stokes flow can be transformed into one another via the transformations

$$(v_i,\ E,\ \sigma) \to (u_i,\ 3\eta,\ 1/2), \quad (u_i,\ \eta) \to (v_i,\ \mu) \qquad [135]$$

Examples of the use of [135] are described in Section 7.04.8.4 on thin-shell theory.

A second useful correspondence principle relates problems in linear viscoelasticity and linear elasticity. Although this principle is valid for any linear viscoelastic body (Biot, 1954), its geophysical application is usually limited to the special case of a linear Maxwell solid, for which the constitutive relation is (e.g., Peltier, 1974)

$$\dot{\sigma}_{ij} + \frac{\mu}{\eta}\left(\sigma_{ij} - \frac{1}{3}\sigma_{kk}\delta_{ij}\right) = 2\mu\left(\dot{v}_{ij} - \frac{1}{3}\dot{v}_{kk}\delta_{ij}\right) + K\dot{v}_{kk}\delta_{ij} \qquad [136]$$

where dots denote time derivatives. Transforming [136] into the frequency domain using a Laplace transform as described in Chapter 7.06, we obtain

$$\bar{\sigma}_{ij} = K\bar{v}_{kk}\delta_{ij} + 2\bar{\mu}(s)\left(\bar{v}_{ij} - \frac{1}{3}\bar{v}_{kk}\delta_{ij}\right) \qquad [137a]$$

$$\bar{\mu}(s) = \frac{\mu s}{s+\mu/\eta} \qquad [137b]$$

where s is the complex frequency and overbars denote Laplace transforms of the quantities beneath. Equation

[137] is identical in form to Hooke's law [132] for an elastic solid, but with a frequency-dependent shear modulus $\bar{\mu}$. Accordingly, any viscoelastic problem can be reduced to an equivalent elastic problem, which can be solved and then inverse-Laplace transformed back into the time domain to yield the solution of the original viscoelastic problem. We now turn to one of the principle geophysical applications of this procedure.

7.04.6.2 Surface Loading of a Stratified Elastic Sphere

The fundamental problem of postglacial rebound is to determine the response of a radially stratified Maxwell Earth to a time-dependent surface load $P(\theta, \phi, t)$ that represents the changing global distribution of glacial ice and meltwater. Formally, this problem can be solved by convolving the load distribution with a Green function that describes the Earth's response to an impulsive point load applied at time t at a point $\mathbf{r}$ on the Earth's surface and then immediately removed. Now an impulse function in the time domain corresponds to a constant in the frequency domain. According to the correspondence principle, therefore, our problem reduces to that of determining the deformation of a stratified elastic sphere by a static point load (Longman, 1962; Farrell, 1972; Peltier, 1974). The derivation below follows Peltier (1995).

The general equations governing the deformation of a self-gravitating elastic sphere are (Backus, 1967)

$$0 = \nabla \cdot \hat{\boldsymbol{\sigma}} + \mathbf{g}_0\hat{\rho} - \rho_0\nabla\hat{\chi} - \nabla(\rho_0 g_0 \hat{u}) \qquad [138a]$$

$$\nabla^2\hat{\chi} = 4\pi G\hat{\rho} \qquad [138b]$$

where $\hat{\mathbf{v}} \equiv \hat{u}\mathbf{e}_r + \hat{v}\,\mathbf{e}_\theta + \hat{w}\mathbf{e}_\phi$ is the displacement vector and the other symbols are the same as in the analogous equations [100] for slow viscous flow.

The elastic equations [138b] differ from their viscous analogs [100] in three ways. First, the stress tensor $\hat{\boldsymbol{\sigma}}$ in [138a] is related to the displacement vector $\hat{\mathbf{v}}$ by the elastic constitutive law [137] with a frequency-dependent shear modulus. Second, because the deformation is driven by surface loading rather than by internal density anomalies, the perturbation density $\hat{\rho} \equiv -\nabla \cdot (\rho_0\hat{\mathbf{v}})$ is determined entirely by the requirement of mass conservation in the deformed solid. Third, [138a] contains an additional term $-\nabla(\rho_0 g_0 \hat{u})$, that corrects for the fact that the strain tensor that appears in the elastic constitutive law is at a fixed material particle and not at a fixed point in space (Backus, 1967, p. 96).

The reduction of the governing equations [138] to solvable form proceeds as for the viscous flow equations in Section 7.04.5.8.2, but with a few significant differences. As in the viscous case, the goal is to reduce [138] to a sixth-order system of ODEs of the form

$$\frac{\mathrm{d}\mathbf{y}}{\mathrm{d}r} = \mathbf{A}\mathbf{y} \qquad [139]$$

where $\mathbf{y}$ is the unknown vector and $\mathbf{A}$ is a 6×6 matrix. Equation [139] contains no inhomogeneous vector $\mathbf{b}$ like the one in the viscous equations [122], because the loads in the elastic problem are applied at the boundaries rather than internally. Another important point is that the reference profiles of density $\rho_0(r)$ and the elastic moduli $\mu(r)$ and $K(r)$ that appear in the equations are essentially continuous functions, given *a priori* by a seismological reference model (e.g., PREM; Dziewonski and Anderson, 1981). Consequently, a discrete-layer solution method like the propagator-matrix technique is not practical, and it is therefore superfluous to reduce [139] to constant-coefficient form via the transformation $z = \ln(r/a_1)$.

We turn now to the definition of the variables $\mathbf{y}$. By symmetry, the deformation of the sphere can depend only on the radius r and the angular distance θ from the point load. The field variables can therefore be expanded as

$$\hat{\mathbf{v}} = \sum_{l=0}^{\infty}[\hat{u}_l(r,\ s)P_l(\cos\theta)\mathbf{e}_r + \hat{v}_l(r,\ s)\partial_\theta P_l(\cos\theta)\mathbf{e}_\theta] \qquad [140a]$$

$$\hat{\chi} = \sum_{l=0}^{\infty}\hat{\chi}_l(r,\ s)P_l(\cos\theta) \qquad [140b]$$

where $P_l(\cos\theta)$ are the Legendre polynomials. Now for each angular degree l, let

$$\mathbf{y} = \left[\hat{u},\ \hat{v},\ \hat{\sigma}_{rr},\ \hat{\sigma}_{r\theta},\ \hat{\chi},\ \partial_r\hat{\chi} + (l+1)\hat{\chi}/r + 4\pi G\rho_0\hat{u}\right]^{\mathrm{T}} \qquad [141]$$

where the subscript l on each variable has been suppressed for simplicity. Apart from factors of r, the definition of y_6, and the replacement of velocities by displacements, [141] is identical to its viscous analog [124]. With the choice [141], the matrix $\mathbf{A}$ in [139] is

$$\mathbf{A} = \begin{bmatrix} -\dfrac{2\lambda}{\beta r} & \dfrac{L\lambda}{\beta r} & \dfrac{1}{\beta} & 0 & 0 & 0 \\ -r^{-1} & r^{-1} & 0 & \bar{\mu}^{-1} & 0 & 0 \\ \dfrac{4}{r}\left(\dfrac{\gamma}{r}-\rho_0 g_0\right) & -\dfrac{L}{r}\left(\dfrac{2\gamma}{r}-\rho_0 g_0\right) & -\dfrac{4\bar{\mu}}{\beta r} & \dfrac{L}{r} & -\dfrac{\rho_0 M}{r} & \rho_0 \\ \dfrac{1}{r}\left(\rho_0 g_0-\dfrac{2\gamma}{r}\right) & \dfrac{L(\gamma+\bar{\mu})-2\bar{\mu}}{r^2} & -\dfrac{\lambda}{\beta r} & -\dfrac{3}{r} & \dfrac{\rho_0}{r} & 0 \\ -4\pi G\rho_0 r & 0 & 0 & 0 & -\dfrac{M}{r} & 1 \\ -\dfrac{4\pi MG\rho_0}{r} & \dfrac{4\pi LG\rho_0}{r} & 0 & 0 & 0 & \dfrac{l-1}{r} \end{bmatrix} \quad [142]$$

where $L = l(l+1)$, $M = l+1$, $\beta = K + 4\bar{\mu}/3$, $\gamma = 3K\bar{\mu}/\beta$, $\lambda = K - 2\bar{\mu}/3$, and $\bar{\mu}$ is defined by [137b]. The system [139] can be solved by a standard numerical method for two-point boundary-value problems (BVPs) (e.g., shooting) subject to appropriate boundary conditions. Inversion of the resulting solution back into the time domain and its subsequent convolution with a given time-dependent surface load function are then performed numerically. The use of this procedure to infer the mantle viscosity profile $\eta(r)$ is reviewed by Peltier (1995).

7.04.7 BL Theory

Many geophysical flows occur in layers or conduits whose length greatly exceeds their thickness: examples include TBLs, subducted oceanic lithosphere, mantle plume stems, and gravity currents of buoyant plume material spreading beneath the lithosphere. In all these cases, the gradients of the fluid velocity and/or temperature across the layer greatly exceed the gradients along it, a fact that can be exploited to simplify the governing equations substantially. The classic example of this approach is BL theory, which describes the flow in layers whose thickness is controlled by a balance of diffusion and advection.

A BL is defined as a thin region in a flow field, usually adjoining an interface or boundary, where the gradients of some quantity transported by the fluid (e.g., vorticity, temperature, or chemical concentration) are large relative to those elsewhere in the flow. Physically, BLs arise when the boundary acts as a source of the transported quantity, which is then prevented from diffusing far from the boundary by strong advection. BLs thus occur when $UL/D \gg 1$, where U and L are characteristic velocity and length scales for the flow and D is the diffusivity of the quantity in question. In classical BL theory, the transported quantity is vorticity, the relevant diffusivity is the kinematic viscosity ν, and BLs form when the Reynolds number $Re \equiv UL/\nu \gg 1$. Such BLs do not occur in the mantle, where $Re \sim 10^{-20}$. However, because the thermal diffusivity $\kappa \sim 10^{-23}\nu$, the Peclet number $UL/\kappa \gg 1$ for typical mantle flows, implying that TBLs will be present.

Although BLs are 3-D structures in general, nearly all BL models used in geodynamics involve one of the three simple geometries shown in **Figure 10**: 2-D flow (1), an axisymmetric plume (2), and axisymmetric flow along a surface of revolution (3). Let x and y be the coordinates parallel to and normal to the boundary (or symmetry axis), respectively, u and v be the corresponding velocity components, and $\delta(x)$ be the thickness of the BL.

The fundamental hypothesis of BL theory is that gradients of the transported quantity (heat in this case) along the BL are much smaller than those across it. Diffusion of heat along the layer is therefore negligible. As an illustration, consider the simplest case of a thermal BL in steady flow with negligible viscous

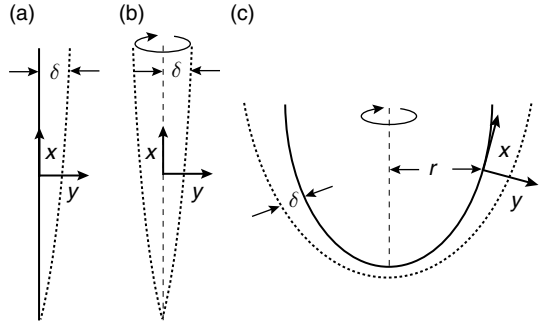

Figure 10 Typical geometries for boundary-layer flows: (a) 2-D flow, (b) an axisymmetric plume, and (c) axisymmetric flow along a surface of revolution. Impermeable boundaries are shown by heavy lines, axes of symmetry by light dashed lines, and the edges of BLs by heavy dashed lines. The coordinates x and y are parallel to and normal to the boundary (or symmetry axis), respectively, $\delta(x)$ is the thickness of the BL, and $r(x)$ is the radius of the surface of revolution.

dissipation of energy. The BL forms of the continuity and energy equations are then

$$u_x + v_y = 0, \qquad [143a]$$

$$uT_x + vT_y = \kappa T_{yy} \qquad [143b]$$

for 2-D flow,

$$u_x + y^{-1}(yv)_y = 0 \qquad [144a]$$

$$uT_x + vT_y = \kappa y^{-1}\left(yT_y\right)_y \qquad [144b]$$

for an axisymmetric plume, and

$$(ru)_x + rv_y = 0 \qquad [145a]$$

$$uT_x + vT_y = \kappa T_{yy} \qquad [145b]$$

for a surface of revolution. As noted in Section 7.04.3.3, the terms uT_x and vT_y are of the same order.

7.04.7.1 Solution of the BL Equations Using Variable Transformations

A powerful technique for solving problems involving BLs is the use of variable transformations to reduce the BL equations to equations of simpler form. One of the most important of these transformations is that of Von Mises (1927), which transforms the 2-D BL equations into the classical heat conduction equation. A second useful transformation, due to Mangler (1948), relates the structure of an axisymmetric BL on a surface of revolution to that of a 2-D BL on a flat surface. After introducing both transformations, we will show how they can be used together to obtain a solution for the heat transfer from a hot sphere moving in a viscous fluid (**Figure 1(a)**).

7.04.7.1.1 Von Mises's transformation

The essential trick involved in this transformation is to use the streamfunction ψ instead of y as the transverse coordinate in the BL. Denoting the streamwise coordinate by a new symbol $s \equiv x$ for clarity, we transform the derivatives in [143b] using the chain rule as

$$\frac{\partial T}{\partial x} = \frac{\partial T}{\partial s}\frac{\partial s}{\partial x} + \frac{\partial T}{\partial \psi}\frac{\partial \psi}{\partial x} \equiv \frac{\partial T}{\partial s} - v\frac{\partial T}{\partial \psi} \qquad [146]$$

$$\frac{\partial T}{\partial y} = \frac{\partial T}{\partial s}\frac{\partial s}{\partial y} + \frac{\partial T}{\partial \psi}\frac{\partial \psi}{\partial y} \equiv u\frac{\partial T}{\partial \psi} \qquad [147]$$

where the streamfunction is defined according to the convention $(u, v) = (\psi_y, -\psi_x)$. Equation [143b] then becomes

$$\frac{\partial T}{\partial s} = \kappa\frac{\partial}{\partial \psi}\left(u\frac{\partial T}{\partial \psi}\right) \qquad [148]$$

Equation [148] takes still simpler forms if the surface $y = \psi = 0$ is either traction-free or rigid. Near a free surface, $u \approx U(s)$ is constant across the BL. Upon introducing a new downstream coordinate τ such that $d\tau = U(s)\mathrm{d}s$, [148] becomes

$$\frac{\partial T}{\partial \tau} = \kappa\frac{\partial^2 T}{\partial \psi^2} \qquad [149]$$

which is just the classical equation for diffusion of heat in a medium with constant thermal diffusivity κ. The units of the time-like variable τ, however, are now those of diffusivity ($\mathrm{m^2\,s^{-1}}$) rather than of time. Near a rigid surface, $u = yf(s)$ and $\psi = y^2 f(s)/2$, implying $u \approx (2\psi f)^{1/2}$, where $f(s)$ is arbitrary. Substituting this result into [148] and introducing a new downstream variable τ such that $\mathrm{d}\tau = (2f)^{1/2}\mathrm{d}s$, we obtain

$$\frac{\partial T}{\partial \tau} = \kappa\frac{\partial}{\partial \psi}\left(\psi^{1/2}\frac{\partial T}{\partial \psi}\right) \qquad [150]$$

which describes the diffusion of heat in a medium with a position-dependent thermal diffusivity $\kappa\psi^{1/2}$ as a function of a time-like variable τ having units of $\mathrm{m\,s^{-1/2}}$.

Of special interest are the self-similar solutions of [149] and [150] that exist when the wall temperature T_0 is constant ($= \Delta T$, say) and the upstream temperature profile is $T(0, \psi) = 0$. The solution of the free-surface equation [149] has the form $T = \Delta T F(\eta)$, where $\eta = \psi/\delta(\tau)$. Separating variables, we obtain $-F''/\eta F' = \delta\dot{\delta}/\kappa = \lambda^2$ (constant), which when solved subject to the conditions $F(0) - 1 = F(\infty) = \delta(0) = 0$ yields

$$T = \Delta T\,\mathrm{erfc}\left(\frac{\psi}{2\sqrt{\kappa\tau}}\right) \qquad [151]$$

The solution of the rigid-surface equation [150] has the form $T = \Delta T F(\eta)$, where $\eta = \sqrt{\psi}/\delta(\tau)$. Separating variables, we find $-F''/4\eta^2 F' = \delta^2\dot{\delta}/\kappa = \lambda^2$ (constant), which when solved subject to $F(0) - 1 = F(\infty) = \delta(0) = 0$ with $\lambda^2 = 1/3$ for convenience gives

$$\frac{T}{\Delta T} = 1 - \frac{3}{\Gamma(1/3)}\left(\frac{4}{9}\right)^{1/3}\int_0^{\eta}\exp\left(-\frac{4}{9}x^3\right)\mathrm{d}x, \qquad \eta = \frac{\psi^{1/2}}{(\kappa\tau)^{1/3}} \qquad [152]$$

where Γ is the gamma function. Below we show how the free-surface solution [151] can be applied to the problems of heat transfer from a sphere (next subsection) and steady cellular convection (Section 7.04.9.3.3.)

7.04.7.1.2 Mangler's transformation

Mangler (1948) showed that the equations governing the axisymmetric BL on a surface of revolution with radius $r(x)$ (**Figure 10**) are related to the 2-D BL equations by the variable transformation

$$\bar{x} = \int_0^x (r/L)^2 \mathrm{d}x, \quad \bar{y} = \frac{r}{L}y, \quad \bar{u} = u, \quad \bar{v} = \frac{L}{r}\left(v + \frac{r'}{r}yu\right), \quad \bar{\psi} = L^{-1}\psi \qquad [153]$$

where the variables with and without overbars are those of the 2-D and the axisymmetric flows, respectively, L is an arbitrary constant length scale, and ψ is the Stokes streamfunction. The transformation [153], which applies equally to vorticity and thermal BLs, allows solutions of the 2-D BL equations to be transformed directly into solutions of the axisymmetric BL equations on a surface of revolution. To illustrate, we determine the heat flow from a traction-free isothermal sphere of radius a and excess temperature ΔT moving at constant speed U in a viscous fluid (**Figure 1**) by transforming the Cartesian BL solution [151], which in terms of the barred variables is

$$T = \Delta T \mathrm{erfc}\left(\frac{\bar{\psi}}{2\sqrt{\kappa\tau}}\right), \quad \tau(\bar{x}) = \int_0^{\bar{x}} \bar{u}\mathrm{d}\bar{x} \qquad [154]$$

For a sphere, $r(x) = a\sin(x/a) \equiv a\sin\theta$, and $L = a$ is the natural choice. The Stokes–Hadamard solution (Section 7.04.5.3.2) gives $\psi \approx (1/2)Uay\sin^2\theta$, and $u \approx (1/2)U\sin\theta$, and [153] implies

$$\bar{\psi} = \frac{1}{2}Uy\sin^2\theta, \quad \bar{x} = \frac{1}{2}x - \frac{a}{4}\sin\frac{2x}{a} \qquad [155]$$

The stretched downstream variable τ is therefore

$$\tau = \int_0^{\bar{x}} \bar{u}\mathrm{d}\bar{x} = \int_0^x u\frac{\mathrm{d}\bar{x}}{\mathrm{d}x}\mathrm{d}x = \frac{2}{3}aU(2 + \cos\theta)\sin^4\frac{\theta}{2} \qquad [156]$$

Substitution of [155] and [156] into [154] yields the temperature $T(y, \theta)$ everywhere in the BL, and the corresponding local Nusselt number is

$$\mathcal{N}(\theta) \equiv -\frac{a}{\Delta T}\frac{\partial T}{\partial y}(y = 0) = \left(\frac{3}{2\pi}\right)^{1/2}\frac{1 + \cos\theta}{(2 + \cos\theta)^{1/2}}Pe^{1/2} \qquad [157]$$

where $Pe = Ua/\kappa$ is the Peclet number.

Table 3 Heat transfer from a hot sphere for $Re \ll 1$: analytical predictions

Technique	Local Nusselt number $\mathcal{N}$	Validity
Dimensional analysis	fct(Pe, θ)	universal
Scaling analysis	$Pe^{1/2}$fct(θ)	$Pe \gg 1$
BL theory	$\left(\frac{3}{2\pi}\right)^{1/2}\frac{1 + \cos\theta}{(2 + \cos\theta)^{1/2}}Pe^{1/2}$	$Pe \gg 1$, $0 < \frac{\pi}{2}$

The result [157], together with our previous treatments of the hot sphere in Sections 7.04.3.1, 7.04.3.2, and 7.04.3.3, shows that BL theory represents a third stage in a hierarchy of techniques (dimensional analysis, scaling analysis, BL theory) that give progressively more detailed information about the structure of the solution in the asymptotic limit of negligible inertia ($Re \ll 1$) and $Pe \to \infty$. **Table 3** summarizes the local Nusselt number $\mathcal{N}(\theta)$ for the (traction-free) sphere predicted by each of the three techniques. Note that the cost of the increasing precision of the results is a decreasing range of validity.

7.04.7.2 The MMAE

We noted in Section 7.04.5.7 that the MMAE is a powerful method for solving problems where the field variables exhibit distinct regions characterized by very different length scales. The method is particularly well suited for BLs, whose characteristic thickness δ is much smaller than the scale L of the flow outside the BL. As an illustration of the method, consider a simple axisymmetric stagnation-point flow model for the steady temperature distribution in a plume upwelling beneath a rigid lithosphere (**Figure 11**), in which fluid with temperature T_1 and upward vertical velocity $-w_1$ at a depth $z = d$ ascends towards a rigid surface with temperature $T = T_0$. If viscous dissipation of energy is negligible, the pressure is (nearly) hydrostatic, and all physical properties of the fluid are constant, then $T(\mathbf{x})$ satisfies

$$\mathbf{u}\cdot\nabla T - \frac{g\alpha}{c_p}\mathbf{u}\cdot\hat{\mathbf{z}}T = \kappa\nabla^2 T \qquad [158]$$

where α is the thermal expansion coefficient and c_p is the heat capacity at constant pressure. The three terms in [158] represent advection of temperature

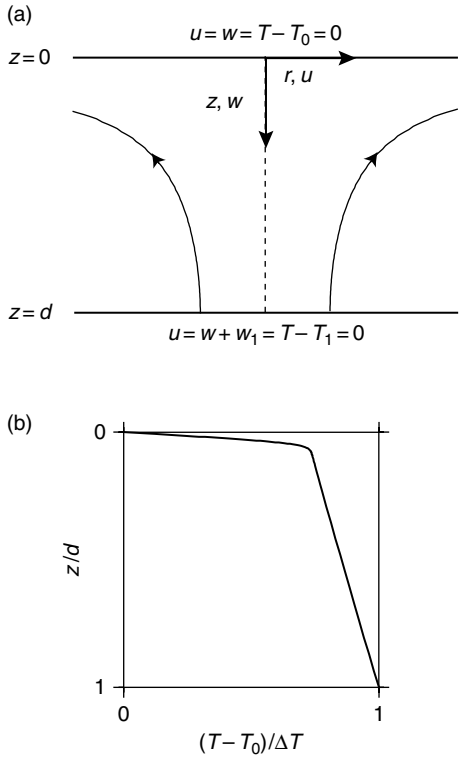

Figure 11 Model for the temperature distribution in a steady stagnation-point flow beneath a rigid lithosphere. (a) The base of the lithosphere $z = 0$ is at temperature T_0, and a uniform upward vertical velocity $w_1 > 0$ is imposed at a depth $z = d$ where the temperature is T_1. The curved lines with arrows are streamlines. (b) Temperature as a function of depth for $\epsilon = 0.0001$, $\beta = 0.1$. and $\lambda = 2.0$.

gradients, adiabatic decompression, and thermal diffusion, respectively.

Let $\mathbf{u} = u(r, z)\mathbf{e}_r + w(r, z)\mathbf{e}_z$. Because $w(r, d) \equiv -w_1$ is constant, $w = w(z)$, whence the continuity equation implies $u = -rw'(z)/2$. Equation [158] therefore admits a 1-D solution $T = T(z)$ that satisfies

$$wT' - \frac{g\alpha}{c_p} wT = \kappa T'' \qquad [159]$$

where primes denote d/dz. By substituting $w = w(z)$ and $u = -rw'(z)/2$ into the constant-viscosity Stokes equations in cylindrical coordinates and solving the resulting equation for $w(z)$ subject to the boundary conditions shown in **Figure 11**, we find

$$\frac{w}{w_1} = 2\left(\frac{z}{d}\right)^3 - 3\left(\frac{z}{d}\right)^2 \qquad [160]$$

Upon introducing dimensionless variables $\tilde{z} = z/d$ and $\tilde{T} = (T - T_0)/(T_1 - T_0) \equiv (T - T_0)/\Delta T$ and then immediately dropping the tildes, [159] together with [160] and the boundary conditions on T become

$$\left(2z^3 - 3z^2\right)[T' - \beta(T + \lambda)] = \epsilon T'' \qquad [161a]$$

$$T(0) = T(1) - 1 = 0 \qquad [161b]$$

where

$$\epsilon = \frac{\kappa}{dw_1} \equiv Pe^{-1}, \quad \beta = \frac{g\alpha d}{c_p}, \quad \lambda = \frac{T_0}{T_1 - T_0} \qquad [162]$$

We wish to solve [161] in the limit $\epsilon \to 0$ ($Pe \to \infty$), assuming for simplicity that $\beta = O(1)$ and $\lambda = O(1)$. However, note that ϵ appears in [161a] as the coefficient of the most highly differentiated term. We therefore cannot simply set $\epsilon = 0$ in [161a], because that would reduce the order of the ODE and make it impossible to satisfy all the boundary conditions. Equations [161] therefore constitute a singular perturbation problem: the solution for small values of $\epsilon > 0$ is not a small perturbation of a solution for $\epsilon = 0$, which in any case does not exist. The resolution of this apparent paradox is that the solution exhibits a thin BL where the term $\epsilon T''$ in [161a] is important, no matter how small ϵ may be.

We therefore anticipate that the solution to [161] will comprise two distinct regions governed by different dynamics: an inner region (the BL) of dimensionless thickness $\delta \ll 1$ in which advection is balanced by diffusion, and an outer region where advection is balanced by adiabatic decompression. Consider the outer region first, and let the temperature there be $T = b(z, \epsilon)$. We seek a solution in the form of an asymptotic expansion

$$b = b_0(z) + \eta_1(\epsilon)b_1(z) + \eta_2(\epsilon)b_2(z) + \cdots \qquad [163]$$

where $\eta_n(\epsilon)$ are (as yet unknown) gauge functions that form an asymptotic sequence such that $\lim_{\epsilon \to 0} \eta_n/\eta_{n-1} = 0$. The function $\eta_0(\epsilon) = 1$ because $T = O(1)$ in the outer region. Substituting [163] into [161a] and retaining only the lowest-order terms, we obtain

$$b_0' - \beta(b_0 + \lambda) = 0 \qquad [164]$$

Because [164] is a first-order ODE, its solution can satisfy only one of the boundary conditions [161b]. Evidently this must be the condition at $z = 1$, because $z = 0$ is the upper limit of a TBL that cannot be described by [164]. The same conclusion can be reached in a more formal algorithmic way by assuming contrary to fact that the BL is at $z = 1$, solving [164] subject to the wrong boundary condition $T(0) = 0$, and finally realizing that the inner solution for the supposed

BL is unphysical because it increases exponentially upward. The lowest-order terms of the (correct) boundary condition are $h_0(1)=1$, and the solution of [164] that satisfies this is

$$h_0 = (1+\lambda)\exp\beta(z-1)-\lambda \qquad [165]$$

Turning now to the inner region, the first task is to determine which term on the LHS of [161a] balances the RHS. Suppose (contrary to fact, as will soon appear) that $\beta(T+\lambda) \gg T'$ (decompression $\gg$ advection). Because $z\sim\delta$ and $z^2 \gg z^3$ in the BL, the balance $z^2\beta(T+\lambda)\sim\epsilon T''$ implies $\delta\sim\epsilon^{1/4}$. But then $T' \gg \beta(T+\lambda)$, which contradicts our original assumption. The correct balance must therefore be $z^2T'\sim\epsilon T''$ (advection $\sim$ diffusion), which implies $\delta\sim\epsilon^{1/3}$ and $T' \gg \beta(T+\lambda)$, consistent with our original assumption. A more physical argument that leads to the same conclusion is to note that the vertical scale length over which adiabatic decompression is significant in the mantle ($\sim$1000 km) is much greater than a typical BL thickness.

Now that we know the thickness of the BL, we can proceed to determine its structure. To discern the thin BL distinctly, we use a sort of mathematical magnifying glass: a new stretched depth coordinate $\hat{z}=z/\delta\equiv z\epsilon^{-1/3}$ that is of order unity in the BL. Denoting the inner solution by $f(\hat{z},\ \epsilon)$ and writing [161a] in terms of $\hat{z}$, we find

$$\left(2\epsilon\hat{z}^3-3\epsilon^{2/3}\hat{z}^2\right)\left[\epsilon^{-1/3}f'-\beta(f+\lambda)\right]=\epsilon^{1/3}f'' \qquad [166]$$

where primes denote differentiation with respect to $\hat{z}$. We now seek a solution in the form

$$f = f_0(z)+\nu_1(\epsilon)f_1(z)+\nu_2(\epsilon)f_2(z)+\cdots \qquad [167]$$

where $\nu_n(\epsilon)$ are unknown gauge functions. Substituting [167] into [166] and retaining only the lowest-order terms, we obtain

$$f_0''+3\hat{z}^2f_0'=0 \qquad [168]$$

The solution of [168] that satisfies the boundary condition $f_0(0)=0$ is

$$f_0 = A\int_0^{\hat{z}}\exp\left(-x^3\right)\mathrm{d}x\equiv\frac{A}{3}\gamma\left(1/3,\ \hat{z}^3\right) \qquad [169]$$

where $\gamma(a,\ x)=\int_0^x\exp(-t)t^{a-1}\mathrm{d}t$ is the incomplete Gamma function and A is an unknown constant that must be determined by matching [169] to the outer solution [165].

The most rigorous way to do the matching is to rewrite both the inner and outer expansions in terms of an intermediate variable $z_{\mathrm{int}}=\xi(\epsilon)z$ such that $\epsilon^{-1/3}\ll\xi\ll1$, and then to choose the values of any unknown constants (A in this case) so that the two expressions agree. However, it is often possible to use a simpler matching principle, due to Prandtl, which states that the inner limit of the outer expansion must be equal to the outer limit of the inner expansion – roughly speaking, that the two expansions must match at the edge of the BL. For our problem, Prandtl's principle is

$$\lim_{\hat{z}\to\infty}f_0(\hat{z})=\lim_{z\to0}h_0(z),\quad \text{whence}\quad A=\frac{3[(1+\lambda)\exp(-\beta)-\lambda]}{\Gamma(1/3)} \qquad [170]$$

where Γ is the Gamma function.

The last step is to construct a composite expansion that is valid both inside and outside the BL. This is just the sum of the inner and outer expansions less their shared common part $h_0(z\to0)$, or

$$T = h_0(z)+[(1+\lambda)\exp(-\beta)-\lambda]\left[\frac{\gamma(1/3,\ z^3/\epsilon)}{\Gamma(1/3)}-1\right] \qquad [171]$$

The procedure described above is a first-order matching that retains only the first terms in the expansions [163] and [167]. If desired, the matching can be carried out to higher order by working back and forth between the inner and outer expansions, determining the gauge functions $\eta_n(\epsilon)$ and $\nu_n(\epsilon)$ and matching at each step. Higher-order matching often requires the use of the more rigorous intermediate matching principle; for examples see Hinch (1991), Kevorkian and Cole (1996), or the somewhat less formal treatments of Nayfeh (1973) or Van Dyke (1975). For many problems, however, first-order matching suffices to reveal the essential structure and physical significance of the solution.

The MMAE has been used to solve a variety of geophysically relevant problems involving BLs, mostly with constant viscosity. Umemura and Busse (1989) studied the axisymmetric convective flow in a cylindrical container of height d with free-slip boundaries, using the MMAE to match the interior flow to the central rising plume and the circumferential downwelling. They found that the vertical velocity in the plume is $w\sim(\kappa/d)(-\ln\epsilon)^{1/2}Ra^{2/3}$, where the dimensionless plume radius $\epsilon\equiv a/d$ satisfies $\epsilon(-\ln\epsilon)^{1/4}\sim Ra^{-1/6}$, $Ra\gg1$ being the Rayleigh number. Whittaker and Lister (2006a) studied creeping plumes from a point heat source with buoyancy flux B on an impermeable plane boundary by matching the BL flow to an outer flow that sees the plume

as a line distribution of Stokeslets. They found that the vertical velocity $w \sim (B/\nu)^{1/2}[\ln(z/z_0)]^{1/2}$, where z is the height and $z_0 = 32\pi\kappa^2\nu/B$. Whittaker and Lister (2006b) studied the dynamics of a plume above a heated disk on a plane boundary, and used the MMAE to match the flow within the plume to both an outer flow and a horizontal BL flow across the disk. The results show that the Nusselt number $N \sim Ra^{1/5}$ for a rigid boundary and $N \sim (Ra/\ln Ra)^{1/3}$ for a free-slip boundary, where $Ra \gg 1$ is defined using the disk radius. An application of the MMAE to a problem with variable viscosity (Morris, 1982) appears in the next subsection.

7.04.7.3 BLs with Strongly Variable Viscosity

In a fluid with constant viscosity and infinite Prandtl number, thermal BLs are not accompanied by vorticity BLs, because the velocity field varies on a length scale much larger than the thickness of the TBL. As a result, the velocity field within the BL can be represented by the first term of its Taylor series expansion (or its multipole expansion in the case of an axisymmetric plume; cf. Whittaker and Lister, 2006a), which greatly simplifies the task of solving the thermal BL equation. This happy state of affairs no longer obtains if the viscosity of the fluid depends on temperature, because the velocity and temperature fields are then coupled.

Most studies of variable-viscosity BLs in the geodynamics literature focus on mantle plumes in either planar (**Figure 10(a)**) or axisymmetric (**Figure 10(b)**) geometry. The basic procedure is to supplement the BL equations [143] or [144] with a simplified BL form of the vertical component of the momentum equation in which derivatives along the BL are neglected relative to those normal to it. In physical terms, this equation simply states that the buoyancy force in the plume is balanced by the lateral gradient of the vertical shear stress τ, or

$$y^{-n}\partial_y(y^n\tau) + \rho g\alpha(T - T_\infty) = 0 \qquad [172]$$

where T_∞ is the temperature far from the plume, y is the coordinate normal to the plume, and $n = 0$ or 1 for planar or axisymmetric geometries, respectively.

An important early study based on [172] in planar geometry was that of Yuen and Schubert (1976), who investigated the buoyant upwelling adjacent to a vertical, isothermal, and traction-free plane of a fluid with temperature-dependent Newtonian or power-law rheology. The governing BL equations governing admit a similarity transformation of the form

$$T = T_\infty + f(\eta), \quad \psi = x^{(n+2)/(n+3)}g(\eta), \quad \eta = yx^{-1/(n+3)} \qquad [173]$$

where ψ is the streamfunction and n is the power-law exponent. The more realistic case of an axisymmetric plume from a point source of heat in a fluid with temperature-dependent viscosity was studied by Morris (1980), Loper and Stacey (1983), and Olson *et al.* (1993). Using a similarity transformation, Morris (1980) found that the temperature on the plume axis decreases exponentially upward with a scale height $Q/12\pi k_c \Delta T_r$, where Q is the total heat flux carried by the plume, ΔT_r is the temperature change required to change the viscosity by a factor e, and k_c is the thermal conductivity. Using a simpler approach in which the functional form of the temperature profile across the plume is assumed, Olson *et al.* (1993) found a scale height equal to three times that determined by Morris (1980). Hauri *et al.* (1994) considered a similar problem, but with an empirical superexponential temperature- and depth-dependent viscosity law.

While plumes involve free or buoyancy-driven convection, variable-viscosity BLs can also arise in situations where a large-scale background flow or wind is imposed externally (forced convection). An example is the previously introduced stagnation-point flow model for the heat transfer from a hot sphere moving in a fluid with strongly temperature-dependent viscosity (**Figure 1(b)**). Using the MMAE, Morris (1982) showed that three distinct dynamical regimes occur: a conduction limit; a Stokes limit in which the flow around the sphere resembles that in an isoviscous fluid; and a lubrication limit in which most of the volume flux is carried by the low-viscosity BL adjoining the hot plate. Solutions in spherical geometry were obtained by Morris (1982) and Ansari and Morris (1985) for the lubrication limit and an intermediate (lubrication/Stokes) limit.

7.04.8 Long-Wave Theories

Long-wave theories comprise a variety of loosely related approaches whose goal is to describe the evolving thickness or shape of a thin layer. The fundamental idea underlying these approaches is the distinction between small amplitude and small slope. To take a simple example, if a 2-D fluid layer has thickness $h_0 + \Delta h \sin kx$, its surface has small

amplitude if $\Delta h/h_0 \ll 1$ and small slope (or long wavelength) if $k\Delta h \ll 1$. Long-wave theories typically exploit the fact that small slope does not imply small amplitude to derive equations governing the nonlinear (finite-amplitude) evolution of long-wave disturbances in a layer.

7.04.8.1 Lubrication Theory

Viscous flows in thin layers are common in geodynamics: examples include lava flows, the deformation of continents, and the spreading of buoyant plume material beneath the lithosphere. Such flows are described by a simplified form of the Navier–Stokes equations, called the lubrication equations because of their importance in the design of industrial lubrication bearings. To develop the theory, we return to the simple model of a viscous drop or gravity current spreading on a rigid surface sketched in **Figure 3(b)**. The lubrication equations that describe such a current can be obtained from the full Navier–Stokes equations by exploiting the fact that $h/R \equiv \epsilon \ll 1$, where h and R are the layer's characteristic thickness and lateral extent, respectively. The thinness of the layer has three important consequences: (1) The horizontal fluid velocity $\mathbf{u} \equiv u\mathbf{e}_x + v\mathbf{e}_y$ along the layer greatly exceeds the velocity w normal to it. The flow is therefore quasi-unidirectional, and inertia is negligible. (2) Derivatives of the velocity components across the layer greatly exceed the derivatives along the layer ($\partial_z \sim h^{-1} \gg \partial_x \sim \partial_y \sim R^{-1}$). (3) The pressure gradient across the layer is approximately hydrostatic. The Navier–Stokes equations then take the simplified forms

$$\nabla_1 \cdot \mathbf{u} + w_z = 0, \quad \nabla_1 p = \eta \mathbf{u}_{zz}, \quad p_z = -\rho g \qquad [174]$$

where w is the vertical velocity and $\nabla_1 = \mathbf{e}_x\partial_x + \mathbf{e}_y\partial_y$ is the horizontal gradient operator.

To illustrate the use of the lubrication equations, we determine the shape and spreading rate of an axisymmetric gravity current with constant volume V (Huppert, 1982). The geometry of this situation is that of **Figure 3(b)** except that the vertical conduit supplying fluid to the current is absent. Let r be the (horizontal) radial coordinate, $u(z, r, t)$ the radial component of the velocity, $h(r, t)$ the thickness of the current, and $R(t)$ its radius. In this (cylindrical) geometry, [174] take the forms

$$r^{-1}(ru)_r + w_z = 0, \quad p_r = \eta u_{zz}, \quad p_z = -\rho g \qquad [175]$$

Integrating [175c] subject to $p(z = h) = 0$, we obtain

$$p = \rho g(h - z) \qquad [176]$$

Next, we substitute [176] into [175b] and integrate subject to the no-slip condition on the plate ($u(0, r, t) = 0$) and vanishing traction at $z = h$. Now because the current's upper surface is nearly horizontal, the traction there $\approx \eta(u_z + w_x)$. However, $w_x \sim (h/R)^2 u_z$ in the lubrication approximation, so the condition of vanishing traction is simply $u_z(h, r, t) = 0$. The profile of radial velocity across the current is therefore

$$u = \frac{\rho g h_r}{2\eta}\left(z^2 - 2hz\right) \qquad [177]$$

where $\rho g h_r$ is the radial gradient of the hydrostatic pressure that drives the flow. Next, the continuity equation [175a] is integrated across the current subject to the impermeability condition $w(0, r, t) = 0$ to obtain

$$0 = w(h, r, t) + r^{-1}\int_0^h (ru)_r \, dz \qquad [178]$$

We now simplify [178] by using the kinematic surface condition to eliminate $w(h, r, t) \equiv h_t + u(h, r, t)h_r$; taking ∂_r outside the integral using the standard expression for the derivative of an integral with a variable limit; and evaluating the integral using [177]. We thereby find that $h(r, t)$ satisfies the nonlinear diffusion equation

$$h_t = 4\sigma r^{-1}\left(rh^3 h_r\right)_r, \quad \sigma = \frac{\rho g}{12\eta} \qquad [179]$$

where σ is the spreadability. Conservation of the current's volume requires

$$2\pi \int_0^R rh \, dr = V \qquad [180]$$

We anticipate that for long times, the current will achieve a universal self-similar shape that retains no memory of the initial shape $h(r, 0)$. Self-similarity requires that h depend on the normalized radius $\eta \equiv r/R(t) \in [0, 1]$, and conservation of volume requires $hR^2 \sim V$. We therefore seek a solution of the form

$$h = \frac{V}{R^2} H\left(\frac{r}{R}\right) \qquad [181]$$

Upon substituting [181] into [179] and [180], separating variables in the now-familiar way (see Section 7.04.4.2), and solving the resulting equations subject to the conditions $H'(0) = H(1) = R(0) = 0$, we obtain

$$H = \frac{4}{3\pi}\left(1 - \eta^2\right)^{1/3}, \quad R = \left(\frac{4096\sigma V^3 t}{81\pi^3}\right)^{1/8} \qquad [182]$$

The radius of the gravity current increases as the 1/8 power of the time.

The solution [182] is a special case of a more general class of similarity solutions of [179] studied by Gratton and Minotti (1990) using a phase-plane formalism. Rather than work with the single PDE [179], Gratton and Minotti (1990) wrote down two coupled PDEs for the thickness h and the mean horizontal velocity v, and then used a similarity transformation to reduce them to coupled ODEs. The solutions of these ODEs can be represented as segments of integral curves on a phase plane that connect singular points representing different boundary conditions such as sources, sinks, and current fronts. Gratton and Minotti (1990) give an exhaustive catalog of the solutions thus found, including a novel second kind similarity solution (cf. Section 7.04.4.2) for the evolution of an axisymmetric gravity current surrounding a circular hole.

Geophysical applications of viscous gravity-current theory include the solutions of Lister and Kerr (1989b) for the spreading of 2-D and axisymmetric currents at a fluid interface, which were applied by Kerr and Lister (1987) to the spread of subducted lithosphere along the boundary between the upper and lower mantle. In the next subsection, we discuss an extension of the theory to currents spreading on moving surfaces, which have been widely used to model the interaction of mantle plumes with a moving or rifting lithosphere.

7.04.8.2 Plume–Plate and Plume–Ridge Interaction Models

The geometry of these models was introduced in Section 7.04.2.3, and is sketched in **Figures 3(c)** and **3(d)**. Motion of a plate (or plates) with a horizontal velocity $\mathbf{U}_0(x, y)$ generates an ambient flow $\mathbf{U}(x, y, z)$ in the mantle below, which is assumed to have uniform density ρ and viscosity η_m. The plume conduit is represented as a volume source of strength Q fixed at $(x, y) = (0, 0)$ that emits buoyant fluid with density $\rho - \Delta\rho$ and viscosity $\eta_p \ll \eta_m$. This fluid spreads laterally beneath the lithosphere to form a thin layer whose thickness $h(x, y, t)$ is governed by a balance of buoyancy-driven spreading and advection by the ambient mantle flow. Strictly speaking, a correct solution of such a problem requires the simultaneous determination of the flow in both fluids subject to the usual matching conditions on velocity and stress at their interface. However, useful results can be obtained via a simpler approach in which the mantle flow $\mathbf{U}(x, y, z)$ is specified *a priori* and is assumed to be unaffected by the flow in the plume layer. Olson (1990) proposed a model of this type for a plume beneath a plate moving at constant speed U_0 (**Figure 3(c)**), and derived a lubrication equation for $h(x, y, t)$ assuming a uniform mantle flow $\mathbf{U}(x,y,z) = U_0\mathbf{e}_x$. For the important special case of a steady-state plume layer, the lubrication equation is

$$U_0 h_x = \bar{\sigma}\nabla_1^2 h^4 + Q\,\delta(x)\delta(y), \quad \bar{\sigma} = \frac{\Delta\rho g}{48\eta_p} \qquad [183]$$

The three terms in [183] represent advection, buoyancy-driven lateral spreading, and injection of the plume fluid, respectively. The spreadability $\bar{\sigma}$ is four times smaller than that for the gravity current (eqn [179]) because Olson (1990) applied a no-slip boundary condition $\mathbf{u}(x,y,h) = U_0\mathbf{e}_x$ at $z = h$, where the plume fluid is in contact with the much more viscous mantle.

The fundamental scales for the thickness h and width L of the plume fluid layer can be found via a scaling analysis of [183]. By requiring the three terms in [183] to be of the same order and noting that $\partial_x \sim \partial_y \sim \delta(x) \sim \delta(y) \sim L^{-1}$, one finds (Ribe and Christensen, 1994)

$$L \sim \frac{Q^{3/4}\bar{\sigma}^{1/4}}{U_0} \equiv L_0, \quad h \sim \left(\frac{Q}{\bar{\sigma}}\right)^{1/4} \equiv h_0 \qquad [184]$$

Further insight is provided by an analytical similarity solution of [183] that is valid far downstream ($x \gg L_0$) from the plume source. We anticipate that at these distances, the layer thickness h will vary more strongly in the direction normal to the plate motion than parallel to it, so that $\nabla_1^2 h^4 \sim (h^4)_{yy}$. Equation [183] now reduces to

$$U_0 h_x = \bar{\sigma}\left(h^4\right)_{yy}, \quad U_0 \int_{-L/2}^{L/2} h\,\mathrm{d}y = Q \qquad [185]$$

where the source strength Q now appears in an integral relation expressing conservation of the downstream volume flux. Equations [185] admit the similarity solution (Ribe and Christensen, 1994)

$$\hat{h} = \left(\frac{3}{40}\right)^{1/3} \hat{x}^{-1/5}\left(C^2 - \hat{y}^2\hat{x}^{-2/5}\right)^{1/3},$$
$$C = \left(\frac{390625}{9\pi^3}\right)^{1/10}\left[\frac{\Gamma(5/6)}{\Gamma(1/3)}\right]^{3/5} \qquad [186]$$

where $\hat{h} = h/h_0$ and $(\hat{x}, \hat{y}) = (x, y)/L_0$. The width of the plume layer increases with downstream distance as $L = 2CL_0(x/L_0)^{1/5}$. This law remains valid for more realistic 3-D numerical models with moderately temperature-and pressure-dependent viscosity (Ribe and

Christensen, 1994, 1999), but must eventually break down if the mantle/plume viscosity contrast becomes too large.

The interaction of a plume with an oceanic spreading ridge has been studied using a modified version of Olson's (1990) model in which the uniform mantle flow $\mathbf{U} = U_0\mathbf{e}_x$ is replaced by a corner flow driven by surface plates diverging with a half-spreading rate U_0 (**Figure 3(d)**; Ribe *et al.*, 1995). The balance of the source term $Q\delta(x)\delta(y)$ with vertical advection directly beneath the ridge yields a new length scale $L_1 \sim (Q/U_0)^{1/2}$, which agrees well with the along-strike extent of the plume fluid beneath the ridge (waist width) determined by laboratory experiments (Feighner and Richards, 1995) and numerical models (Ribe *et al.*, 1995.)

An important extension of the theory for geodynamical applications is to currents in which both the buoyancy and viscosity depend on temperature. Such a theory was developed by Bercovici (1994) and Bercovici and Lin (1996), who supplemented the usual lubrication theory equations with an energy equation describing the temperature distribution inside the current. They found that variable viscosity and buoyancy strongly influence the current's shape and spreading rate, which typically no longer exhibit the self-similar behavior typical of currents with constant properties.

7.04.8.3 Long-Wave Analysis of Buoyant Instability

In convecting systems such as the Earth's mantle, plumes arise as instabilities of horizontal TBLs. A long-wave model for this process has been proposed by Lemery *et al.* (2000; henceforth LRS00), based on two assumptions: that the wavelength of the initial instability greatly exceeds the BL thickness, and that the horizontal velocity of the fluid is approximately constant across the BL. These assumptions allow the coupled 3-D dynamics of the BL and the fluid outside it to be reduced to 2-D equations for the lateral velocity at the edge of the BL and a temperature moment that describes the distribution of buoyancy within it.

The domain of the model is a fluid half-space bounded by a cold traction-free surface $x_3 = 0$ held at temperature $-\Delta T$ relative to the fluid far from it (**Figure 2(b)**) The BL occupies the depth interval $x_3 < h(x_1, x_2, t)$, where x_α are Cartesian coordinates parallel to the BL and t is time. In the following, hatted and unhatted variables are those in the BL and in the interior, respectively, and an argument in parentheses indicates a value of x_3. The (constant) viscosity of the outer fluid is η_0, and the viscosity within the BL is $\hat{\eta}(x_3)$.

The starting point is the momentum equation within the BL, namely, $-\partial_i\hat{p} + \partial_j\hat{\tau}_{ij} = \rho_0\alpha g\hat{T}\delta_{i3}$, where $\hat{\tau}_{ij}$ is the deviatoric part of the stress tensor. Taking the curl of this equation, applying the continuity equation $\hat{\tau}_{33} = -\hat{\tau}_{\gamma\gamma}$, and noting that $(\partial_{11}^2\hat{\tau}_{\alpha 3}, \partial_{12}^2\hat{\tau}_{\alpha 3}, \partial_{22}^2\hat{\tau}_{\alpha 3}) \ll \partial_{33}\hat{\tau}_{\alpha 3}$ in the long-wavelength approximation, we obtain

$$\partial_{33}^2\hat{\tau}_{\alpha 3} + \partial_3\hat{A}_\alpha = -\rho_0\alpha g\partial_\alpha\hat{T}, \quad \hat{A}_\alpha = \partial_\alpha\hat{\tau}_{\gamma\gamma} + \partial_\gamma\hat{\tau}_{\alpha\gamma} \quad [187]$$

Physically, [187] are the lateral ($\alpha = 1$ or 2) components of the vorticity equation. Now multiply [187] by x_3, integrate across the BL from $x_3 = 0$ to $x_3 = h$, and take lateral derivatives outside the integral signs by neglecting the small lateral variation of the upper limit $h(x_1, x_2, t)$. The result is

$$-\hat{\tau}_{\alpha 3}(h) + h\partial_3\hat{\tau}_{\alpha 3}(h) + h\hat{A}_\alpha(h) - \langle\hat{A}_\alpha\rangle = \rho_0\alpha g\partial_\alpha M \quad [188]$$

where $\langle\rangle = \int_0^h \mathrm{d}x_3$ and

$$M = -\langle x_3\hat{T}\rangle \quad [189]$$

is the temperature moment. Now $h\partial_3\hat{\tau}_{\alpha 3}(h) \ll \hat{\tau}_{\alpha 3}(h)$ in the long-wave limit, and continuity of shear stress at $x_3 = h$ requires $\hat{\tau}_{\alpha 3}(h) = \tau_{\alpha 3}(h)$. But because the interior fluid sees the BL as a skin with zero thickness, $\tau_{\alpha 3}(h) \approx \tau_{\alpha 3}(0) \approx \eta_0\partial_3 u_\alpha(0)$. Moreover, the lateral velocity components are constant across the layer to lowest order and must match those in the interior fluid, requiring $\hat{u}_\alpha = u_\alpha(0)$ and $\hat{\tau}_{\alpha\beta} = \hat{\eta}(x_3)[\partial_\alpha u_\beta(0) + \partial_\beta u_\alpha(0)]$. Substituting these expressions into [188], we find

$$-\partial_3\mathbf{u} - \boldsymbol{\nabla}\cdot[\sigma(2\mathbf{e} - \mathbf{I}\boldsymbol{\nabla}\cdot\mathbf{u})] - \boldsymbol{\nabla}(3\sigma\boldsymbol{\nabla}\cdot\mathbf{u}) = \frac{\rho_0 g\alpha}{\eta_0}\boldsymbol{\nabla}M \quad [190]$$

where

$$\sigma = \left\langle\frac{\hat{\eta}(x_3) - \eta_0}{\eta_0}\right\rangle \quad [191]$$

is a relative excess surface viscosity, $\mathbf{u}$ is the horizontal velocity vector, $\mathbf{e}$ is the 2-D strain-rate tensor, $\boldsymbol{\nabla}$ is the 2-D gradient operator, $\mathbf{I}$ is the identity tensor, and all terms are evaluated at $x_3 = 0$. Equation [191] is an effective boundary condition that represents the influence of the BL on the interior fluid. It shows that the BL acts like an extensible skin with shear viscosity $\sigma\eta_0$ and compressional viscosity $3\sigma\eta_0$ that applies a shear stress proportional to $\boldsymbol{\nabla}M$ to the outer fluid.

The next step is to determine explicitly the flow in the outer fluid that is driven by lateral variations in M by solving the Stokes equations in the half-space $x_3 \geq 0$ subject to [190]. Evaluating the resulting solution at $x_3 = 0$, we obtain the closure relationship (LRS00, eqn [2.41])

$$\bar{\mathbf{u}}(\mathbf{k}) = \frac{i\mathbf{k}}{2k(1+2\sigma k)} \frac{\rho_0 g\alpha}{\eta_0} \bar{M}(\mathbf{k}) \qquad [192]$$

where $\mathbf{k}$ is the horizontal wave vector, $k = |\mathbf{k}|$, and overbars denote the Fourier transform. Equation [192] is only valid if σ does not vary laterally. Finally, an evolution equation for M is obtained by taking the first moment of the energy equation, yielding

$$\partial_t M + \mathbf{u} \cdot \nabla M + 2M \nabla \cdot \mathbf{u} = \kappa \left(\nabla^2 M + \Delta T \right) \qquad [193]$$

Equations [192] and [193] are three equations for $u_\alpha(x_1, x_2, t)$ and $M(x_1, x_2, t)$ that can be solved numerically subject to periodic boundary conditions in the lateral directions for a specified initial condition $M(x_1, x_2, 0)$.

An important special case of the above equations is the R–T instability of a layer with density $\rho_0 + \Delta\rho$ and viscosity $\eta_1 = \gamma\eta_0$, obtained by the transformation

$$M \to h^2 \Delta\rho / 2\rho_0 \alpha, \quad \sigma \to h(\gamma - 1), \quad \kappa \to 0 \qquad [194]$$

A linear stability analysis of [192] and [193] can now be performed by setting $h = h_0 + \tilde{h} \exp(i\mathbf{k} \cdot \mathbf{x}) \exp(st)$ and $\mathbf{u} = \tilde{\mathbf{u}} \exp(i\mathbf{k} \cdot \mathbf{x}) \exp(st)$ and linearizing in the perturbations $\tilde{h}$ and $\tilde{u}$. The resulting growth rate is $s/s_1 = \epsilon\gamma/2[1 + 2\epsilon(\gamma - 1)]$, where $\epsilon = h_0 k$ and $s_1 = g\Delta\rho h_0/\eta_1$, which agrees with the exact analytical expression [29] if $\gamma \gg \epsilon$. Equations [190]–[193] are therefore valid as long as the BL is not too much less viscous than the outer fluid.

The above equations also describe the finite-amplitude evolution of the R–T instability of a dense viscous layer over a passive half-space (Canright and Morris, 1993 ≡ CM93). Because the half-space is effectively inviscid ($\gamma \to \infty$), the closure law (192) is not meaningful, and the relevant equations are [190] and [193]. Rewriting these using [194] and noting that the first term in [190] (shear stress applied by the inviscid fluid) is negligible, we obtain

$$\nabla \left(\frac{g\Delta\rho}{4\eta_1} h^2 + h \nabla \cdot \mathbf{u} \right) + \nabla \cdot (h\mathbf{e}) = 0 \qquad [195]$$

$$\partial_t h + \nabla \cdot (h\mathbf{u}) = 0 \qquad [196]$$

which are just the dimensional forms of eqns [3.8] and [3.7], respectively, of CM93.

A remarkable feature of the eqns [192]–[193] and [195]–[196] is the existence of similarity solutions in which M or h becomes infinite at a finite time t_s, corresponding to the runaway escape of the plume from its source layer. The general form of the solution for h or $M^{1/2}$ is

$$h \text{ or } M^{1/2} = (t_s - t)^a \text{fct}\left(\frac{x}{(t_s - t)^b} \right) \qquad [197]$$

where x is the lateral or radial distance from the peak of the instability and a and b are exponents. CM93's solution of [195]–[196] gives $a = -1$ for a Newtonian fluid, whereas LRS00 solved [192]–[193] in the limit $\sigma \gg 1$ to find $a = -1/2$. The discrepancy appears to be due to the fact that LRS00 treated σ as a constant, whereas $\sigma \propto h$ in the problem studied by CM93.

7.04.8.4 Theory of Thin Shells, Plates, and Sheets

A central problem in geodynamics is to determine the response of the lithosphere to applied loads such as seamounts, plate boundary forces (ridge push, slab pull, etc.), and tractions imposed by underlying mantle convection. Such problems can be solved effectively using thin-shell theory, a branch of applied mechanics concerned with the behavior of sheet-like objects whose thickness h is much smaller than their typical radius of curvature R. This condition is evidently satisfied for the Earth's lithosphere, for which $h \approx 100$ km and $R \approx 6300$ km. A further assumption of thin-shell theory is that the stresses within the shell vary laterally on a length scale $L \gg h$. Thin-shell theory therefore properly belongs to the general class of long-wave theories.

The basic idea of thin-shell theory is to exploit the smallness of h/R to reduce the full 3-D dynamical equations to equivalent 2-D equations for the dynamics of the shell's mid-surface. Let the 3-D Cartesian coordinates of any point on this surface be $\mathbf{x}_0(\theta_1, \theta_2)$, where θ_α are coordinates on the mid-surface itself. In the most general formulations of shell theory (e.g., Niordson, 1985), θ_α are allowed to be arbitrary and nonorthogonal. Such a formulation is useful for problems involving large finite deformation, because θ_α can be treated as Lagrangian coordinates. If the deformation is small, however, it makes sense to define θ_α as orthogonal lines-of-curvature coordinates whose isolines are parallel to the two directions of principal curvature of the mid-surface at each point. This less elegant but more

readily understandable formulation is the one used in most geodynamical applications of shell theory.

Relative to lines-of-curvature coordinates, the fundamental quantities that describe the shape of the mid-surface are the principal radii of curvature R_α and the Lamé parameters $A_\alpha = |\partial_\alpha \mathbf{x}_0|$, where $\partial_\alpha = \partial/\partial_{\theta_\alpha}$. For notational convenience, let $B_\alpha = 1/A_\alpha$ and $K_\alpha = 1/R_\alpha$. All vector and tensor quantities defined on the mid-surface are expressed relative to a local orthonormal basis comprising two surface-parallel unit vectors $\mathbf{d}_1$, $\mathbf{d}_2$ and a normal vector $\mathbf{d}_3$ defined by

$$\mathbf{d}_1 = B_1\partial_1\mathbf{x}_0, \quad \mathbf{d}_2 = B_2\partial_2\mathbf{x}_0, \quad \mathbf{d}_3 = \mathbf{d}_1 \times \mathbf{d}_2 \qquad [198]$$

In the following, z is a coordinate normal to the mid-surface $z = 0$. Moreover, the repeated subscript α is not summed unless explicitly indicated, and $\beta = 2$ when $\alpha = 1$ and vice versa.

The general equilibrium equations for a shell without inertia are (Novozhilov, 1959, p. 39)

$$\begin{aligned}&\partial_\alpha(A_\beta T_\alpha) + \partial_\beta(A_\alpha S) + S\partial_\beta A_\alpha - T_\beta\partial_\alpha A_\beta \\ &\quad + K_\alpha\left[\partial_\alpha(A_\beta M_\alpha) - M_\beta\partial_\alpha A_\beta\right. \\ &\quad \left. + 2\partial_\beta(A_\alpha H) + 2R_\alpha K_\beta H\partial_\beta A_\alpha\right] = -A_1A_2P_\alpha \qquad [199a]\end{aligned}$$

$$\begin{aligned}&\sum_{\alpha=1}^{2}\left\{B_1B_2\partial_\alpha\left[B_\alpha\left(\partial_\alpha(A_\beta M_\alpha) - M_\beta\partial_\alpha A_\beta\right.\right.\right. \\ &\quad \left.\left.\left. + \partial_\beta(A_\alpha H) + H\partial_\beta A_\alpha\right)\right] - K_\alpha T_\alpha\right\} = -P_3 \qquad [199b]\end{aligned}$$

where

$$\begin{aligned}T_\alpha &= \int_{-b/2}^{b/2}(1 + K_\beta z)\sigma_{\alpha\alpha}\,\mathrm{d}z, \\ S &= \int_{-b/2}^{b/2}(1 - K_1K_2z^2)\sigma_{12}\,\mathrm{d}z \qquad [200a]\end{aligned}$$

$$\begin{aligned}M_\alpha &= \int_{-b/2}^{b/2} z(1 + K_\beta z)\sigma_{\alpha\alpha}\,\mathrm{d}z, \\ H &= \int_{-b/2}^{b/2} z[1 + (K_1 + K_2)z/2]\sigma_{12}\,\mathrm{d}z \qquad [200b]\end{aligned}$$

P_i is the total load vector (per unit midsurface area), and $\sigma_{\gamma\lambda}$ is the usual Cauchy stress tensor. The essential content of [199] is that a loaded shell can deform in two distinct ways: by in-plane stretching and shear, the intensity of which is measured by the stress resultants T_α and S, and by bending, which is measured by the bending moments M_α and H. In general both modes are present, in a proportion that depends in a complicated way on the mid-surface shape. Shells that deform only by extension and in-plane shear ($M_\alpha = H = 0$) are called membranes.

Equations [199] are valid for a shell of any material. To solve them, we need constitutive relations that link T_α, S, M_α, and H to the displacement v_i (for an elastic shell) or the velocity u_i (for a fluid shell) of the mid-surface. For an elastic shell with Young's modulus E and Poisson's ratio σ, these are (Novozhilov, 1959, pp. 24, 48)

$$\begin{aligned}T_\alpha &= \frac{Eh}{1-\sigma^2}(\epsilon_\alpha + \sigma\epsilon_\beta), \\ M_\alpha &\frac{Eh^3}{12(1-\sigma^2)}(\kappa_\alpha + \sigma\kappa_\beta) \qquad [201a]\end{aligned}$$

$$S = \frac{Eh}{2(1+\sigma)}\omega, \quad H = \frac{Eh^3}{12(1+\sigma)}\tau \qquad [201b]$$

where

$$\epsilon_\alpha = B_\alpha\partial_\alpha v_a + B_1B_2v_\beta\partial_\beta A_\alpha + K_\alpha v_3 \qquad [202a]$$

$$\omega = \sum_{\alpha=1}^{2} A_\beta B_\alpha\partial_\alpha(B_\beta v_\beta) \qquad [202b]$$

$$\begin{aligned}\kappa_\alpha = &-B_\alpha\partial_\alpha(B_\alpha\partial_\alpha v_3 - K_\alpha v_\alpha) \\ &- B_1B_2\partial_\beta A_\alpha(B_\beta\partial_\beta v_3 - K_\beta v_\beta) \qquad [202c]\end{aligned}$$

$$\begin{aligned}\tau = &-B_1B_2\partial_{12}^2 v_3 + \sum_{\alpha=1}^{2}\left\{B_1B_2B_\alpha(\partial_\beta A_\alpha)\partial_\alpha v_3\right. \\ &\left. + K_\alpha(B_\beta\partial_\beta v_\alpha - B_1B_2u_3\partial_\beta A_\alpha)\right\} \qquad [202d]\end{aligned}$$

are the six independent quantities that describe the deformation of the mid-surface: the elongations ϵ_α and the changes of curvature κ_α in the two coordinate directions, the in-plane shear deformation ω, and the torsional (twist) deformation τ. The analogous expressions for a fluid shell are obtained by applying the transformation [135] to [201] and [202].

The above equations include all the special cases commonly considered in geodynamics. The first is that of a flat ($R_1 = R_2 = \infty$, $A_1 = A_2 = 1$) elastic plate with constant thickness h. The (uncoupled) equations governing the flexural and membrane modes are (Landau and Lifshitz, 1986)

$$\frac{Eh^3}{12(1-\sigma^2)}\nabla_1^4 v_3 = P_3 \qquad [203a]$$

$$\frac{Eh}{2(1-\sigma^2)}\left[(1-\sigma)\nabla^2\mathbf{v} + (1+\sigma)\boldsymbol{\nabla}(\boldsymbol{\nabla}\cdot\mathbf{v})\right] = -P_1\mathbf{e}_1 - P_2\mathbf{e}_2 \qquad [203b]$$

where ∇^2, $\boldsymbol{\nabla}$, and $\mathbf{v}$ are the 2D (in-plane) Laplacian operator, gradient operator, and displacement vector,

respectively, v_3 is the normal displacement, and $\mathbf{P}$ is the 3D load vector. The quantity $Eh^3/12(1-\sigma^2) \equiv D$ is called the flexural rigidity. Equation [203a] has been widely used to model the deformation of the lithosphere caused by topographic loading (e.g., Watts, 1978). McKenzie and Bowin (1976) generalized [203a] to a thick incompressible plate that need not be thin relative to the load wavelength.

A second important special case is that of a spherical shell with radius $R = R_1 = R_2$. If $\theta_1 = \theta$ (colatitude) and $\theta_2 = \phi$ (longitude), then $A_1 = R$ and $A_2 = R\sin\theta$. Turcotte (1974) used these equations in the membrane limit to estimate the magnitude of the stresses generated in the lithosphere when it moves relative to the Earth's equatorial bulge, and found that they may be large enough to cause propagating fractures. Tanimoto (1998) used the complete (membrane plus flexural) equations to estimate the displacement and state of stress in subducting lithosphere, and concluded that the state of stress is strongly influenced by the spherical geometry.

A third case is pure membrane flow in a flat fluid sheet. A well-known application is the thin-sheet model for continental deformation of England and McKenzie (1983), whose eqn, (16) is just the fluid version of [203b] with a power-law rheology of the form [31f] and an expression for P_1 and P_2 representing the lateral forces arising from variations in crustal thickness.

A final limiting case of interest is the finite-amplitude deformation of a 2-D Newtonian fluid sheet. By symmetry, $\partial_2 = u_2 = K_2 = \epsilon_2 = \omega = \kappa_2 = \tau = S = H = 0$ for this case. If $\theta_1 \equiv s$ is the arclength along the mid-surface, then $A_1 = A_2 = 1$. The instantaneous mid-surface velocity $\mathbf{u}(s, t)$ produced by a given loading distribution $P_i(s, t)$ is governed by the fluid analogs of [199]–[202], while the evolution of the mid-surface position $\mathbf{x}_0(s, t)$ and the sheet thickness $h(s, t)$ are described by the kinematic equations

$$\mathcal{D}_t \mathbf{x}_0 = \mathbf{u}, \quad \mathcal{D}_t h = -h\epsilon_1 \qquad [204]$$

where $\mathcal{D}_t$ is a convective derivative that follows the motion of material points on the (stretching) mid-surface (Buckmaster *et al.*, 1975.) Ribe (2003) used these equations to determine scaling laws for the periodic buckling instability of a viscous sheet falling onto a horizontal surface. Ribe *et al.* (2007) subsequently showed that these scaling laws predict well the anomalous apparent widening of subducted lithosphere imaged by seismic tomography at 700–1200 km depth beneath some subduction zones (e.g., Central America, Java).

7.04.8.5 Effective Boundary Conditions From Thin-Layer Flows

The interaction of a convective flow with a rheologically distinct lithosphere can be studied using a simple extension of thin-shell theory in which the shell's dynamics is reduced to an equivalent boundary condition on the underlying flow. For simplicity, we consider a flat fluid sheet with constant thickness h and laterally variable viscosity $\hat{\eta}(x_1, x_2)$, overlying a mantle whose viscosity just below the sheet is $\bar{\eta}(x_1, x_2)$. In the following, superposed hats and bars denote quantities within the sheet and in the mantle just below it, respectively.

Suppose that the sheet deforms as a membrane (cf. Section 7.04.8.4), so that the lateral velocities $\hat{u_\alpha}$ and the pressure $\hat{p}$ are independent of the depth x_3, where $x_3 = 0$ and $x_3 = -h$ are the upper and lower surfaces of the sheet, respectively. Integrating the lateral force balance $\partial_\alpha \hat{\sigma}_{\alpha\beta} + \partial_3 \hat{\sigma}_{\beta 3} = 0$ across the sheet subject to the free-surface condition $\hat{\sigma}_{\beta 3}|_{z=0} = 0$, we obtain

$$h\partial_\alpha \left[-\hat{p}\delta_{\alpha\beta} + 2\hat{\eta}\hat{e}_{\alpha\beta}\right] - \hat{\sigma}_{\beta 3}|_{z=-h} = 0 \qquad [205]$$

where $e_{\alpha\beta} = (\partial_\alpha u_\beta + \partial_\beta u_\alpha)/2$ is the strain-rate tensor. Now continuity of the velocity and stress at $x_3 = -h$ requires $\hat{u_i} = \bar{u}_i$, $\hat{e}_{\alpha\beta} = \bar{e}_{\alpha\beta}$, $\hat{\sigma}_{\beta 3}|_{z=-h} = \bar{\sigma}_{\beta 3}$, and $-\hat{p} + 2\hat{\eta}\hat{e}_{33} \equiv -\hat{p} - 2\hat{\eta}\bar{e}_{\lambda\lambda} = \bar{\sigma}_{33}$, where the continuity equation $\hat{e}_{33} = -\hat{e}_{\lambda\lambda}$ has been used. Substituting these relations into [205], we obtain an effective boundary condition that involves only mantle (barred) variables and the known viscosity $\hat{\eta}$ of the sheet:

$$h^{-1}\bar{\sigma}_{\beta 3} = 2\partial_\alpha \left[\hat{\eta}\left(\bar{e}_{\alpha\beta} + \bar{e}_{\lambda\lambda}\delta_{\alpha\beta}\right)\right] + \partial_\beta \bar{\sigma}_{33} \qquad [206]$$

Equation [206] remains valid even if the sheet has a power-law rheology [31f], because $\hat{I} \approx (\hat{e}_{\alpha\beta}\hat{e}_{\alpha\beta} + \hat{e}_{\lambda\lambda}^2)^{1/2}$ can be written in terms of the mantle variables using the matching condition $\hat{e}_{\alpha\beta} = \bar{e}_{\alpha\beta}$.

In reality, the sheet thickness is governed by the conservation law $\partial_t h = -\partial_\alpha(h\hat{u_\alpha})$, and will therefore not in general remain constant. However, this effect is ignored in most applications. Weinstein and Olson (1992) used the 1-D version of (206) with a power-law rheology for $\hat{\eta}$ to study the conditions under which a highly non-Newtonian sheet above a vigorously convecting Newtonian fluid exhibits plate-like behavior. Ribe (1992) used the spherical-coordinate analog of [206] to investigate the generation of a toroidal component of mantle flow by lateral viscosity variations in the lithosphere.

7.04.8.6 Solitary Waves

Another flow that can be studied using a long-wave approximation is the motion of finite-amplitude solitary waves in a two-fluid system. The potential importance of such waves in geodynamics was first demonstrated theoretically using equations describing the migration of a low-viscosity melt phase in a viscous porous matrix (Richter and McKenzie, 1984; Scott and Stevenson, 1984; see also Chapter 7.06) Scott *et al.* (1986) and Olson and Christensen (1986) subsequently showed that similar waves can exist in a cylindrical conduit of low-viscosity fluid embedded in a fluid of higher viscosity. These waves are examples of kinematic waves (Whitham, 1974), which occur when there is a functional relation between the density or amplitude of the medium and the flux of a conserved quantity like mass; other examples include the propagation of a pulse of wastewater down a gutter and the flow of traffic on a crowded highway.

To illustrate the basic principles, we follow here the derivation of Olson and Christensen (1986) for solitary waves in viscous conduits. Consider an infinite vertical conduit with a circular cross-section of radius $R(z, t)$ and area $A(z, t)$, where z is the height and t is time. The conduit contains fluid with density ρ_L and viscosity η_L, and is embedded in an infinite fluid with density $\rho_M \equiv \rho_L + \Delta\rho$ and viscosity $\eta_M \gg \eta_L$. Conservation of mass in the conduit requires

$$A_t + \underline{Q}_z = 0 \qquad [207]$$

where $\underline{Q}(z, t)$ is the volume flux and subscripts indicate partial derivatives. Because $\eta_M \gg \eta_L$, the fluid in the conduit sees the wall as rigid. The volume flux is therefore given by Poiseuille's law

$$\underline{Q} = -\frac{A^2}{8\pi\eta_L} P_z \qquad [208]$$

where the nonhydrostatic pressure P in the conduit is determined by the requirement that the normal stress σ_{rr} in the radial (r) direction be continuous at $r = R$. Now the pressure in the matrix is hydrostatic, and the deviatoric component of σ_{rr} in the conduit is negligible relative to that in the matrix because $\eta_M \gg \eta_L$. Continuity of σ_{rr} therefore requires $\rho_L g z - P = \rho_M g z + 2\eta_M u_r(R)$. However, because the flow in the matrix is dominantly radial, the continuity equation requires $u \propto r^{-1}$, whence $u_r(R) = -u(R)/R = -A_t/2A$ and

$$P = -\Delta\rho g z + \eta_M A^{-1} A_t \qquad [209]$$

Substituting [209] into [208] and using [207], we obtain

$$\underline{Q} = \frac{A^2}{8\pi\eta_L}\left[\Delta\rho g + \eta_M \left(A^{-1}\underline{Q}_z\right)_z\right] \qquad [210]$$

The nonlinear coupled equations [207] and [210] admit finite-amplitude traveling wave solutions wherein $A = A(z - ct)$ and $\underline{Q} = \underline{Q}(z - ct)$, where c is the wave speed. Substitution of these forms into [207] and [210] yields a dispersion relation for c as a function of the minimum and maximum amplitudes of the wave (Olson and Christensen, 1986, eqn, (22)). The most interesting case is that of an isolated solitary wave that propagates without change of shape along an otherwise uniform conduit with $A = A_0$ and $\underline{Q} = \Delta\rho g A_0^2 / 8\pi\eta_L \equiv \underline{Q}_0$. In the limit of large amplitude, the velocity of such a wave is

$$c = 2c_0 \ln(A_{max}/A_0) \qquad [211]$$

where $c_0 \equiv \underline{Q}_0/A_0$ is the average Poiseuille velocity in the conduit far from the wave and A_{max} is the maximum cross-sectional area of the wave. The speed of the wave thus increases with its amplitude.

The mathematical properties of solitary waves in deformable porous media were further investigated by Barcilon and Richter (1986), who concluded that such waves are probably not solitons, that is, that they do not possess an infinite number of conservation laws. Whitehead and Helfrich (1986) showed that the equations describing solitary waves in both porous media and fluid conduits reduce to the Korteweg–de Vries equation in the limit of small amplitude. Geophysical applications of conduit solitary waves include Whitehead and Helfrich's (1988) suggestion that such waves might transport deep-mantle material rapidly to the surface with little diffusion or contamination. Schubert *et al.* (1989) subsequently showed numerically that solitary waves can also propagate along the conduits of thermal plumes in a fluid with temperature-dependent viscosity. Such solitary waves have been invoked to explain the origin of the 'V-shaped' topographic ridges on the ocean floor south of Iceland (Albers and Christensen, 2001; Ito, 2001).

7.04.9 Hydrodynamic Stability and Thermal Convection

Not every correct solution of the governing equations of fluid mechanics can exist in nature or in the laboratory. To be observable, the solution must also

be stable, that is, able to maintain itself against the small disturbances or perturbations that are ubiquitous in any physical environment. Whether this is the case can be determined by linear stability analysis, wherein one solves the linearized equations that govern infinitesimal perturbations of a solution of interest (the basic state) to determine the conditions under which these perturbations grow (instability) or decay (stability). Typically, one expands the perturbations in normal modes that satisfy the equations and boundary conditions, and then determines which modes have a rate of exponential growth with a positive real part. However, linear stability analysis describes only the initial growth of perturbations, and is no longer valid when their amplitude is sufficiently large that nonlinear interactions between the modes become important. Various nonlinear stability methods have been developed to describe the dynamics of this stage.

Here we illustrate these methods for two geodynamically important instabilities: the R–T instability of a buoyant layer, and Rayleigh–Bénard convection between isothermal surfaces. The Section concludes with a discussion of how similar methods have been applied to thermal convection in more complex and realistic systems.

7.04.9.1 R–T Instability

We have already encountered the R–T instability in Section 7.04.4.3, where it served as an example of how intermediate asympotic limits of a function can be identified and interpreted. We now outline the linear stability analysis that leads to the expression [28] for the growth rate of infinitesimal perturbations.

The model geometry is shown in **Figure 2(a)**. The flow in both fluids satisfies the Stokes equations $\boldsymbol{\nabla} p = \eta \boldsymbol{\nabla}^2 \mathbf{u}$, which must be solved subject to the appropriate boundary and matching conditions. Let the velocities in the two layers be $\mathbf{u}_n \equiv (u_n, v_n, w_n)$. The vanishing of the normal velocity and the shear stress at $z = -h_0$ requires

$$w_1(-h_0) = \partial_z u_1(-h_0) = \partial_z v_1(-h_0) = 0 \qquad [212]$$

where the arguments x_1, x_2, and t of the variables have been suppressed. The velocity must vanish at $z = \infty$, which requires

$$u_2(\infty) = v_2(\infty) = w_2(\infty) = 0 \qquad [213]$$

Finally, continuity of the velocity and traction at the interface requires

$$[\mathbf{u} \cdot \mathbf{t}] = [\mathbf{u} \cdot \mathbf{n}] = [\mathbf{t} \cdot \boldsymbol{\sigma} \cdot \mathbf{n}] = [\mathbf{n} \cdot \boldsymbol{\sigma} \cdot \mathbf{n}] + g\Delta\rho\zeta = 0 \qquad [214]$$

where $[\ldots]$ denotes the jump in the enclosed quantity from fluid 1 to fluid 2 across the interface $z = \zeta$, σ is the nonhydrostatic stress tensor,

$$\mathbf{n} = \left(1 + |\boldsymbol{\nabla}_1 \zeta|^2\right)^{-1/2} (\mathbf{e}_z - \boldsymbol{\nabla}_1 \zeta) \qquad [215]$$

is the unit vector normal to the interface, and $\mathbf{t}$ is any unit vector tangent to the interface. Because the hydrostatic pressure gradients $-\mathbf{e}_z g\rho_n$ in the two fluids are different, the nonhydrostatic part of the normal stress jumps by an amount $-g\Delta\rho\zeta$ across the interface even though the total normal stress is continuous there. The final relation required is the kinematic condition

$$\partial_t \zeta + \mathbf{u}(\zeta) \cdot \boldsymbol{\nabla}_1 \zeta = w(\zeta) \qquad [216]$$

which expresses the fact that the interface $z = \zeta$ is a material surface.

Because the Stokes equations are linear, the nonlinearity of the problem resides entirely in the conditions [214] and [216]. To linearize them, we expand all field variables in Taylor series about the undisturbed position $z = 0$ of the interface and eliminate all terms of order ζ^2 and higher, noting that $\mathbf{u} \propto \zeta$ because the flow is driven entirely by the buoyancy associated with the disturbance of the interface. The resulting linearized matching and kinematic conditions are

$$[u] = [v] = [w] = [\sigma_{xz}] = [\sigma_{yz}] = [\sigma_{zz}] + g\Delta\rho\zeta = 0 \qquad [217]$$

$$\partial_t \zeta = w(0) \qquad [218]$$

To lowest order in η, the flow is purely poloidal (Ribe, 1998) and can be described by two poloidal potentials $\mathcal{P}_n$ (one for each of the layers $n = 0$ and 1) that satisfy $\nabla_1^2 \nabla^4 \mathcal{P}_n = 0$ (see Section 7.04.5.2). Let the (exponentially growing) deformation of the interface be $\zeta = \zeta_0 f(x, y) e^{st}$, where s is the growth rate and f is a planform function satisfying $\nabla_1^2 f = -k^2 f$, where $k \equiv |\mathbf{k}|$ is the magnitude of the horizontal wave vector $\mathbf{k}$. Then the solutions for $\mathcal{P}_n$ must have the form

$$\mathcal{P}_n = P_n(z) f(x, y) e^{st} \qquad [219]$$

Substitution of [219] into [43], [212], [213], and [217] yields the two-point BVP

$$\left(D^2 - k^2\right)^2 P_n = 0 \qquad [220a]$$

$$P_1(-h_0) = D^2P_1(-h_0) = P_2(\infty) = DP_2(\infty) = 0 \quad [220b]$$

$$[P] = [DP] = \left[\eta\left(D^2 + k^2\right)P\right]$$
$$= \left[\eta D\left(3k^2 - D^2\right)P\right] - g\Delta\rho\zeta_0 = 0 \qquad [220c]$$

where $D = \mathrm{d}/\mathrm{d}z$. The general solution of [220a] is

$$P_n = (A_n + B_n z)\mathrm{e}^{-kz} + (C_n + D_n z)\mathrm{e}^{kz} \qquad [221]$$

Substitution of [221] into [220b] and [220c] yields eight algebraic equations which can be solved for the constants $A_n - D_n$. The growth rate is then determined from the transformed kinematic condition $\zeta_0 s = -k^2 P_1(0)$, yielding [28].

The R–T instability has been used to model a variety of mantle processes. The instability of a thin layer beneath an infinite fluid half-space was studied by Selig (1965) and Whitehead and Luther (1975), and used by the latter as a model for the initiation of mantle plumes. Lister and Kerr (1989a) studied analytically the instability of a rising horizontal cylinder of buoyant fluid, motivated in part by suggestions that the R–T instability in this geometry might explain the characteristic spacing of island-arc volcanoes (Marsh and Carmichael, 1974) and of volcanic centers along mid-ocean ridges (Whitehead *et al.*, 1984). They found that the growth rate s and the most unstable wavelength are independent of the ambient fluid/cylinder viscosity ratio γ when $\gamma \gg 1$, unlike flat layers for which $s \propto \gamma^{1/3}$. Canright and Morris (1993) performed a detailed scaling analysis of the instability for two layers of finite depth (see Section 7.04.4.3), and studied the nonlinear evolution of a Newtonian or power-law layer above an effectively inviscid half-space as a model for the initiation of subduction (see Section 7.04.8.3.) Ribe (1998) used a weakly nonlinear analysis to study planform selection and the direction of superexponential growth (spouting) in the R–T instability of a two-layer system. Finally, analytical solutions of the R–T instability with more complicated rheological and density structures have been used to model the delamination of the lowermost lithosphere (Conrad and Molnar, 1997; Houseman and Molnar, 1997; Molnar and Houseman, 2004).

7.04.9.2 Rayleigh–Bénard Convection

Rayleigh–Bénard (R–B) convection in a fluid layer is the paradigmatic case of a pattern-forming instability. The classic R–B configuration (**Figure 12**) comprises fluid with constant kinematic viscosity ν and thermal diffusivity κ confined between horizontal planes $z = \pm d/2$ held at temperatures $\mp\Delta T/2$. The fluid density depends on temperature as $\rho = \rho_0(1 - \alpha T)$, where α is the coefficient of thermal expansion. The planes $z = \pm d/2$ may be either rigid or traction-free, and k is the characteristic horizontal wave number of the convection pattern. In the rest of this subsection, all variables will be nondimensionalized using d, d^2/κ, κ/d, and ΔT as scales for length, time, velocity, and temperature, respectively, and $\{x_1, x_2, x_3\} \equiv \{x, y, z\}$.

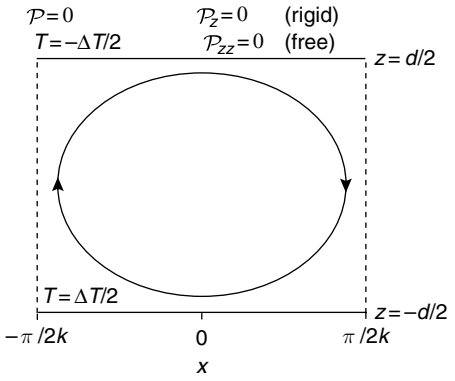

Figure 12 Geometry of Rayleigh–Bénard convection. Fluid with constant kinematic viscosity ν, thermal diffusivity κ, and thermal expansivity α is confined between horizontal planes $z = \pm d/2$ held at temperatures $\mp\Delta T/2$. The characteristic horizontal wave number of the convection pattern is k. For the special case of 2-D rolls, the roll axis is parallel to the y- direction. The boundary conditions on the poloidal scalar $\mathcal{P}$ for free and rigid boundaries are indicated above the top boundary, and subscripts denote partial differentiation.

The basic state is a motionless ($u_i = 0$) layer with a linear (conductive) temperature profile $T = -z$. Because the viscosity is constant, buoyancy forces generate a purely poloidal flow

$$u_i = \mathcal{L}_i\mathcal{P}, \quad \mathcal{L}_i = \delta_{i3}\nabla^2 - \partial_i\partial_3 \qquad [222]$$

where $\mathcal{P}$ is the poloidal potential defined by [41]. In the geodynamically relevant limit of negligible inertia, the equations satisfied by $\mathcal{P}$ and the perturbation θ of the conductive temperature profile are

$$\nabla^4\mathcal{P} = -Ra\,\theta \qquad [223a]$$

$$\theta_t + \mathcal{L}_j\mathcal{P}\partial_j\theta - \nabla_1^2\mathcal{P} = \nabla^2\theta \qquad [223b]$$

where $\nabla_1^2 = \partial_{11}^2 + \partial_{22}^2$ and

$$Ra = \frac{g\alpha d^3\Delta T}{\nu\kappa} \qquad [224]$$

is the Rayleigh number. The boundary conditions at $z = \pm 1/2$ are obtained from [41] with $\mathcal{T} = 0$, noting that $\mathcal{P}$ is arbitrary to within an additive function of z

and/or an additive function $f(x, y)$ satisfying $\nabla_1^2 f = 0$. Impermeability requires $\nabla_1^2 \mathcal{P} = 0$, which can be replaced by the simpler condition $\mathcal{P} = 0$. The no-slip condition at a rigid surface requires $\partial_{13}^2 \mathcal{P} = \partial_{23}^2 \mathcal{P} = 0$, which can be replaced by $\partial_3 \mathcal{P} = 0$. Finally, the vanishing of the tangential stress at a free surface requires $\partial_1 \left(\nabla_1^2 - \partial_{33}^2\right) \mathcal{P} = \partial_2 \left(\nabla_1^2 - \partial_{33}^2\right) \mathcal{P} = 0$, which can be replaced by $\partial_{33}^2 \mathcal{P} = 0$. In summary, the boundary conditions are

$$\theta = \mathcal{P} = \partial_{33}^2 \mathcal{P} = 0 \,(\text{free}) \qquad [225a]$$

or

$$\theta = \mathcal{P} = \partial_3 \mathcal{P} = 0 \,(\text{rigid}) \qquad [225b]$$

7.04.9.2.1 Linear stability analysis

The initial/BVP describing the evolution of small perturbations to the basic state is obtained by linearizing [223] about $(\mathcal{P},\ \theta) = (0, 0)$, reducing the resulting equations to a single equation for $\mathcal{P}$ by cross-differentiation, and recasting the boundary conditions $\theta(\pm 1/2) = 0$ in terms of $\mathcal{P}$ with the help of [223a]. For the (analytically simpler) free-boundary case, the result is

$$\left[\nabla^4 \left(\nabla^2 - \partial_t\right) - Ra \nabla_1^2\right] \mathcal{P} = 0 \qquad [226a]$$

$$\mathcal{P} = \partial_{33}^2 \mathcal{P} = \partial_{3333}^4 \mathcal{P} = 0 \text{ at } z = \pm 1/2 \qquad [226b]$$

Equations [226] admit normal mode solutions of the form

$$\mathcal{P} = P(z) f(x,\ y) e^{st} \qquad [227]$$

where σ is the growth rate and $f(x,y)$ is the planform function satisfying $\nabla_1^2 f = -k^2 f$. Substituting [227] into [226], we obtain

$$\left[\left(D^2 - k^2\right)^2 \left(D^2 - k^2 - s\right) + Ra k^2\right] P = 0 \qquad [228a]$$

$$P = D^2 P = D^4 P = 0 \text{ at } z = \pm 1/2 \qquad [228b]$$

where $D = \mathrm{d}/\mathrm{d}z$. Equations [228] define an eigenvalue problem whose solution is

$$P = \sin n\pi \left(z + \frac{1}{2}\right), \quad s = \frac{Ra\, k^2}{\left(n^2\pi^2 + k^2\right)^2} - n^2\pi^2 - k^2 \qquad [229]$$

where the index n defines the vertical wavelength of the mode. The growth rate s becomes positive when Ra exceeds a value $Ra_0(k)$ that corresponds to marginal stability. This occurs first for the mode $n = 1$, for which

$$Ra_0 = \frac{\left(\pi^2 + k^2\right)^3}{k^2} \qquad [230]$$

The most unstable wave number k_c and the corresponding critical Rayleigh number Ra_c are found by minimizing $Ra_0(k)$, yielding

$$Ra_c = \frac{27\pi^4}{4} \approx 657.5, \quad k_c = \frac{\pi}{\sqrt{2}} \approx 2.22 \qquad [231]$$

The corresponding results for convection between rigid surfaces must be obtained numerically (Chandrasekhar, 1981, pp. 36–42), and are $Ra_c \approx 1707.8$, $k_c \approx 3.117$. The marginally stable Rayleigh number $Ra_0(k)$ is shown for both free and rigid surfaces in **Figure 13(a)**. For future reference, we note that [229] can be written

$$s = \left(\pi^2 + k^2\right) \frac{Ra - Ra_0}{Ra_0} \qquad [232]$$

7.04.9.2.2 Order-parameter equations for finite-amplitude thermal convection

Linear stability analysis predicts the initial growth rate of a normal mode with wave number **k**. Typically, however, many different modes have the same or nearly the same growth rate: examples include convection rolls with the same wave number but different orientations, and rolls with the same orientation but slightly different wave numbers within a narrow band around the most unstable wave number k_c. The question therefore arises: among a set of modes with equal (or nearly equal) growth rates, which mode or combination of modes is actually realized for a given (supercritical) Rayleigh number? The answer depends on a combination of two factors: the nonlinear coupling between different modes due to the nonlinear terms in the governing equations, and external biases imposed by the initial and/or boundary conditions. Linear stability analysis is powerless to help us here, and more complicated nonlinear theories are required.

An especially powerful method of this type is to reduce the full 3-D equations governing convection to 2-D equations for one or more order parameters that describe the degree of order or patterning in the system. Newell *et al.* (1993) identified four distinct classes of such equations, depending on whether the degree of supercriticality $\epsilon \equiv \left[(Ra - Ra_c)/Ra_c\right]^{1/2}$ is small or of order unity, and whether the horizontal spectrum of the allowable modes is discrete or (quasi-) continuous (**Table 4**). The spectrum is discrete for convection in an infinite layer with a periodic planform characterized by a single fundamental wave number k, and also for a layer of finite extent $L = O(d)$ when only a few of the allowable wave

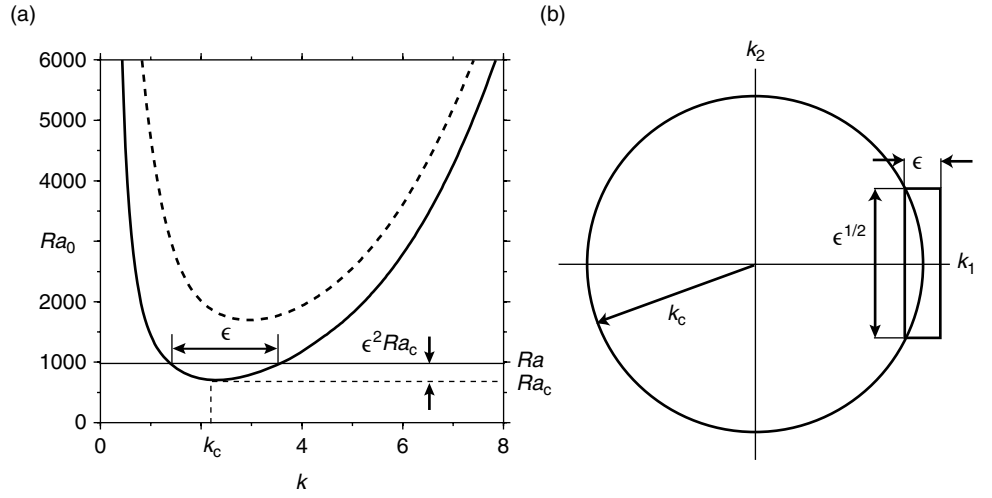

Figure 13 (a) Marginally stable Rayleigh number Ra_0 as a function of wave number k for Rayleigh–Bénard convection between traction-free (solid line) and rigid (dashed line) surfaces. The critical Rayleigh number Ra_c and wave number k_c are indicated for the free-surface case. For a slightly super-critical Rayleigh number $Ra = (1 + \epsilon^2)Ra_c$, a band of wave numbers of width $\sim \epsilon$ is unstable. (b) The most unstable wave vector $\mathbf{k} = (k_1, k_2)$ for Rayleigh–Bénard convection lies on a circle of radius k_c. Changing $|\mathbf{k}|$ by an amount $\sim \epsilon$ in the vicinity of the wave vector $(k_c, 0)$ for rolls with axes parallel to the x_2-direction corresponds to changing k_1 and k_2 by amounts $\sim \epsilon$ and $\sim \epsilon^{1/2}$, respectively (rectangle).

Table 4 Order-parameter equations for Rayleigh–Bénard convection

Spectrum	$\epsilon \ll 1$	$\epsilon = O(1)$
Discrete	amplitude equations	finite-amplitude convection rolls
Continuous	envelope equations	slowly modulated patterns

numbers $2n\pi/L$ are unstable for a given Rayleigh number. The wave numbers of the unstable modes become ever more closely spaced as L increases, until in the limit $L/d \gg 1$ they can be regarded as forming a quasi-continuous spectrum.

Historically, the first case to be studied (Malkus and Veronis, 1958) was that of a single mode with $\epsilon \ll 1$. Here the order parameter is the amplitude $A(t)$ of the dominant mode, whose temporal evolution is described by a nonlinear Landau equation (Landau, 1944). Subsequently, these weakly nonlinear results were extended to $\epsilon = O(1)$ by Busse (1967a), who used a Galerkin method to obtain numerical solutions for convection rolls and to examine their stability. The more complicated case of a continuous spectrum was first studied by Segel (1969) and Newell and Whitehead (1969), who derived the evolution equation governing the slowly varying (in time and space) amplitude envelope $A(\epsilon x, \epsilon^{1/2} y, \epsilon^2 t)$ of weakly nonlinear ($\epsilon \ll 1$) convection with modes contained in a narrow band surrounding the critical wave vector $\mathbf{k}_c = (k_c, 0)$ for straight parallel rolls. Finally, Newell *et al.* (1990) extended these results to $\epsilon = O(1)$ by deriving the phase diffusion equation that governs the slowly varying phase Φ of a convection pattern that locally has the form of straight parallel rolls. We now examine each of these four cases in turn.

7.04.9.2.3 Amplitude equation for convection rolls

Consider convection between traction-free boundaries in the form of straight rolls with axes parallel to $\mathbf{e}_y$. The equations and boundary conditions satisfied by $\mathcal{P}$ and θ are [223], where $\mathcal{P}$ and θ are independent of y and $\partial_2 \equiv 0$.

The basic idea of weakly nonlinear analysis is to expand the dependent variables in powers of a small parameter ϵ that measures the degree of supercriticality. By substituting these expansions into the governing equations and gathering together the terms proportional to different powers of ϵ, one reduces the original nonlinear problem to a sequence of linear (but inhomogeneous) problems that can be solved sequentially. Thus we write

$$\mathcal{P} = \sum_{n=1}^{\infty} \epsilon^n \mathcal{P}_n, \quad \theta = \sum_{n=1}^{\infty} \epsilon^n \theta_n,$$
$$Ra = Ra_0 + \sum_{n=1}^{\infty} \epsilon^n Ra_n \qquad [233]$$

where the last expansion can be regarded as an implicit definition of the supercriticality $\epsilon(Ra)$. Now because the boundary conditions are the same on both surfaces, the hot and cold portions of the flow are mirror images of each other. The problem is therefore invariant under the transformation $\{\mathcal{P} \to -\mathcal{P},\ \theta \to -\theta\}$ or (equivalently) $\epsilon \to -\epsilon$. Application of the latter transformation to the expanded form of [223a] shows that $Ra_n = 0$ for all odd n. To lowest order, therefore,

$$Ra - Ra_0 \approx \epsilon^2 Ra_2 \qquad [234]$$

where $Ra_2 = O(1)$ is to be determined. Now comparison of [234] with [232] shows that $s \propto \epsilon^2$. We therefore introduce a slow time $T \equiv \epsilon^2 t$ which is of order unity during the initial stage of exponential growth, whence

$$\partial_t = \epsilon^2 \partial_T \qquad [235]$$

Substituting [233], [234], and [235] into [223] and collecting terms proportional to ϵ, we obtain

$$\nabla^4 \mathcal{P}_1 + Ra_0 \theta_1 = 0, \quad \nabla^2 \theta_1 + \partial_{11}^2 \mathcal{P}_1 = 0 \qquad [236]$$

subject to the boundary conditions $\mathcal{P}_1 = \partial_{33}^2 \mathcal{P}_1 = \theta_1 = 0$ at $z = \pm 1/2$. This is just the linear stability problem, for which the solution is

$$\mathcal{P}_1 = -\frac{C}{k^2} \cos \pi z \cos kx, \quad \theta_1 = \frac{C}{\pi^2 + k^2} \cos \pi z \cos kx,$$
$$Ra_0 = \frac{(\pi^2 + k^2)^3}{k^2} \qquad [237]$$

where the amplitude $C(T)$ of the vertical velocity $w_1 \equiv \partial_{11}^2 \mathcal{P}_1$ remains to be determined. Next, we collect terms proportional to ϵ^2 to obtain

$$\nabla^4 \mathcal{P}_2 + Ra_0 \theta_2 = -Ra_1 \theta_1 \equiv 0 \qquad [238a]$$

$$\nabla^2 \theta_2 + \partial_{11}^2 \mathcal{P}_2 = \mathcal{L}_j \mathcal{P}_1 \partial_j \theta_1 \equiv -\frac{C^2 \pi}{2(\pi^2 + k^2)} \sin 2\pi z \qquad [238b]$$

Now because the inhomogeneous term in [238b] depends only on z, we must seek solutions of [238] of the forms

$$\mathcal{P}_2 = \tilde{\mathcal{P}}_2(x, z), \quad \theta_2 = \tilde{\theta}_2(x, z) + \bar{\theta}_2(z) \qquad [239]$$

where $\tilde{\mathcal{P}}_2$ and $\tilde{\theta}_2$ are the fluctuating (periodic in x) parts of the solution and $\bar{\theta}_2$ is the mean (x-independent) part. The mean part of $\mathcal{P}_2$ is set to zero because the poloidal scalar is arbitrary to within an additive function of z, as can be verified by inspection of [41]. Now the equations satisfied by $\tilde{\mathcal{P}}_2$ and $\tilde{\theta}_2$ are just the homogeneous forms of [238], which are identical to the order ϵ equations [236]. We may therefore set $\tilde{\mathcal{P}}_2 = \tilde{\theta}_2 = 0$ with no loss of generality. The solution for $\bar{\theta}_2$ is then obtained by integrating [238b] subject to the boundary conditions $\bar{\theta}_2(\pm 1/2) = 0$. We thereby find

$$\mathcal{P}_2 = 0, \quad \theta_2 \equiv \bar{\theta}_2 = \frac{C^2}{8\pi(\pi^2 + k^2)} \sin 2\pi z \qquad [240]$$

Physically, $\bar{\theta}_2(z)$ describes the average heating (cooling) of the upper (lower) half of the layer that is induced by the convection. Despite appearances, [240] is consistent with [238a] because $\mathcal{P}_2$ is arbitrary to within an additive function of z.

The parameter Ra_2 is still not determined, so we must proceed to order ϵ^3, for which the equations are

$$\nabla^4 \mathcal{P}_3 + Ra_0 \theta_3 = -Ra_2 \theta_1 \qquad [241a]$$

$$\nabla^2 \theta_3 + \partial_{11}^2 \mathcal{P}_3 = \partial_T \theta_1 + \mathcal{L}_j \mathcal{P}_1 \partial_j \theta_2 \qquad [241b]$$

We now evaluate the RHSs of [241], set $\mathcal{P}_3 = \tilde{\mathcal{P}}_3(z, T) \cos kx$ and $\theta_3 = \tilde{\theta}_3(z, T) \cos kx$, and reduce the resulting equations to a single equation for $\tilde{\mathcal{P}}_3$, obtaining

$$\left[\left(D^2 - k^2\right)^3 + k^2 Ra_0\right] \tilde{\mathcal{P}}_3 = -\left[\frac{Ra_0\left(C^3 \cos 2\pi z + 4\dot{C}\right)}{4(\pi^2 + k^2)} - Ra_2 C\right] \cos \pi z \qquad [242]$$

where $D = \mathrm{d}/\mathrm{d}z$ and a superposed dot denotes $\mathrm{d}/\mathrm{d}T$. Now the homogeneous form of [242] is identical to the eigenvalue problem at order ϵ, and thus has a solution $\propto \cos \pi z$ that satisfies the boundary conditions. The Fredholm alternative theorem then implies that the inhomogeneous equation [242] will have a solution only if the RHS satisfies a solvability condition. In the general case, this condition is found by multiplying the inhomogeneous equation by the solution of the homogeneous adjoint problem and then integrating over the domain of the dependent variable. For our (self-adjoint) problem, the homogeneous adjoint solution is $\propto \cos \pi z$, and the procedure just described yields

$$\int_{-1/2}^{1/2} \left[\left(D^2 - k^2\right)^3 + k^2 Ra_0\right] \tilde{\mathcal{P}}_3 \cos \pi z \, \mathrm{d}z = -\frac{\left[Ra_0\left(C^3 + 8\dot{C}\right) - 8\left(\pi^2 + k^2\right) Ra_2 C\right]}{16\left(\pi^2 + k^2\right)} \qquad [243]$$

Now the LHS of [243] is identically zero, as one can easily show by integrating repeatedly by parts and applying the boundary conditions on $\tilde{\mathcal{P}}_3$. The RHS of [243] must therefore vanish. Now by [233] and [237], the amplitude of the vertical velocity is $\epsilon C \equiv W$. Because only the product of ϵ and C is physically meaningful, the definition of ϵ itself – or,

equivalently, of Ra_2 – is arbitrary. Making the most convenient choice $Ra_2 = Ra_0$, we find that the vanishing of the RHS of [243] yields the following evolution equation for the physical amplitude W:

$$\frac{\mathrm{d}W}{\mathrm{d}T} = \left(\pi^2 + k^2\right) W - \frac{Ra_0}{8(Ra - Ra_0)} W^3 \qquad [244]$$

Initially, W grows exponentially with a growth rate $W^{-1}\dot{W} = \pi^2 + k^2$. At long times, however, $\dot{W} \to 0$ and the amplitude approaches a steady value

$$W(T \to \infty) = \left[\frac{8(\pi^2 + k^2)(Ra - Ra_0)}{Ra_0}\right]^{1/2} \qquad [245]$$

7.04.9.2.4 Finite-amplitude convection rolls and their stability

The extension of the above results to strongly nonlinear rolls ($\epsilon = O(1)$) between rigid surfaces is due to Busse (1967a), whose development we follow here with some changes of notation. The first step is to determine steady roll solutions of [223] using a Galerkin method (Fletcher, 1984) whereby θ and $\mathcal{P}$ are expanded in orthogonal functions that satisfy the boundary conditions and the coefficients are then chosen to satisfy approximately the governing equations.

We begin by expanding θ into a complete set of Fourier modes that satisfy the boundary conditions $\theta(x, \pm 1/2) = 0$:

$$\theta = \sum_{m,n} c_{mn} \mathrm{e}^{imkx} f_n(z), \quad f_n(z) = \sin n\pi\left(z + \frac{1}{2}\right) \qquad [246]$$

where $2\pi/k$ is the wavelength of the convection rolls, $c_{mn} = \bar{c}_{n-m}$, where the overbar denotes complex conjugation, and the summations are over $-\infty \le m \le \infty$ and $1 \le n \le \infty$. Now substitute [246] into [223a] and solve the resulting equation to obtain

$$\mathcal{P} = -Ra \sum_{m,n} c_{mn} \mathrm{e}^{imkx} Q_n(mk,\ z) \qquad [247a]$$

$$Q_n(r,\ z) = \frac{f_n(z) + n\pi h_n(r)}{\left(r^2 + n^2\pi^2\right)^2} \qquad [247b]$$

$$h_n(r) = \begin{cases} (2SC + r)^{-1}(2zC \sin h\, rz - S\cosh rz) & \text{(n odd)} \\ (2SC - r)^{-1}(C \sin h\, rz - 2zS\cosh rz) & \text{(n even)} \end{cases} \qquad [247c]$$

$$S = \sinh\frac{r}{2}, \quad C = \cosh\frac{r}{2} \qquad [247d]$$

To determine the coefficients c_{mn}, we substitute [247] into [223b], multiply the result by $f_q(z)\mathrm{e}^{-ipkx}$, and integrate over the fluid layer. By using for p and q all integers in the ranges of m and n, respectively, we obtain an infinite set of nonlinear algebraic equations for $c_{mn}(Ra)$ that can be truncated and solved numerically (Busse, 1967a.)

Another advantage of the Galerkin method is that a stability analysis of the solution can easily be performed. The linearized equations governing infinitesimal perturbations $(\tilde{\mathcal{P}},\ \tilde{\theta})$ to the steady roll solution $(\mathcal{P}_0,\ \theta_0)$ are

$$\nabla^4 \tilde{\mathcal{P}} = -Ra\tilde{\theta} \qquad [248a]$$

$$\tilde{\theta}_t + \mathcal{L}_j \mathcal{P}_0 \partial_j \tilde{\theta} + \partial_j \theta_0 \mathcal{L}_j \tilde{\mathcal{P}} - \nabla_1^2 \tilde{\mathcal{P}} = \nabla^2 \tilde{\theta} \qquad [248b]$$

subject to $\tilde{\theta} = \tilde{\mathcal{P}} = \partial_3 \tilde{\mathcal{P}} = 0$ at $z = \pm 1/2$. Now [248] are linear PDEs with coefficients that are periodic in the x-direction but independent of both z and t. The general solution can be written as a sum of solutions which depend exponentially on x, y, and t, multiplied by a function of x having the same periodicity as the stationary solution (Busse, 1967a.) We therefore write

$$\tilde{\theta} = \left\{\sum_{m,n} \tilde{c}_{mn} \mathrm{e}^{imkx} f_n(z)\right\} \mathrm{e}^{\mathrm{i}(ax+by)+st} \qquad [249]$$

and note further that [248a] and the boundary conditions on $\mathcal{P}$ are satisfied exactly if

$$\tilde{\mathcal{P}} = -Ra\left\{\sum_{m,n} \tilde{c}_{mn} \mathrm{e}^{imkx} Q_n\left(\sqrt{(mk + a)^2 + b^2},\ z\right)\right\} \times \mathrm{e}^{\mathrm{i}(ax+by)+st} \qquad [250]$$

Substituting [249] and [250] into [248b], multiplying by $f_q(z)\mathrm{e}^{-\mathrm{i}(pkx + ax + by) - st}$, and averaging over the fluid layer, we obtain an infinite system of linear equations for the coefficients $\tilde{c}_{mn}$. The system is then truncated and the largest eigenvalue $s(Ra, k, a, b)$ is determined numerically, assuming that s is real in view of the fact that $\Im(s) = 0$ at the onset of convection (Busse, 1967a).

The results show that convection rolls are stable ($s < 0$) in an elongate region of the (Ra, k) space often called the Busse balloon (**Figure 14**). Above $Ra \approx 22600$, convection rolls of any wave number are unstable. The lower left edge of the balloon (denoted by Z in **Figure 14**) represents the onset of a zigzag instability in the form of rolls oblique to the original ones. Around the rest of the balloon (denoted by C), the stability of rolls is limited by the crossroll instability, which grows in the form of perpendicularly aligned rolls. The results of Busse (1967a) were extended to the case of traction-free boundaries by Straus (1972), Busse and Bolton (1984), and Bolton and Busse (1985).

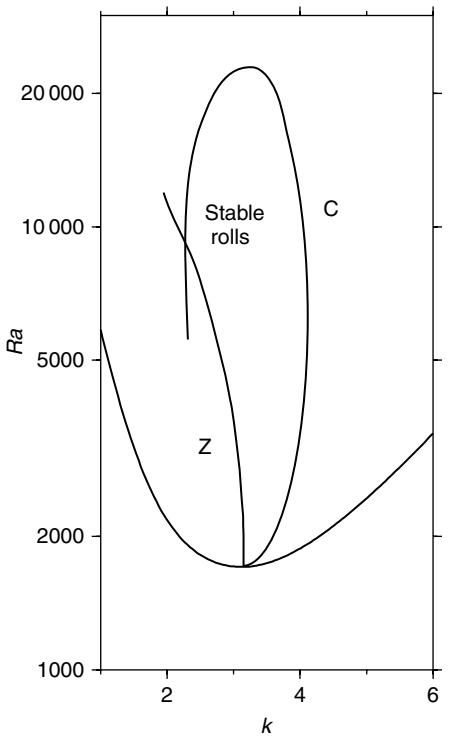

Figure 14 Region of stability in the Rayleigh number/wave number plane of 2-D convection rolls between rigid isothermal surfaces (Busse balloon). Portions of the boundary of the balloon labeled *Z* and *C* correspond to the onset of the zigzag and cross-roll instabilities, respectively.

7.04.9.2.5 Envelope equation for modulated convection rolls

The analyses in Sections 7.04.9.2.3 and 7.04.9.2.4 assume convection in the form of straight parallel rolls with a single dominant wave number k. In the laboratory, however, rolls often exhibit a more irregular pattern in which both the magnitude and direction of the wave vector $\mathbf{k} = (k_1, k_2)$ vary slowly as functions of time and position. To describe this behavior, Newell and Whitehead (1969) and Segel (1969) derived an envelope equation for modulated convection rolls whose wave vectors form a continuous spectrum within a narrow band centered on the wave vector $(k_c, 0)$ for straight parallel rolls. The envelope equation is derived via a multiscale expansion that accounts in a self-consistent way for both the fast and slow variations of the flow field in time and space. Richter (1973) applied a similar method to convection modulated by long-wavelength variations in the boundary temperatures.

The first step is to determine the scales over which the slow (i.e., long-wavelength) spatial variations occur. Because the marginal stability curve $Ra_0(k)$ is a parabola in the vicinity of its minimum $(k, Ra_0) = (k_c, Ra_c)$, the wave numbers $|\mathbf{k}|$ that become unstable when Ra exceeds Ra_c by an amount $\epsilon^2 Ra_c$ comprise a continuous band of width $\sim\epsilon$ centered on k_c (**Figure 13(a)**). However, the orientation of the rolls, measured by the ratio k_2/k_1, may also vary. Now the most unstable wave vector lies on a circle of radius k_c (**Figure 13(b)**). Therefore if we change $|\mathbf{k}|$ by an amount $\sim\epsilon$ in the vicinity of the straight-roll wave vector $(k_c, 0)$, the (maximum) corresponding changes of k_1 and k_2 are $\sim\epsilon$ and $\sim\epsilon^{1/2}$, respectively. The appropriate slow variables are therefore

$$X = \epsilon x, \quad Y = \epsilon^{1/2} y, \quad T = \epsilon^2 t \qquad [251]$$

where the expression for T derives from the argument preceeding [235].

The essence of the multiscale procedure is to treat the flow fields (here, $\mathcal{P}$ and θ) as functions of both the fast variables (x, y, t) and the slow variables (X, Y, T). Accordingly, the asympotic expansions analogous to [233] are

$$\begin{aligned} \mathcal{P} &= \sum_{n=1}^{\infty} \epsilon^n \mathcal{P}_n(X, Y, T, x, z) \\ \theta &= \sum_{n=1}^{\infty} \epsilon^n \theta_n(X, Y, T, x, z) \end{aligned} \qquad [252]$$

Because the solution for steady straight rolls is independent of y and t, $\mathcal{P}_n$ and θ_n depend on these variables only through the variables Y and T that measure the slow modulation of the pattern. By the chain rule, derivatives of the expansions [252] with respect to the fast variables transform as

$$\begin{aligned} &\partial_t \to \epsilon^2 \partial_T, \quad \partial_x \to \partial_x + \epsilon \partial_X, \\ &\partial_y \to \epsilon^{1/2} \partial_Y, \quad \partial_z \to \partial_z \end{aligned} \qquad [253]$$

We now substitute [252] into the governing equations [223] and collect terms proportional to like powers of ϵ, just as in Section 7.04.9.2.3. The solutions at order ϵ analogous to [237] are

$$\mathcal{P}_1 = -\frac{1}{2k_c^2}\left[C e^{ik_c x} + \bar{C} e^{-ik_c x}\right] \cos \pi z \qquad [254a]$$

$$\theta_1 = \frac{1}{2\left(\pi^2 + k_c^2\right)}\left[C e^{ik_c x} + \bar{C} e^{-ik_c x}\right] \cos \pi z \qquad [254b]$$

where $C = C(X, Y, T)$ is the slowly varying envelope of the roll solution and overbars denotes complex

conjugation. The solution at order ϵ^2 analogous to [240] is

$$\mathcal{P}_2 = 0, \quad \theta_2 = \frac{C\bar{C}}{8\pi\left(\pi^2 + k_c^2\right)} \sin 2\pi z \qquad [255]$$

The temperature θ_2 also contains free modes proportional to $\partial_X(C, \bar{C})$ and $\partial_{YY}(C, \bar{C})$, but these do not change the solvability condition at order ϵ^3 and can therefore be neglected. Evaluating this solvability condition as in Section 7.04.9.2.3 and setting $k_c = \pi/\sqrt{2}$, we obtain the Newell–Whitehead–Segel equation for the envelope $W \equiv \epsilon C$ of the vertical velocity field:

$$\frac{\partial W}{\partial T} - \frac{4}{3}\left(\frac{\partial}{\partial X} - \frac{\mathrm{i}}{\sqrt{2}\pi}\frac{\partial^2}{\partial Y^2}\right)^2 W = \frac{3\pi^2}{2} W - \frac{Ra_c}{8(Ra - Ra_c)}|W|^2 W \qquad [256]$$

Equation [256] differs from [244] by the addition of a diffusion-like term on the LHS, which represents the interaction of neighboring rolls via the buoyant torques they apply to each other. Equations generalizing [256] to N interacting wavepackets are given by Newell and Whitehead (1969).

7.04.9.2.6 Phase diffusion equation for thermal convection

The final case is that of large-amplitude ($\epsilon = O(1)$) convection in the form of modulated rolls, which can be described by a phase diffusion equation. The derivation below follows Newell *et al.* (1990) ≡ NPS90.

The basic assumption is that the flow field consists locally of straight parallel rolls whose wave vector varies slowly over the fluid layer. This wave vector can be written as $\mathbf{k} \equiv \nabla\phi$, where ϕ is the phase of the roll pattern. The phase is the crucial dynamical variable far from onset, because the amplitude is an algebraic function of the wave number k and the Rayleigh number and no longer an independent parameter. The amplitude is therefore slaved to the phase gradients, and the phase diffusion equation alone suffices to describe the dynamics.

The problem involves two very different length scales, the layer depth d and the tank width $L \gg d$, and may therefore be solved using a multiscale expansion. Because the convection is strongly nonlinear, however, the relevant small parameter is no longer the degree of supercriticality (as in Section 7.04.9.2.5), but rather the inverse aspect ratio $d/L \equiv \Gamma^{-1}$. Now the lateral scale of the variation of $\mathbf{k}$ is the tank width $L \equiv \Gamma d$, and its characteristic timescale is the lateral thermal diffusion time $L^2/\kappa \equiv \Gamma^2 d^2/\kappa$. Accordingly, the slow variables that characterize the modulation of the basic roll pattern are

$$X = \Gamma^{-1}x, \quad Y = \Gamma^{-1}y, \quad T = \Gamma^{-2}t \qquad [257]$$

The starting point of the analysis is the Galerkin representation [246]–[247] for large-amplitude steady rolls with axes parallel to the y-direction and wave vector $\mathbf{k} = (k, 0)$. Let A be some measure of the amplitude of this solution, which can be calculated via the Galerkin procedure as a function of Ra and k. Next, we seek modulated roll solutions for the dependent variables $\mathbf{v} = (\mathcal{P}, \theta)$ in the form

$$\mathbf{v} = \mathbf{F}(\phi = \Gamma\Phi(X, Y, T), z; A(X, Y, T)) \qquad [258]$$

In [258], Φ is a slow phase variable defined such that

$$\mathbf{k} = \nabla_x\phi = \nabla_X\Phi \qquad [259]$$

where ∇_x and ∇_X are the horizontal gradient operators with respect to the variables (x, y) and (X, Y), respectively. Because derivatives act on functions of ϕ, z, X, Y, and T, the chain rule implies the transformations

$$\begin{aligned} &\partial_z \to \partial_z, \quad \nabla_x \to \mathbf{k}\partial_\phi + \Gamma^{-1}\nabla_X, \\ &\partial_t \to \Gamma^{-1}\partial_T\Phi\partial_\Theta + \Gamma^{-2}\partial_T, \\ &\nabla^2 \to k^2\partial^2_{\phi\phi} + \partial^2_{zz} + \Gamma^{-1}D\partial_\phi + \Gamma^{-2}\nabla^2_X, \\ &D = 2\mathbf{k}\cdot\nabla_X + \nabla_X\cdot\mathbf{k} \end{aligned} \qquad [260]$$

where $\mathbf{k} = (k_1, k_2)$.

Because of the slow modulation, [258] is no longer an exact solution of the Boussinesq equations. We therefore seek solutions in the form of an asympotic expansion in powers of Γ^{-1},

$$\mathbf{v} = \mathbf{v}_0 + \Gamma^{-1}\mathbf{v}_1 + \Gamma^{-2}\mathbf{v}_2 + \cdots \qquad [261]$$

where v_0 is the Galerkin solution for steady parallel rolls. Substituting [261] into the Boussinesq equations, using [260], and collecting terms proportional to Γ^{-1}, we obtain a BVP for $\mathbf{v}_1$ which has a solution only if a solvability condition is satisfied. This condition yields the phase diffusion equation

$$\frac{\partial\Phi}{\partial T} + \frac{1}{\tau(k)}\nabla\cdot[\mathbf{k}B(k)] = 0 \qquad [262]$$

where the functions $\tau(k)$ and $B(k)$ are determined numerically. The diffusional character of [262] becomes obvious when one recalls that $\mathbf{k} = \nabla_X\Phi$. In writing [262], we have neglected an additional mean drift term that is nonzero only for finite values of the

Prandtl number (NPS90, eqn. (1.1)). NPS90 show that a linear stability analysis of [262] reproduces closely all the portions of the boundary of the Busse balloon for which the wavelength of the instability is long relative to the layer depth.

7.04.9.3 Convection at High Rayleigh Number

Even though convection in the form of steady 2-D rolls is unstable when $Ra > 22\,600$ (Section 7.04.9.2.4), much can be learned by studying the structure of such rolls in the limit $Ra \to \infty$. Because temperature variations are now confined to thin TBLs around the edges of the cells, scaling analysis and BL theory are particularly effective tools for this purpose.

7.04.9.3.1 Scaling analysis

The essential scalings for cellular convection at high Rayleigh number can be determined by a scaling analysis of the governing equations. The following derivation (for the cell geometry shown in **Figure 6**) generalizes the analysis of McKenzie *et al.* (1974) to include both traction-free and rigid-surface boundary conditions. For simplicity, we assume in this subsection only that the aspect ratio β does not differ much from unity.

The analysis proceeds by determining six equations relating six unknown quantities: the thicknesses δ_p of the thermal plumes and δ_h of the horizontal TBLs, the maximum vertical velocity v_p and the vorticity ω in the plumes, the vertical velocity $v(\delta_h)$ in the plume at the edge of the horizontal BLs, and the heat flux q across the layer (per unit length along the roll axes). The heat flux carried by an upwelling plume is

$$q \sim \rho c_p v_p \Delta T \delta_p \qquad [263]$$

where c_p is the heat capacity at constant pressure. Because the convection is steady, the flux [263] must equal that lost by conduction through the top horizontal BL, implying

$$q \sim k_c d \Delta T / \delta_h \qquad [264]$$

where k_c is the thermal conductivity. The thickness δ_h of the horizontal BLs is controlled by the balance $vT_y \sim \kappa T_{yy}$ of advection and diffusion, which implies

$$v(\delta_h)\Delta T/\delta_h \sim \kappa \Delta T/\delta_h^2 \qquad [265]$$

Now $v(\delta_h)$ depends on whether the horizontal surfaces are free or rigid. Because the velocity parallel to the boundary is constant to lowest order across a TBL at a free surface ($n = 0$ say) and varies linearly across a TBL at a rigid surface ($n = 1$),

$$v(\delta_h) \sim v_p(\delta_h/d)^{n+1} \qquad [266]$$

The force balance in the plumes is scaled using the vorticity equation $\nu\nabla^2\omega = g\alpha T_x$, which implies

$$\omega \sim g\alpha\Delta T\delta_p/\nu \qquad [267]$$

Finally, the vorticity ω in the plumes is of the same order as the rotation rate of the isothermal core, or

$$\omega \sim v_p/d \qquad [268]$$

The simultaneous solution of [263]–[268] yields scaling laws for each of the six unknown quantities as a function of R. **Table 5** shows the results for v_p, δ_p, and the Nusselt number $Nu \equiv d/\delta_h$. The free-surface heat transfer law $Nu \sim Ra^{1/3}$ corresponds to a dimensional heat flux $q \equiv k_c \Delta T Nu/d$ that is independent of the layer depth d, whereas $q \propto d^{-2/5}$ for rigid surfaces. A revealing check of the results is to note that $v_p d/\kappa$ (column 2) is just the effective Peclet number Pe for the flow. The scaling laws for Nu (column 4) then imply $Nu \sim Pe^{1/(n+2)}$, in agreement with our previous expression [12] for the heat transfer from a hot sphere moving in a viscous fluid.

7.04.9.3.2 Flow in the isothermal core

Given the fundamental scales of **Table 5**, we can now carry out a more detailed analysis based on BL theory. This approach, pioneered by Turcotte (1967) and Turcotte and Oxburgh (1967) and extended by Roberts (1979), Olson and Corcos (1980), and Jimenez and Zufiria (1987) (henceforth JZ87), is applicable to convection in a layer bounded by either free or rigid surfaces. Here we consider only the former case, following JZ87 with some changes of notation.

The dimensional equations governing the flow are

$$\nu\nabla^4\psi = -g\alpha T_x \qquad [269a]$$

$$u\theta_x + v\theta_y = \kappa\nabla^2 T \qquad [269b]$$

Table 5 Scaling laws for vigorous Rayleigh–Bénard convection

Boundaries	$v_p d/\kappa$	δ_p/d	$Nu \equiv d/\delta_h$
Free	$Ra^{2/3}$	$Ra^{-1/3}$	$Ra^{1/3}$
Rigid	$Ra^{3/5}$	$Ra^{-2/5}$	$Ra^{1/5}$

where T is the temperature, $\mathbf{u} = u\mathbf{e}_x + v\mathbf{e}_y \equiv -\psi_y\mathbf{e}_x + \psi_x\mathbf{e}_y$ is the velocity, and ψ is the streamfunction. In the limit $Ra \to \infty$, each cell comprises a nearly isothermal core surrounded by thin vertical plumes and horizontal BLs. Because temperature gradients are negligible in the core, the principal agency driving the flow within it is the shear stresses applied to its vertical boundaries by the plumes. Our first task is therefore to derive a boundary condition on the core flow that represents this agency.

Consider for definiteness the upwelling plume at the left boundary $x = -\beta d/2 \equiv x_-$ of the cell (**Figure 6**), and let its half-width be δ_p. The (upward) buoyancy force acting on the right half of this plume must be balanced by a downward shear stress at its edge $x = x_- + \delta_p$ (the shear stress on $x = x_-$ is zero by symmetry). This requires

$$\nu v_x|_{x=x_-+\delta_p} = -g\alpha \int_{x_-}^{x_-+\delta_p} (T - T_c)\mathrm{d}x \qquad [270]$$

where T_c ($\equiv 0$) is the temperature in the core. Multiplying [270] by v_p, we obtain

$$v_p v_x|_{x=x_-+\delta_p} = -\frac{\alpha g}{\nu \rho c_p}\left[\rho c_p \int_{x_-}^{x_-+\delta_p} v_p (T - T_c)\mathrm{d}x\right] \qquad [271]$$

where we have used the fact that $v_p \equiv \psi_x$ is constant to first order across the plumes to take it inside the integral on the RHS. Now the quantity $[\ldots]$ in [270] is just the heat flux carried by the right half of the plume, which is $k_c \Delta T Nu/2$. Moreover, because the plume is thin, $v_x \equiv \psi_{xx}$ can be evaluated at $x = x_-$ rather than at $x = x_- + \delta_p$. Equation [271] then becomes

$$\psi_x \psi_{xx}|_{x=x_-} = -\frac{1}{2}\frac{g\kappa\alpha\Delta T}{\nu} Nu \qquad [272]$$

which is a nonlinear and inhomogeneous boundary condition on the core flow. The corresponding condition at $x = +\beta d/2$ is obtained from [272] by reversing the sign of the RHS.

We now invoke the results of the scaling analysis (**Table 5**) to nondimensionalize the equations and boundary conditions for the core flow. We first write the scaling law for Nu as

$$Nu = C(\beta) Ra^{1/3} \qquad [273]$$

where $C(\beta)$ (to be determined) measures the dependence of the heat transfer on the aspect ratio. Rewriting the equations and boundary conditions in terms of the dimensionless variables $(x', z') = (x, z)/d$ and $\psi' = \psi/\kappa C(\beta)^{1/2} Ra^{2/3}$ and then dropping the primes, we obtain

$$\nabla^4 \psi = 0 \qquad [274a]$$

$$\psi(x, \pm 1/2) = \psi_{yy}(x, \pm 1/2) = 0 \qquad [274b]$$

$$\psi(\pm\beta/2, y) = \psi_x(\pm\beta/2, y) \times \psi_{xx}(\pm\beta/2, y) \mp 1/2 = 0 \qquad [274c]$$

The problem [274] can be solved either numerically (JZ87) or using a superposition method (Section 7.04.5.4.1).

7.04.9.3.3 TBLs and heat transfer

The next step is to determine the temperature in the plumes and the horizontal TBLs using BL theory. The temperature in all these layers is governed by the transformed BL equation [149]. Turcotte and Oxburgh (1967) solved this equation assuming self-similarity, obtaining solutions of the form [151]. However, Roberts (1979) pointed out that this is not correct, because the fluid traveling around the margins of the cell sees a periodic boundary condition which is alternatingly isothermal (along the horizontal boundaries) and insulating (in the plumes). Now because [149] is parabolic, its solution can be written in convolution-integral form in terms of an arbitrary boundary temperature $T_b(\tau)$ and an initial temperature profile $T(\psi, 0)$ at $\tau = 0$, where $\tau = \int U(s)\mathrm{d}s$ is the time-like variable introduced in Section 7.04.7.1.1 and the velocity $U(s)$ parallel to the boundary is determined (to within the unknown scale factor $C(\beta)$) from the core flow streamfunction ψ that satisfies [274]. However, in the limit $\tau \to \infty$ corresponding to an infinite number of transits around the cell, the convolution integral describing the evolution of the initial profile vanishes, and the solution is (JZ87)

$$T(\psi, \tau) = -\frac{\psi}{2(\pi\kappa)^{1/2}} \times \int_0^\infty \frac{T_b(\tau - t)}{t^{3/2}} \exp\left(-\frac{\psi^2}{4\kappa t}\right)\mathrm{d}t \qquad [275]$$

where all variables are dimensional. Now T_b is known only on the top and bottom surfaces. Along the (insulating) plume centerlines, it can be found by setting to zero the temperature gradient $\partial_\psi T|_{\psi=0}$ calculated from [275] and solving numerically the resulting integral equation. The temperature everywhere in the plumes and horizontal BLs can then be determined from [275]. The final step is to determine the unknown scale factor $C(\beta)$ by matching the heat flow advected vertically by the plumes to the

conductive heat flux across the upper boundary (JZ87, eqn [23]).

The solution of JZ87 shows that the scale factor $C(\beta)$ (and hence the Nusselt number $Nu = CRa^{1/3}$) is maximum for $\beta \approx 0.75$, which may therefore be the preferred cell aspect ratio (Malkus and Veronis, 1958). A particularly interesting result from a geophysical perspective is that the temperature profile in the TBL beneath the cold upper surface exhibits a hot asthenosphere, that is, a range of depths where the temperature exceeds that of the cell's interior.

7.04.9.3.4 Structure of the flow near the corners

The solutions described above break down near the corners of the cell, where the vorticity of the core flow solution becomes infinite and the BL approximation is no longer valid. The (dimensional) characteristic radius r_c of this corner region can be determined using a scaling argument. Consider for definiteness the corner above the upwelling plume, and let (r, φ) be polar coordinates with origin at the corner such that $\varphi = 0$ on the upper surface and $\varphi = \pi/2$ on the plume centerline. Close to the corner, the streamfunction has the self-similar form $\psi(r, \varphi) = r^{\lambda} F(\varphi)$ for some λ, where F is given by [64]. Near the corner, the dimensional forms of the boundary conditions [274b] and [274c] are

$$\psi(r, 0) = \psi(r, \pi/2) = \psi_{\varphi\varphi}(r, 0) = 0 \qquad [276a]$$

$$r^{-3}\psi_{\varphi}(r, \pi/2)\psi_{\varphi\varphi}(r, \pi/2) = \frac{1}{2}\frac{g\kappa\alpha\Delta T}{\nu} Nu \qquad [276b]$$

Equation [276b] immediately implies $\lambda = 3/2$, and the streamfunction which satisfies all the conditions [276] is

$$\psi = \frac{\kappa}{2}\left(\frac{r}{d}\right)^{3/2} C(\beta)^{1/2} Ra^{2/3}\left(\sin\frac{3}{2}\varphi - \sin\frac{1}{2}\varphi\right) \qquad [277]$$

Note that the vorticity $\omega \sim -(\kappa/d^2)Ra^{2/3}(r/d)^{-1/2}$ becomes infinite at the corner. Now the balance between viscous forces and buoyancy in the corner region requires $\nu\nabla^4\psi \sim -g\alpha T_x$, or

$$\psi \sim \kappa Ra(r_c/d)^3 \qquad [278]$$

Equating [278] with the scale $\psi \sim \kappa Ra^{2/3}(r_c/d)^{3/2}$ implied by [277], we find (Roberts, 1979)

$$r_c \sim Ra^{-2/9} d \qquad [279]$$

A corrected solution for the flow in the corner region that removes the vorticity singularity was proposed by JZ87.

7.04.9.3.5 Howard's scaling for high-Ra convection

While the above solution for cellular convection is illuminating, we know that rolls between rigid boundaries with $R > 22\,600$ are not stable to small perturbations (Section 7.04.9.2.4). In reality, convection at high Rayleigh number $Ra > 10^6$ is a quasi-periodic process in which the TBLs grow by thermal diffusion, become unstable, and then empty rapidly into plumes, at which point the cycle begins again. The characteristic timescale of this process can be estimated via a simple scaling argument (Howard, 1964). The thickness δ of both TBLs initially increases by thermal diffusion as $\delta \approx (\pi\kappa t)^{1/2}$. Instability sets in when the growth rate of R–T instabilities in the layers (see Section 7.04.9.1) becomes comparable to the thickening rate $\dot{\delta}/\delta$, or (equivalently) when the Rayleigh number $Ra(\delta) \equiv g\alpha\Delta T\delta^3/\nu\kappa$ based on the TBL thickness attains a critical value $Ra_c \approx 10^3$. This occurs after a time

$$t_c \approx \frac{1}{\pi\kappa}\left(\frac{\kappa\nu Ra_c}{g\alpha\Delta T}\right)^{2/3} \qquad [280]$$

that is independent of the layer depth. The scaling law [280] has been amply confirmed by laboratory experiments (e.g., Sparrow *et al.*, 1970.)

7.04.9.4 Thermal Convection in More Realistic Systems

As the simplest and most widely studied example of thermal convection, the R–B configuration is the source of most of what has been learned about thermal convection during the past century. From a geophysical point of view, however, it lacks many crucial features that are important in the Earth's mantle: the variation of viscosity as a function of pressure, temperature, and stress; the presence of solid-state phase changes; internal production of heat by radioactive decay; density variations associated with differences in chemical composition; and a host of other factors such as rheological anisotropy, the effect of volatile content, etc. Because analytical methods thrive on simple model problems, the addition of each new complexity reduces their room for manoeuvre; but many important analytical results have been obtained nevertheless. Here we review briefly some of these, focussing on the effects of variable viscosity, phase transitions, and chemical heterogeneity.

A variety of important analytical results have been obtained for fluids with temperature-dependent viscosity. Stengel *et al.* (1982) performed a linear stability analysis of convection in a fluid whose viscosity $\nu(T)$ varies strongly (by up to a factor of 2×10^4) with temperature. For fluids for which $\nu(T)$ is an exponential function, the critical Rayleigh number (based on the viscosity at the mean of the boundary temperatures) first increases and then decreases as the total viscosity contrast across the layer increases, reflecting the fact that convection begins first in a low-viscosity sublayer near the hot bottom boundary. A nonlinear stability analysis of convection in a fluid with a weak linear dependence of viscosity on temperature was carried out by Palm (1960), using a method like that described in Section 7.04.9.2.3. Because the variation of the viscosity breaks the symmetry between upwelling and downwelling motions, the amplitude equation analogous to [244] contains a quadratic term that permits transcritical bifurcation. Subsequent work (e.g., Busse, 1967b, Palm *et al.*, 1967) showed that the stable planforms are hexagons, hexagons and 2D rolls, or 2D rolls alone, depending on the Rayleigh number. Busse and Frick (1985) used a Galerkin method (Section 7.04.9.2.4) to study convection in a fluid whose viscosity depends strongly (but linearly) on temperature, and found that a square planform becomes stable when the viscosity contrast is sufficiently large.

Convection at high Rayleigh number in fluids with strongly variable viscosity is a particularly difficult analytical challenge, but some noteworthy results have been obtained. Morris and Canright (1984) and Fowler (1985) used BL analyses similar to that described in Section 7.04.9.3 to determine the Nusselt number in the stagnant lid limit $\Delta T/\Delta T_r \rightarrow \infty$ for convection in a fluid whose viscosity depends on temperature as $\nu = \nu_0 \exp[-(T - T_0)/\Delta T_r]$. Both studies find the Nusselt number to be $Nu \sim (\Delta T/\Delta T_r)^{-1} Ra_r^{1/5}$ where $Ra_\gamma = \alpha g \Delta T_\mathrm{r} d^3/\nu_0 \kappa$ is the Rayleigh number based on the rheological temperature scale ΔT_r and the viscosity ν_0 at the hot bottom boundary. Solomatov (1995) presented a comprehensive scaling analysis for convection in fluids with temperature- and stress-dependent viscosity. He found that three different dynamical regimes occur as the total viscosity contrast across the layer increases: quasi-isoviscous convection, a transitional regime with a mobile cold upper BL, and a stagnant-lid regime in which the upper BL is motionless and convection is confined beneath it. Busse *et al.* (2006) generalized Turcotte and Oxburgh's (1967) BL analysis of steady cellular convection to include thin low-viscosity layers adjoining the top and bottom boundaries, whose presence increases the cell aspect ratio that maximizes the heat transport.

The influence of a phase transition on the stability of convection in a fluid with constant viscosity was analyzed by Schubert and Turcotte (1971). The novel elements here are two matching conditions at the depth of the phase change: one of these equates the energy released by the transformation to the difference in the perturbation heat flux into and out of the phase boundary, while the second requires the phase boundary to lie on the Clapeyron slope. The resulting eigenvalue problem yields the critical Rayleigh number $Ra_\mathrm{c}(S, Ra_{\underline{Q}})$, where

$$S = \frac{\Delta\rho/\rho}{\alpha d(\rho g/\gamma - \beta)}, \qquad Ra_{\underline{Q}} = \frac{\alpha g d^3 \underline{Q}}{8 c_p \nu \kappa} \qquad [281]$$

$\Delta\rho$ is the density difference between the phases, $\underline{Q}$ is the energy per unit mass required to change the denser phase into the lighter, γ is the Clapeyron slope, and β is the magnitude of the temperature gradient in the basic state. Ra_c is a decreasing function of S (which measures the destabilizing effect of the density change) but an increasing function of $Ra_{\underline{Q}}$ (which measures the stabilizing influence of latent heat). These results were extended to a divariant phase change by Schubert *et al.* (1972).

Convection in a chemically layered mantle was first studied by Richter and Johnson (1974), who performed a linear stability analysis of a system comprising two superposed fluid layers of equal depth and viscosity but different densities. The critical Rayleigh number Ra_c depends on the value of a second Rayleigh number $Ra_\rho = g\Delta\rho d^3/\nu\kappa$ proportional to the magnitude of the stabilizing density difference $\Delta\rho$ between the layers. Three distinct modes of instability are possible: convection over the entire depth of the fluid with advection of the interface; separate convection within each layer; and standing waves on the interface, corresponding to an imaginary growth rate at marginal stability. Busse (1981) extended these results to layers of different thicknesses. Rasenat *et al.* (1989) examined a still larger region of the parameter space, and demonstrated the possibility of an oscillatory two-layer regime with no interface deformation, in which the coupling between the layers oscillates between thermal and mechanical. Le Bars and Davaille (2002) mapped out the linear stability of two-layer

convection as a function of the interlayer viscosity contrast γ and the layer depth ratio r, and showed that the transition from oscillatory to stratified convection occurs at a critical value of the buoyancy ratio $B \equiv Ra_\rho / Ra$ that depends on γ and r.

For the time being, studies like those discussed above represent the limit of what can be learned about convection in complex systems using analytical methods alone. The impressive additional progress that has been made using experimental and numerical approaches is discussed in Chapters 7.02 and 7.04 of this volume.

Acknowledgment

This is IPGP contribution number 2202.

References

Albers M and Christensen UR (2001) Channeling of plume flow beneath mid-ocean ridges. *Earth and Planetary Science Letters* 187: 207–220.

Ansari A and Morris S (1985) The effects of a strongly temperature-dependent viscosity on Stokes's drag law: Experiments and theory. *Journal of Fluid Mechanics* 159: 459–476.

Backus GE (1958) A class of self-sustaining dissipative spherical dynamos. *Annals of Physics* 4: 372–447.

Bai Q, Mackwell SJ, and Kohlstedt DL (1991) High-temperature creep of olivine single crystals. Part 1: Mechanical results for buffered samples. *Journal of Geophysical Research* 96: 2441–2463.

Backus GE (1967) Converting vector and tensor equations to scalar equations in spherical co-ordinates. *Geophysical Journal of the Royal Astronomical Society* 13: 71–101.

Barcilon V and Richter FM (1986) Nonlinear waves in compacting media. *Journal of Fluid Mechanics* 164: 429–448.

Barenblatt GI (1996) *Scaling, Self-Similarity, and Intermediate Asymptotics*. Cambridge: Cambridge University Press.

Batchelor GK (1967) *An Introduction to Fluid Dynamics*. Cambridge: Cambridge University Press.

Batchelor GK (1970) Slender-body theory for particles of arbitrary crosssection in Stokes flow. *Journal of Fluid Mechanics* 44: 419–440.

Bercovici D (1994) A theoretical model of cooling viscous gravity currents with temperature-dependent viscosity. *Geophysical Research Letters* 21: 1177–1180.

Bercovici D and Lin J (1996) A gravity current model of cooling mantle plume heads with temperature-dependent buoyancy and viscosity. *Journal of Geophysical Research* 101: 3291–3309.

Biot MA (1954) Theory of stress-strain relations in anisotropic viscoelasticity and relaxation phenomena. *Journal of Applied Physics* 25: 1385–1391.

Bird RB, Armstrong RC, and Hassager O (1987) *Dynamics of Polymeric Liquids, Vol 1: Fluid Mechanics,* 2nd edn. New York, NY: John Wiley & Sons.

Blake JR (1971) A note on the image system for a Stokeslet in a no-slip boundary. *Proceedings of the Cambridge Philosophical Society* 70: 303–310.

Bloor MIG and Wilson MJ (2006) An approximate analytic solution method for the biharmonic problem. *Proceedings of the Royal Society of London A* 462: 1107–1121.

Bolton EW and Busse FH (1985) Stability of convection rolls in a layer with stress-free boundaries. *Journal of Fluid Mechanics* 150: 487–498.

Buckingham E (1914) On physically similar systems; illustrations of the use of dimensional equations. *Physical Review* 4: 345–376.

Buckmaster JD, Nachman A, and Ting L (1975) The buckling and stretching of a viscida. *Journal of Fluid Mechanics* 69: 1–20.

Busse FH (1967a) On the stability of two-dimensional convection in a layer heated from below. *Journal of Mathematical Physics* 46: 140–150.

Busse FH (1967b) The stability of finite amplitude cellular convection and its relation to an extremum principle. *Journal of Fluid Mechanics* 30: 625–649.

Busse FH (1981) On the aspect ratio of two-layer mantle convection. *Physics of the Earth and Planetary Interiors* 24: 320–324.

Busse FH and Bolton EW (1984) Instabilities of convection rolls with stress-free boundaries near threshold. *Journal of Fluid Mechanics* 146: 115–125.

Busse FH and Frick H (1985) Square-pattern convection in fluids with strongly temperature-dependent viscosity. *Journal of Fluid Mechanics* 150: 451–465.

Busse FH, Richards MA, and Lenardic A (2006) A simple model of high Prandtl and high Rayleigh number convection bounded by thin low-viscosity layers. *Geophysical Journal International* 164: 160–167.

Canright DR (1987) *A Finite-Amplitude Analysis of the Buoyant Instability of a Highly Viscous Film over a Less Viscous Half-Space*. PhD Thesis, University of California, Berkeley.

Canright D and Morris S (1993) Buoyant instability of a viscous film over a passive fluid. *Journal of Fluid Mechanics* 255: 349–372.

Chandrasekhar S (1981) *Hydrodynamic and Hydromagnetic Stability*. New York, NY: Dover.

Conrad CP and Molnar P (1997) The growth of Rayleigh–Taylor-type instabilities in the lithosphere for various rheological and density structures. *Geophysical Journal International* 129: 95–112.

Cox RG (1970) The motion of long slender bodies in a viscous fluid. Part 1: General theory. *Journal of Fluid Mechanics* 44: 791–810.

Davaille A (1999) Two-layer thermal convection in miscible viscous fluids. *Journal of Fluid Mechanics* 379: 223–253.

Dziewonski AM and Anderson DL (1981) Preliminary reference Earth model. *Physics of the Earth and Planetary Interiors* 25: 297–356.

England P and McKenzie D (1983) Correction to: A thin viscous sheet model for continental deformation. *Geophysical Journal of the Royal Astronomical Society* 73: 523–532.

Farrell WE (1972) Deformation of the Earth by surface loads. *Review of Geophysics and Space Physics* 10: 761–797.

Feighner M and Richards MA (1995) The fluid dynamics of plume-ridge and plume-plate interactions: An experimental investigation. *Earth and Planetary Science Letters* 129: 171–182.

Fenner RT (1975) On local solutions to non-Newtonian slow viscous flows. *International Journal of Non-Linear Mechanics* 10: 207–214.

Fleitout L and Froidevaux C (1983) Tectonic stresses in the lithosphere. *Tectonics* 2: 315–324.

Fletcher CAJ (1984) *Computational Galerkin Methods*. New York, NY: Springer Verlag.

Forte AM and Peltier WR (1987) Plate tectonics and aspherical Earth structure: The importance of poloidal-toroidal coupling. *Journal of Geophysical Research* 92: 3645–3679.
Fowler AC (1985) Fast thermoviscous convection. *Studies in Applied Mathematics* 72: 189–219.
Gantmacher FR (1960) *Matrix Theory,* 2 vols. Providence, RI: AMS Chelsea Publishing.
Gomilko AM, Malyuga VS, and Meleshko VV (2003) On steady Stokes flow in a trihedral rectangular corner. *Journal of Fluid Mechanics* 476: 159–177.
Gratton J and Minotti F (1990) Self-similar viscous gravity currents: Phase-plane formalism. *Journal of Fluid Mechanics* 210: 155–182.
Griffiths RW (1986) Thermals in extremely viscous fluids, including the effects of temperature-dependent viscosity. *Journal of Fluid Mechanics* 166: 115–138.
Hager BH and O'Connell RJ (1981) A simple global model of plate tectonics and mantle convection. *Journal of Geophysical Research* 86: 4843–4867.
Hager BH, Clayton RW, Richards MA, Comer RP, and Dziewonski AM (1985) Lower mantle heterogeneity, dynamic topography and the geoid. *Nature* 313: 541–545.
Happel J and Brenner H (1991) *Low Reynolds Number Hydrodynamics,* 2nd rev. edn. Dordrecht: Kluwer Academic.
Hauri EH, Whitehead JA, Jr., and Hart SR (1994) Fluid dynamic and geochemical aspects of entrainment in mantle plumes. *Journal of Geophysical Research* 99: 24275–24300.
Hinch EJ (1991) *Perturbation Methods*. Cambridge: Cambridge University Press.
Houseman GA and Molnar P (1997) Gravitational (Rayleigh–Taylor) instability of a layer with non-linear viscosity and convective thinning of continental lithosphere. *Geophysical Journal International* 128: 125–150.
Howard LN (1964) Convection at high Rayleigh number. In: Görtler H (ed.) *Proceedings of the 11th International Congress in Applied Mechanics*, pp. 1109–1115. Berlin: Springer.
Huppert HE (1982) The propagation of two-dimensional and axisymmetric viscous gravity currents over a rigid horizontal surface. *Journal of Fluid Mechanics* 121: 43–58.
Ito G (2001) Reykjanes 'V'-shaped ridges originating from a pulsing and dehydrating mantle plume. *Nature* 411: 681–684.
Jackson JD (1975) *Classical Electrodynamics*. New York, NY: John Wiley & Sons.
Jimenez J and Zufiria JA (1987) A boundary-layer analysis of Rayleigh–Bénard convection at large Rayleigh number. *Journal of Fluid Mechanics* 178: 53–71.
Jeong J-T and Moffatt HK (1992) Free-surface cusps associated with flow at low Reynolds number. *Journal of Fluid Mechanics* 241: 1–22.
Johnson RE (1980) Slender-body theory for slow viscous flow. *Journal of Fluid Mechanics* 75: 705–714.
Katopodes FV, Davis AMJ, and Stone HA (2000) Piston flow in a two-dimensional channel. *Physics of Fluids* 12: 1240–1243.
Keller JB and Rubinow SI (1976) An improved slender-body theory for Stokes flow. *Journal of Fluid Mechanics* 99: 411–431.
Kerr RC and Lister JR (1987) The spread of subducted lithospheric material along the mid-mantle boundary. *Earth and Planetary Science Letters* 85: 241–247.
Kevorkian J and Cole JD (1996) *Multiple Scale and Singular Perturbation Methods*. New York, NY: Springer.
Kim S and Karrila SJ (1991) *Microhydrodynamics: Principles and Selected Applications*. Boston, MA: Butterworth-Heinemann.
Koch DM and Koch DL (1995) Numerical and theoretical solutions for a drop spreading below a free fluid surface. *Journal of Fluid Mechanics* 287: 251–278.
Koch DM and Ribe NM (1989) The effect of lateral viscosity variations on surface observables. *Geophysical Research Letters* 16: 535–538.
Lachenbruch AH and Nathenson M (1974) Rise of a variable viscosity fluid in a steadily spreading wedge-shaped conduit with accreting walls. *Open File Report.* 74–251, 27 pp. US Geological Survey, Menlo Park, CA.
Ladyzhenskaya OA (1963) *The Mathematical Theory of Viscous Incompressible Flow*. New York, NY: Gordon and Breach.
Lamb H (1932) *Hydrodynamics*. Cambridge: Cambridge University Press.
Landau LD (1944) On the problem of turbulence. *Comptes Rendus de l'Academie des Sciences URSS* 44: 311–314.
Landau LD and Lifshitz EM (1986) *Theory of Elasticity,* 3rd edn. Oxford: Pergamon.
Langlois WE (1964) *Slow Viscous Flow*. New York, NY: Macmillan.
Le Bars M and Davaille A (2002) Stability of thermal convection in two superposed miscible viscous fluids. *Journal of Fluid Mechanics* 471: 339–363.
Lee SH and Leal LG (1980) Motion of a sphere in the presence of a plane interface. Part 2: An exact solution in bipolar co-ordinates. *Journal of Fluid Mechanics* 98: 193–224.
Lemery C, Ricard Y, and Sommeria J (2000) A model for the emergence of thermal plumes in Rayleigh-Bénard convection at infinite Prandtl number. *Journal of Fluid Mechanics* 414: 225–250.
Lister JR and Kerr RC (1989a) The effect of geometry on the gravitiational instability of a region of viscous fluid. *Journal of Fluid Mechanics* 202: 577–594.
Lister JR and Kerr RC (1989b) The propagation of two-dimensional and axisymmetric viscous gravity currents at a fluid interface. *Journal of Fluid Mechanics* 203: 215–249.
Longman IM (1962) A Green's function for determining the deformation of the Earth under surface mass loads. *Journal of Geophysical Research* 67: 845–850.
Loper DE and Stacey FD (1983) The dynamical and thermal structure of deep mantle plumes. *Physics of the Earth and Planetary Interiors* 33: 305–317.
Malkus WVR and Veronis G (1958) Finite amplitude cellular convection. *Journal of Fluid Mechanics* 4: 225–260.
Manga M (1996) Mixing of heterogeneities in the mantle: Effect of viscosity differences. *Geophysical Research Letters* 23: 403–406.
Manga M (1997) Interactions between mantle diapirs. *Geophysical Research Letters* 24: 1871–1874.
Manga M and Stone HA (1993) Buoyancy-driven interaction between two deformable viscous drops. *Journal of Fluid Mechanics* 256: 647–683.
Manga M, Stone HA, and O'Connell RJ (1993) The interaction of plume heads with compositional discontinuities in the Earth's mantle. *Journal of Geophysical Research* 98: 19979–19990.
Mangler W (1948) Zusammenhang zwischen ebenen und rotationssymmetrischen Grenzschichten in kompressiblen Flüssigkeiten. *Zeitschrift für Angewandte Mathematik und Mechanik* 28: 97–103.
Marsh BD (1978) On the coolling of ascending andesitic magma. *Philosophical Transactions of the Royal Society of London* 288: 611–625.
Marsh BD and Carmichael ISE (1974) Benioff zone magmatism. *Journal of Geophysical Research* 79: 1196–1206.
McKenzie DP (1969) Speculations on the consequences and causes of plate motions. *Geophysical Journal of the Royal Astronomical Society* 18: 1–32.
McKenzie DP and Bowin C (1976) The relationship between bathymetry and gravity in the Atlantic ocean. *Journal of Geophysical Research* 81: 1903–1915.

McKenzie DP, Roberts JM, and Weiss NO (1974) Convection in the Earth's mantle: Towards a numerical simulation. *Journal of Fluid Mechanics* 62: 465–538.
Meleshko VV (1996) Steady Stokes flow in a rectangular cavity. *Proceedings of the Royal Society of London A* 452: 1999–2022.
Mitrovica JX and Forte AM (2004) A new inference of mantle viscosity based upon joint inversion of convection and glacial isostatic adjustment data. *Earth and Planetary Science Letters* 225: 177–189.
Moffatt HK (1964) Viscous and resistive eddies near a sharp corner. *Journal of Fluid Mechanics* 18: 1–18.
Molnar P and Houseman GA (2004) The effects of buoyant crust on the gravitational instability of thickened mantle lithosphere at zones of intracontinental convergence. *Geophysical Journal International* 158: 1134–1150.
Morris S (1980) *An Asymptotic Method for Determining the Transport of Heat and Matter by Creeping Flows with Strongly Variable Viscosity; Fluid Dynamic Problems Motivated by Island Arc Volcanism*. PhD Thesis, The Johns Hopkins University
Morris S (1982) The effects of a strongly temperature-dependent viscosity on slow flow past a hot sphere. *Journal of Fluid Mechanics* 124: 1–26.
Morris S and Canright D (1984) A boundary-layer analysis of Benard convection in a fluid of strongly temperature-dependent viscosity. *Physics of the Earth and Planetary Interiors* 36: 355–373.
Muskhelishvili NI (1953) *Some Basic Problems in the Mathematical Theory of Elasticity*. Groningen: P. Noordhoff.
Nayfeh A (1973) *Perturbation Methods*. New York, NY: John Wiley & Sons.
Newell A C, Passot T, and Lega J (1993) Order parameter equations for patterns. *Annual Reviews of Fluid Mechanics* 25: 399–453.
Newell AC, Passot T, and Souli M (1990) The phase diffusion and mean drift equations for convection at finite Rayleigh numbers in large containers. *Journal of Fluid Mechanics* 220: 187–252.
Newell AC and Whitehead JA, Jr. (1969) Finite bandwidth, finite amplitude convection. *Journal of Fluid Mechanics* 38: 279–303.
Niordson FI (1985) *Shell Theory*. Amsterdam: North-Holland.
Novozhilov VV (1959) *Theory of Thin Shells*. Groningen: P. Noordhoff.
Olson P (1990) Hot spots, swells and mantle plumes. In: Ryan MP (ed.) *Magma Transport and Storage*, pp. 33–51. New York, NY: John Wiley.
Olson P and Christensen U (1986) Solitary wave propagation in a fluid conduit within a viscous matrix. *Journal of Geophysical Research* 91: 6367–6374.
Olson P and Corcos GM (1980) A boundary-layer model for mantle convection with surface plates. *Geophysical Journal of the Royal Astronomical Society* 62: 195–219.
Olson P, Schubert G, and Anderson C (1993) Structure of axisymmetric mantle plumes. *Journal of Geophysical Research* 98: 6829–6844.
Olson P and Singer H (1985) Creeping plumes. *Journal of Fluid Mechanics* 158: 511–531.
Palm E (1960) On the tendency towards hexagonal cells in steady convection. *Journal of Fluid Mechanics* 8: 183–192.
Palm E, Ellingsen T, and Gjevik B (1967) On the occurrence of cellular motion in Bénard convection. *Journal of Fluid Mechanics* 30: 651–661.
Parsons B and Daly S (1983) The relationship between surface topography, gravity anomalies, and the temperature structure of convection. *Journal of Geophysical Research* 88: 1129–1144.
Peltier WR (1974) The impulse response of a Maxwell Earth. *Reviews of Geophysics and Space Physics* 12: 649–669.
Peltier WR (1995) Mantle viscosity. In: Peltier WR (ed.) *Mantle Convection: Plate Tectonics and Global Dynamics*, pp. 389–478. New York, NY: Gordon and Breach Science Publishers.
Pozrikidis C (1990) The deformation of a liquid drop moving normal to a plane wall. *Journal of Fluid Mechanics* 215: 331–363.
Pozrikidis C (1992) *Boundary Integral and Singularity Methods for Linearized Viscous Flow*. Cambridge: Cambridge University Press.
Rasenat S, Busse FH, and Rehberg I (1989) A theoretical and experimental study of double-layer convection. *Journal of Fluid Mechanics* 199: 519–540.
Rayleigh L (1922) *Theory of Sound*, vol. II, 313 pp. New York, NY: Dover.
Ribe NM (1992) The dynamics of thin shells with variable viscosity and the origin of toroidal flow in the mantle. *Geophysical Journal International* 110: 537–552.
Ribe NM (1998) Spouting and planform selection in the Rayleigh–Taylor instability of miscible viscous fluids. *Journal of Fluid Mechanics* 234: 315–336.
Ribe NM (2003) Periodic folding of viscous sheets. *Physical Review E* 68: 036305.
Ribe NM and Christensen U (1994) Three-dimensional modeling of plume-lithosphere interaction. *Journal of Geophysical Research* 99: 669–682.
Ribe NM and Christensen U (1999) The dynamical origin of Hawaiian volcanism. *Earth and Planetary Science Letters* 171: 517–531.
Ribe NM, Christensen UR, and Theissing J (1995) The dynamics of plume-ridge interaction. Part 1: Ridge-centered plumes. *Earth and Planetary Science Letters* 134: 155–168.
Ribe NM and Delattre WL (1998) The dynamics of plume-ridge interaction-III. The effects of ridge migration. *Geophysical Journal International* 133: 511–518.
Ribe NM, Stutzmann E, Ren Y, and van der Hilst R (2007) Buckling instabilities of subducted lithosphere beneath the transition zone. *Earth and Planetary Science Letters* 254: 173–179.
Ricard Y, Fleitout L, and Froidevaux C (1984) Geoid heights and lithospheric stresses for a dynamic earth. *Annals of Geophysics* 2: 267–286.
Richards MA and Hager BH (1984) Geoid anomalies in a dynamic Earth. *Journal of Geophysical Research* 89: 5987–6002.
Richards MA, Hager BH, and Sleep NH (1988) Dynamically supported geoid highs over hotspots: Observation and theory. *Journal of Geophysical Research* 893: 7690–7708.
Richter FM (1973) Dynamical models for sea floor spreading. *Reviews of Geophysics and Space Physics* 11: 223–287.
Richter FM and Johnson CE (1974) Stability of a chemically layered mantle. *Journal of Geophysical Research* 79: 1635–1639.
Richter FM and McKenzie DP (1984) Dynamical models for melt segregation from a deformable matrix. *Journal of Geology* 92: 729–740.
Roberts GO (1979) Fast viscous Bénard convection. *Geophysical and Astrophysical Fluid Dynamics* 12: 235–272.
Schubert G, Olson P, Anderson C, and Goldman P (1989) Solitary waves in mantle plumes. *Journal of Geophysical Research* 94: 9523–9532.
Schubert G and Turcotte DL (1971) Phase changes and mantle convection. *Journal of Geophysical Research* 76: 1424–1432.
Schubert G, Yuen DA, and Turcotte DL (1972) Role of phase transitions in a dynamic mantle. *Geophysical Journal of the Royal Astronomical Society* 42: 705–735.
Scott DR and Stevenson DJ (1984) Magma solitons. *Geophysical Research Letters* 11: 1161–1164.

Scott DR, Stevenson DJ, and Whitehead JA, Jr. (1986) Observations of solitary waves in a deformable pipe. *Nature* 319: 759–761.

Segel L (1969) Distant side-walls cause slow amplitude modulation of cellular convection. *Journal of Fluid Mechanics* 38: 203–224.

Selig F (1965) A theoretical prediction of salt dome patterns. *Geophysics* 30: 633–643.

Shankar PN (1993) The eddy structure in Stokes flow in a cavity. *Journal of Fluid Mechanics* 250: 371–383.

Shankar PN (2005) Eigenfunction expansions on arbitrary domains. *Proceedings of the Royal Society of London A* 461: 2121–2133.

Sleep NH (1987) Lithospheric heating by mantle plumes. *Geophysical Journal of the Royal Astronomical Society* 91: 1–11.

Solomatov VS (1995) Scaling of temperature- and stress-dependent viscosity convection. *Physics of Fluids* 7: 266–274.

Sparrow EM, Husar RB, and Goldstein RJ (1970) Observations and other characteristics of thermals. *Journal of Fluid Mechanics* 41: 793–800.

Stengel KC, Oliver DS, and Booker JR (1982) Onset of convection in a variable-viscosity fluid. *Journal of Fluid Mechanics* 120: 411–431.

Stevenson DJ and Turner JS (1977) Angle of subduction. *Nature* 270: 334–336.

Stimson M and Jeffrey GB (1926) The motion of two spheres in a viscous fluid. *Proceedings of the Royal Society of London A* 111: 110–116.

Stokes GG (1845) On the theories of the internal friction of fluids and of the equilibrium and motion of elastic solids. *Transactions of the Cambridge Philosophical Society* 8: 287–347.

Straus JM (1972) Finite amplitude doubly diffusive convection. *Journal of Fluid Mechanics* 56: 353–374.

Tanimoto T (1998) State of stress within a bending spherical shell and its implications for subducting lithosphere. *Geophysical Journal International* 134: 199–206.

Tovish A, Schubert G, and Luyendyk BP (1978) Mantle flow pressure and the angle of subduction: Non-Newtonian corner flows. *Journal of Geophysical Research* 83: 5892–5898.

Turcotte DL (1967) A boundary-layer theory for cellular convection. *International Journal of Heat and Mass Transfer* 10: 1065–1074.

Turcotte DL (1974) Membrane tectonics. *Geophysical Journal of the Royal Astronomical Society* 36: 33–42.

Turcotte DL and Oxburgh ER (1967) Finite amplitude convection cells and continental drift. *Journal of Fluid Mechanics* 28: 29–42.

Umemura A and Busse FH (1989) Axisymmetric convection at large Rayleigh number and infinite Prandtl number. *Journal of Fluid Mechanics* 208: 459–478.

Van Dyke M (1975) *Perturbation Methods in Fluid Mechanics*. Stanford, CA: Parabolic Press.

Von Mises R (1927) Bemerkungen zur Hydrodynamik. *Zeitschrift für Angewandte Mathematik und Mechanik* 7: 425–431.

Watts AB (1978) An analysis of isostasy in the world's oceans. Part 1: Hawaiian-Emperor Seamount chain. *Journal of Geophysical Research* 83: 5989–6004.

Weinstein SA and Olson PL (1992) Thermal convection with non-Newtonian plates. *Geophysical Journal International* 111: 515–530.

Whitehead JA, Jr., Dick HBJ, and Schouten H (1984) A mechanism for magmatic accretion under spreading centers. *Nature* 312: 146–148.

Whitehead JA, Jr. and Helfrich KR (1986) The Korteweg-de Vries equation from laboratory conduit and magma migration equations. *Geophysical Research Letters* 13: 545–546.

Whitehead JA, Jr. and Helfrich KR (1988) Wave transport of deep mantle material. *Nature* 335: 59–61.

Whitehead JA, Jr. and Luther DS (1975) Dynamics of laboratory diapir and plume models. *Journal of Geophysical Research* 80: 705–717.

Whitham GB (1974) *Linear and Non-Linear Waves*. Sydney: Wiley-Interscience.

Whittaker RJ and Lister JR (2006a) Steady axisymmetric creeping plumes above a planar boundary. Part I: A point source. *Journal of Fluid Mechanics* 567: 361–378.

Whittaker RJ and Lister JR (2006b) Steady axisymmetric creeping plumes above a planar boundary. Part II: A distributed source. *Journal of Fluid Mechanics* 567: 379–397.

Yale MM and Phipps Morgan J (1998) Asthenosphere flow model of hotspot-ridge interactions: A comparison of Iceland and Kerguelen. *Earth and Planetary Science Letters* 161: 45–56.

Yuen DA and Peltier WR (1980) Mantle plumes and the thermal stability of the *D″* layer. *Geophysical Research Letters* 7: 625–628.

Yuen DA and Schubert G (1976) Mantle plumes: a boundary-layer approach for Newtonian and non-Newtonian temperature-dependent rheologies. *Journal of Geophysical Research* 81: 2499–2510.